Study on Spectral Sizing for CO_2 Observations:

Error analysis for CarbonSat scenarios and different spectral sizing

Technical Note

ESA Study
"Study on Spectral Sizing for CO_2 Observations"
ESA Contract N° 4000118601/16/NL/FF/gp

Author:
Michael.Buchwitz@iup.physik.uni-bremen.de,
Institute of Environmental Physics (IUP) / Institute of Remote Sensing (IFE),
University of Bremen (UB), Bremen, Germany

Change log

Version	Date	Status	Author	Reason for change
1.0	11-Apr-2017	Submitted	M. Buchwitz, IUP-UB	New document
2.0	23-May-2017	Submitted (for MTR)	M. Buchwitz	Update of straylight assessment using updated version of SRON-CSS-TN-2016-002 (incl. improved error estimation procedure) Some editorial improvements (e.g., Fig. numbering issue)
3.0	29-June-2017	Submitted	M. Buchwitz	Update of straylight assessment considering new information from ESA Summary figure for linear error analysis added
3.1	6-July-2017	Submitted	M. Buchwitz	Improved summary figures 36 (improved colors) and 47 (improved colors and annotation)
4.0	30-April-2018	Submitted	M. Buchwitz	Additional results added: New Sects. 9 and 10

Table of Contents

1. Abstract

In the context of optimizing CarbonSat (also in terms of costs) it had been investigated in the past if high spectral resolution is mandatory for precise and accurate XCO_2 retrieval or if a somewhat less demanding spectral resolution is also acceptable taking into account that other parameters (such as spectral coverage and signal-to-noise performance) can be optimized simultaneously for compensation. According to the initial specification of CarbonSat - as given in the CarbonSat Mission Requirements Document, MRDv1.0 – a rather high spectral resolution was required. Using this specification as a starting point it had been investigated in the past to what extent the spectral resolution can be reduced. That investigation was primarily based on simulated retrievals which have been carried out by University of Bremen using the BESD/C retrieval algorithm and independently by University of Leicester using University of Leicester's XCO_2 retrieval algorithm. In addition, real GOSAT data had been analysed by SRON. Based on these past investigations it was concluded that the spectral resolution can be reduced if the signal-to-noise performance is enhanced and the spectral coverage is extended. These findings had been adopted for the final version of the CarbonSat Mission Requirements Document - MRDv1.2 - which had been used for sub-sequent assessments conducted to quantify in detail the performance of CarbonSat in the context of the Earth Explorer 8 (EE8) Report for Mission Selection (RfMS) of CarbonSat.

The purpose of this follow-on study is to repeat and extend (parts of) those past investigations, which had been carried out to define CarbonSat's instrument spectral sizing point (SSP), where SSP is defined as spectral resolution, spectral coverage and signal-to-noise performance. Specifically, it was requested to repeat the analysis as had been carried out for CarbonSat by the University of Bremen but (i) using the latest version of the BESD/C retrieval algorithm (as available at the end of the CarbonSat EE8 related activities), (ii) using the latest information on systematic instrument related errors and (iii) using four different pre-defined instrument concepts: instrument A (similar as CarbonSat MRDv1.0), instrument B (similar a CarbonSat MRDv1.2), instrument C (similar as NASA's OCO-2) and instrument D (similar as CNES's MicroCarb). Here instrument B has the lowest spectral resolution compared to the other three instruments but instrument B has highest signal-to-noise ratio and covers the largest spectral region. The purpose of this investigation is to find out if the past recommendation - which led to a CarbonSat similar as instrument B - is still valid, namely that instrument B is equivalent or even better in terms of XCO_2 random and systematic errors compared to other higher spectral resolution instrument concepts (note that instrument B is preferred for cost reasons if equivalent in terms of XCO_2 quality).

As shown in this document the following error sources have been considered: (i) instrument noise, (ii) geophysical errors (e.g., aerosols, cirrus, sun-induced fluorescence), (iii) zero-level-offset, (iv) distortions of the Instrument Spectral Response Function, (v) straylight, (vi) detector non-linearity and (vii) polarization. It is shown that instrument B has the smallest XCO_2 random error ("best precision"). For systematic errors the situation is less clear. Using full iterative retrievals it is shown that instrument B often has the smallest systematic error for the investigated scenarios but according to linear error analysis (performed to isolate instrument specific errors) the differences to the other instruments are much less pronounced (here the results show that instruments A, B and C are nearly identical). It is therefore concluded that the past recommendations - which resulted in MRDv1.2 - are still valid.

2. Executive summary

In this document an updated (and extended) analysis of a past analysis is presented. That past analysis had been conducted for the ESA Earth Explorer 8 (EE8) candidate mission CarbonSat. The results of that past analysis are reported in the Final Report (FR) of the ESA study "Level-2 and Level-1B Requirements Consolidation Study" **/Bovenmann et al., 2014/** in particular in Sect. 5.1 - 5.3. In the following that past study is referred to as CS-L1L2-I study.

A key result of that past analysis was that the spectral resolution of CarbonSat can be reduced (w.r.t. to the initial instrument configuration) - without degradation in terms of biases and precision of the main data products XCO_2 and XCH_4 - if the spectral coverage of (the initial specification of) CarbonSat bands is extended and the signal-to-noise ratio (SNR) is enhanced.

As a result, it had been recommended (and later also decided) to aim at a new "spectral sizing point" (SSP) for CarbonSat, where SSP is defined as a certain combination of spectral resolution, spectral coverage and SNR performance. The decision about the new SSP has been made quite early in CarbonSat Phase A and the resulting instrument specification had been used to update the CarbonSat Mission Requirements Document (MRD) from versions 1.0/1.1 to version 1.2.

Document MRDv1.2 had been used as input for many sub-sequent assessments and, ultimately, for the results presented in the CarbonSat EE8 Report for Mission Selection (RfMS) **/CS RfMS, 2015/**. All these assessments confirmed that a CarbonSat instrument with the new MRDv1.2 SSP will be able to meet the demanding XCO_2 and XCH_4 requirements concerning random and systematic errors (see **/Buchwitz et al., 2013a, 2013b, 2015/ /Bovensmann et al., 2015/ /CS RfMS, 2015/**).

At present, however, more details are available on various instrument related errors such as detector non-linearity and straylight. It is therefore of interest to know if the past CarbonSat findings and recommendations concerning its SSP are still valid or not. This is relevant in the context of ongoing activities related to a possible future European satellite mission to monitor fossil CO_2 emissions (see "Towards a European Operational Observing System to Monitor Fossil CO_2 emissions" **/Ciais et al., 2015/**).

In this document results from a new analysis are reported which are an update and extension of the above mentioned past analysis. Specifically, simulated retrievals have been performed for four different SSPs referred to as instrument concepts A, B, C and D in this document.

Instruments A and B correspond to CarbonSat MRD v1.0 and v1.2, respectively, except for the SNR performance (which had been updated based on the most recent information). Instrument C is similar to NASA's OCO-2 and Instrument D is similar to MicroCarb/CNES.

Simulated retrievals have been performed primarily for the 15 geophysical scenarios also used for the previous CarbonSat SSP assessments (see **/Bovenmann et al., 2014/**, in particular Sects. 5.1 to 5.3). They are defined by different CO_2, CH_4, and aerosol vertical profiles, different aerosol types, cirrus amounts and cirrus altitudes and different amounts of Sun-Induced Fluorescence (SIF). These parameters are input parameters for radiative transfer simulations. The high spectral resolution radiances - as computed with the radiative transfer model SCIATRAN - have been converted to simulated satellite instrument radiance observations using an instrument model.

The simulated radiance observations have then been inverted using the BESD/C retrieval method, which has also been used for previous CarbonSat assessments. The main output of the retrieval step is the retrieved XCO_2 and its uncertainty (essentially the XCO_2 random error due to instrument noise). Systematic XCO_2 retrieval errors are obtained by computing the difference of the retrieved and the "true" XCO_2 (the "true" XCO_2 has been computed from the known model atmosphere).

The main question to be answered via the activities described in this document is:

- Is instrument B equivalent (or even better) in terms of XCO_2 data quality compared to (some or all of) the other (higher spectral resolution) instruments or not?

This question is relevant as high spectral resolution implies high costs. This means that instrument concept B is the preferred concept if equivalent in terms of XCO_2 quality.

This question has been answered by performing simulated XCO_2 retrievals for different SSPs (i.e., different instrument concepts) using different scenarios and different instrument / calibration related errors such as straylight, detector non-linearity and zero-level-offset.

The findings can be summarized as follows: It is shown that instrument B has the smallest XCO_2 random error ("best precision") (**Figure 1**). For systematic errors the situation is less clear. Concerning systematic errors (biases) it is shown using full iterative retrievals that instrument B often has the smallest bias for the investigated scenarios (**Figure 1**). In addition, a linear error analysis has been performed in particular to (better) isolate instrument related biases. Also here instrument B shows good performance but the differences between the four instruments is much less pronounced (esp. for A, B and C) (**Figure 2**). It is therefore concluded that the past recommendations - which resulted in CarbonSat MRDv1.2 - are still valid.

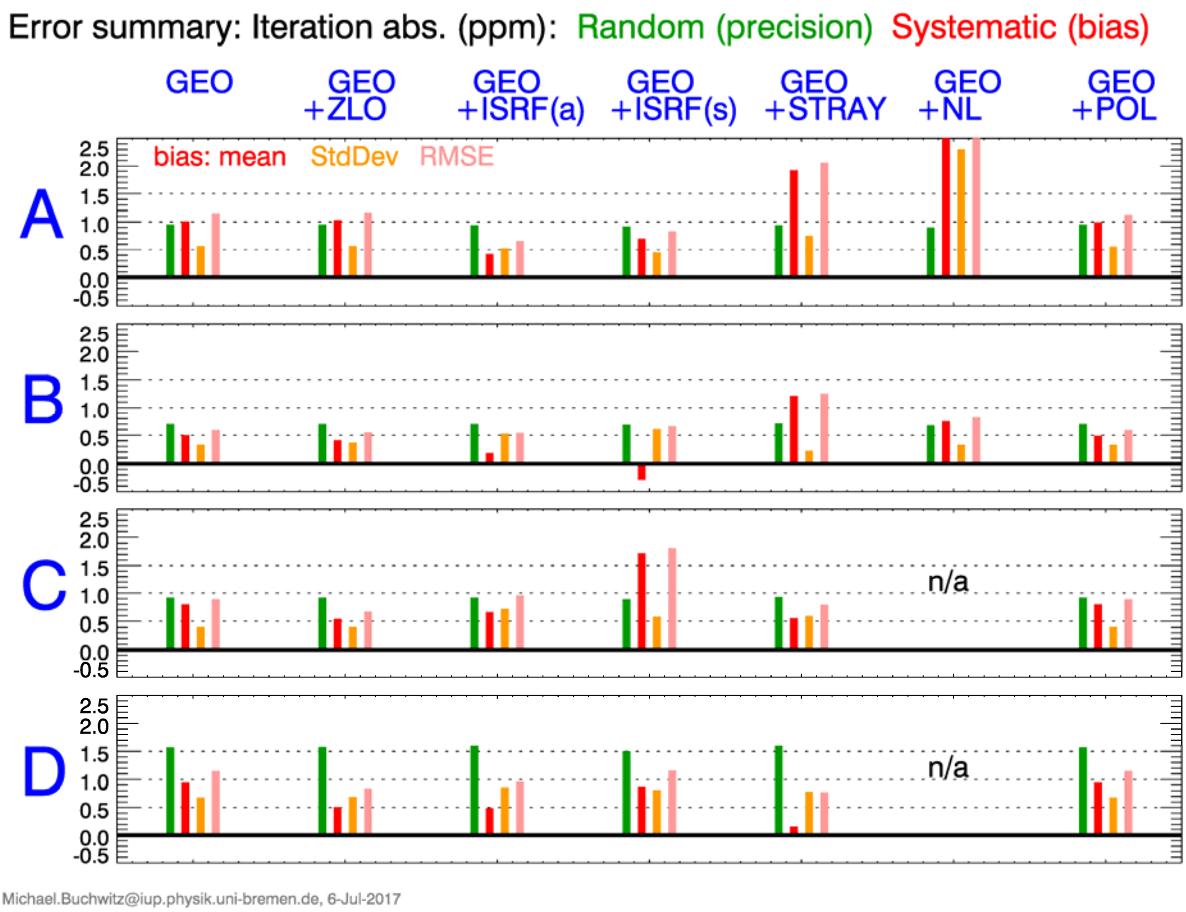

Figure 1: Summary of the error analysis results obtained using full iterative retrievals. A row corresponds to one of the four instruments A, B, C and D. A column corresponds to a certain systematic error or combination of errors: GEO: geophysical error (i.e., XCO_2 error due to aerosols, clouds, etc.), GEO+ZLO: zero-level-offset (radiance) error in addition to GEO error, ISRF: Instrument Spectral Response Function (two type of ISRF errors have been investigated (a = anti-symmetrial shape error, s = symmetrical error)), STRAY: straylight, NL: detector non-linearity (only input data for the instruments A and B were available), and POL: polarization related radiance error. The green bars show the XCO_2 random error ("precision"). The red bars show the three numbers computed to characterize XCO_2 biases (from left to right): mean bias, standard deviation of bias and root-mean-square error. As can be seen, instrument B has "best precision" (smallest random error) and typically also smallest bias (smallest systematic error). For additional details see **Sect. 6**.

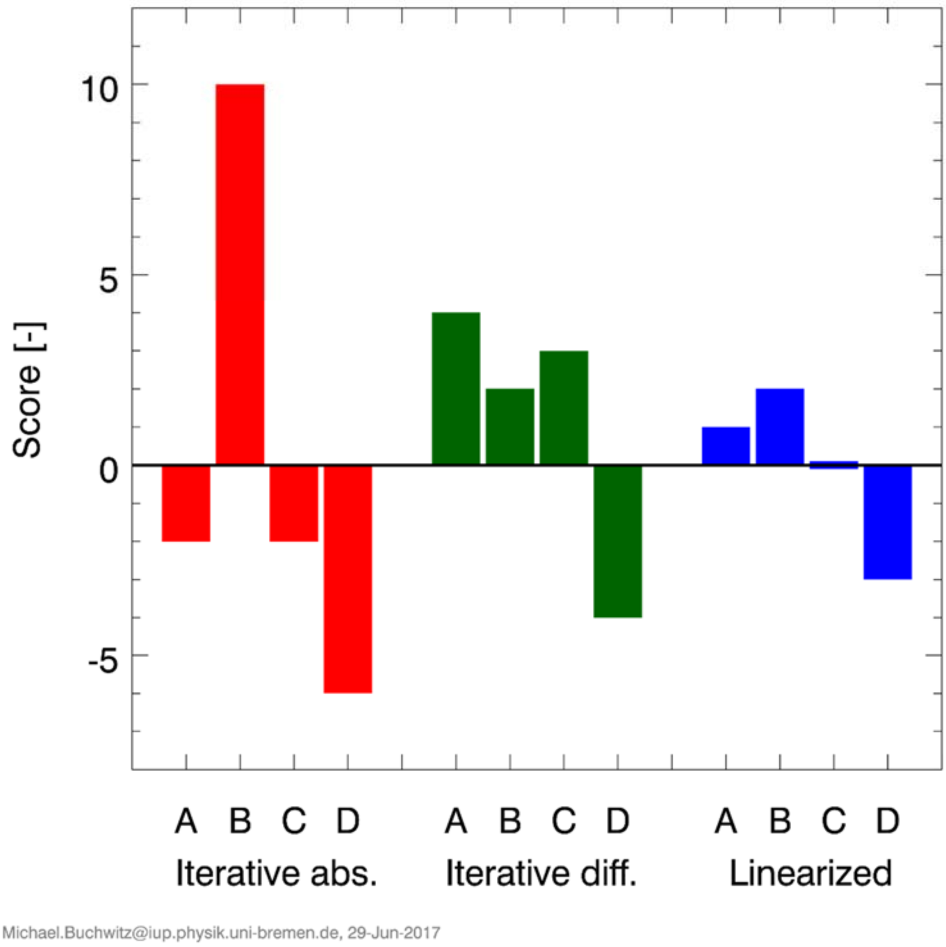

Figure 2: Overall summary of the error analysis results using scores (see **Sect. 8.1**). The higher the score, the better the instrument in terms of smaller XCO_2 biases. The red bars ("Iterative abs.") show the scores for the results obtained using full iterative retrievals. The blue bars ("Linearized") show the scores using linearized retrievals. As can be seen, instrument B is "the winner" for both methods. For additional details incl. explanation of "Iterative diff." (green bars), where the results are somewhat difficult to interpret, see **Sect. 8.1.2**.

3. Used set-up and simulation tools

3.1. Overview

The goal of this study is to investigate four different satellite instrument concepts in order to determine their characteristics with respect to the retrieval of column-averaged dry-air mole fractions of carbon dioxide (CO_2), i.e., XCO_2. Essentially it is of interest to find out which instrument is "the best" for this application and how large the XCO_2 data quality differences are (if the differences are "negligible", then other criteria for instrument selection are more relevant, e.g., costs).

However, none of the instruments is directly measuring XCO_2. Each instrument measures a radiance spectrum. This radiance spectrum needs to be "interpreted" w.r.t. XCO_2 using an inversion (or retrieval) algorithm, which is typically a quite complex algorithm using atmospheric radiative transfer modelling and a large number of input parameters. The instrument observes the atmosphere, which is defined by many parameters including CO_2. The atmospheric radiance, which enters the instrument, is modified by the instrument and is measured using a detector. The detector signals can be converted to the observed radiance using a "Level 0 to Level 1" algorithm (essentially the inverse of the instrument model) and calibration parameters. This observed radiance can then be converted to the desired quantity XCO_2. This retrieved XCO_2 can be compared with the "true XCO_2" (which is known for simulations) in order to determine the bias characteristics of the retrieved XCO_2. These characteristics depend NOT ONLY on the instrument but ALSO on the inversion (or retrieval) algorithm, i.e., on the entire Observing System (**Figure 3**). This means that - strictly speaking - the results shown in this document are valid only for the observing system, which uses BESD/C as inversion algorithm. The influence of the inversion algorithm is however considered in this study by using also other algorithms (see the corresponding technical reports and the Final Report of this study). Furthermore, linear error analysis is used in addition to full iterative retrievals.

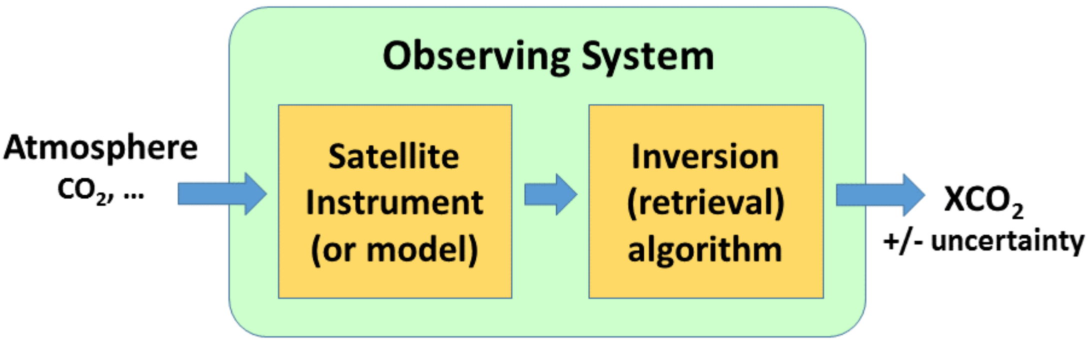

Figure 3: The XCO_2 observing system.

For the purpose of this study, it is essential to determine how certain characteristics of the Level 1 radiance spectra determine the quality of the XCO_2 Level 2 data products of the proposed CarbonSat-like instrument. To perform these assessments, the IUP-UB CarbonSat (CS) analysis system has been used, which is described in detail in **/Buchwitz et al., 2013a, 2013b, 2015/ /Bovenmann et al., 2014/**.

A more detailed overview about this analysis system is shown in **Figure 4**. The key components are:

- a Radiative Transfer Model (RTM) which computes high spectral resolution radiances based on given atmospheric, surface parameters and other parameters such as the solar zenith angle. A given set of parameters is referred to as "geophysical scenario" in the following.
- an instrument model which converts the high resolution RTM radiances into simulated satellite instrument observations taking into account the instrument characteristics as given by instrument requirements (or performance estimates) for parameters such as spectral range, spectral resolution and signal-to-noise ratio (SNR).
- the Level 1-2 retrieval program ("BESD/C") which inverts the radiance spectra in order to obtain the desired parameter XCO_2 (and XCH_4) and its statistical uncertainty (random error). The XCO_2 systematic error (bias) is computed as "retrieved minus true", where the true value of XCO_2 is obtained from the used model atmosphere.

More details on these components are given in the following sub-sections.

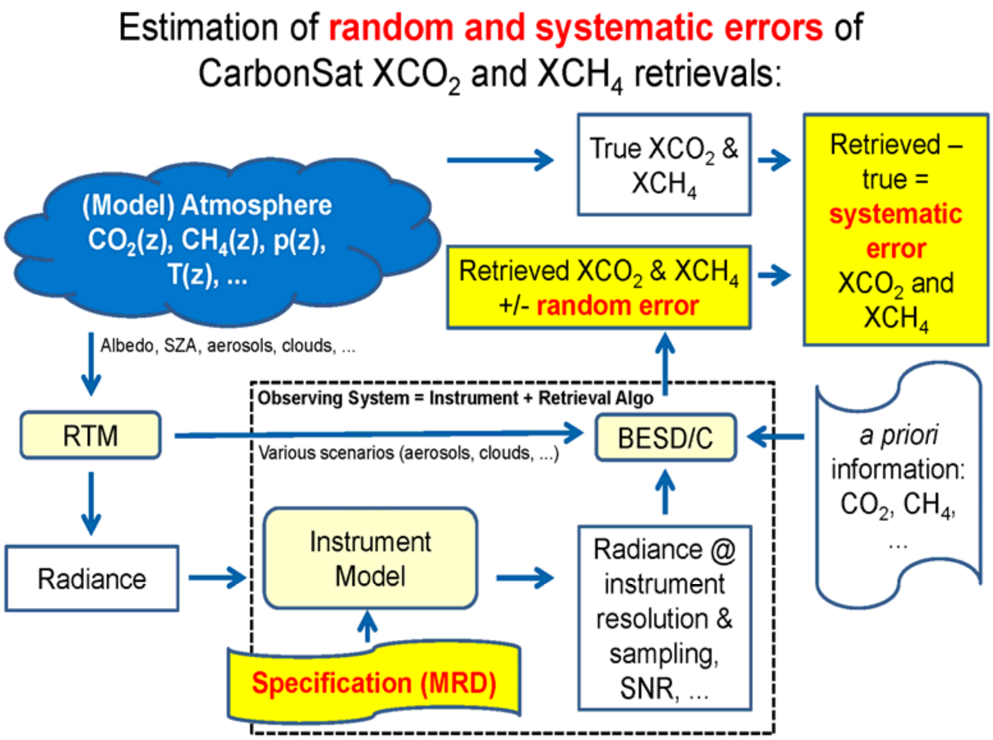

Figure 4: Overview of the IUP-UB satellite instrument Level 1 to Level 2 analysis system as used for past for CarbonSat assessments and also used in this study. Figure from **/Buchwitz et al., 2013b/**.

3.2. Retrieval Algorithm BESD/C

The retrieval algorithm used for the assessment results presented in this document is BESD/C **/Bovensmann et al., 2010/ /Buchwitz et al. 2013a/**. BESD stands for "Bremen optimal Estimation DOAS". BESD/C is an algorithm primarily designed to retrieve atmospheric dry-air column-averaged mole fractions of CO_2 and CH_4, i.e., XCO_2 and XCH_4 from satellite observed radiance spectra in the Near-Infrared / Shortwave-Infrared (NIR/SWIR) spectral region. In addition, a number of other parameters, such as Sun-Induced Fluorescence (SIF) (also referred to as Vegetation Chlorophyll Fluorescence (VCF) in this document) and cirrus optical depth (COD), can also be retrieved with this algorithm.

BESD/C is based on Optimal Estimation (OE) **/Rodgers, 2000/** and uses SCIATRAN as the forward (RT) model. SCIATRAN is a powerful state of the art RT simulation software which has been developed at the IUP of University of Bremen **/Rozanov et al. 2014/**.

BESD/C has been designed to simultaneously evaluate multiple spectral regions (e.g., O_2 A band and SWIR bands) and to retrieve scattering parameters (aerosols, clouds) in addition to XCO_2, as well as other parameters (e.g., SIF).

The radiance as used for the purpose of this study are high spectral resolution radiances (computed with SCIATRAN), which are converted to simulated satellite radiance observations using an instrument model, which is described in the following.

The same (full iterative) BESD/C retrieval algorithm has been applied to simulated radiance of all 4 instruments investigated in this study. However, some of the retrieval algorithm settings had to be adjusted due to the fact that the instruments cover different spectral regions. The only differences are the following:

- All instruments: Spectral fitting windows according to instrument specification.
- SIF and COD pre-processing:
    - A: SIF: yes (via 758 nm region); COD: no
    - B: SIF: yes (via 758 nm region); COD: yes (via 1939 nm region)
    - C: SIF: no; COD: no
    - D: SIF: no; COD: no

3.3. Instrument Simulator

The satellite instrument simulator as used for the presented assessments converts the high spectral resolution radiance and irradiance spectra as computed with RTMs such as SCIATRAN **/Rozanov et al. 2014/** into simulated spectra as measured by a satellite instrument by

- convolving the spectra using the assumed Instrument Spectral Response Function (ISRF) (spectral resolution),
- computing the wavelength grid of the satellite radiance observations using the definition of the instrument's spectral bands, spectral resolution and Spectral Sampling Ratios (SSR),
- spectral interpolation of the convolved spectra onto the instrument spectral grid and
- computation of the measurement error using the instrument signal-to-noise ratio (SNR).

Figure 5 shows example spectra for instrument B. The instrument parameters are from **/Landgraf et al., 2017b/** and described in **Sect. 5**.

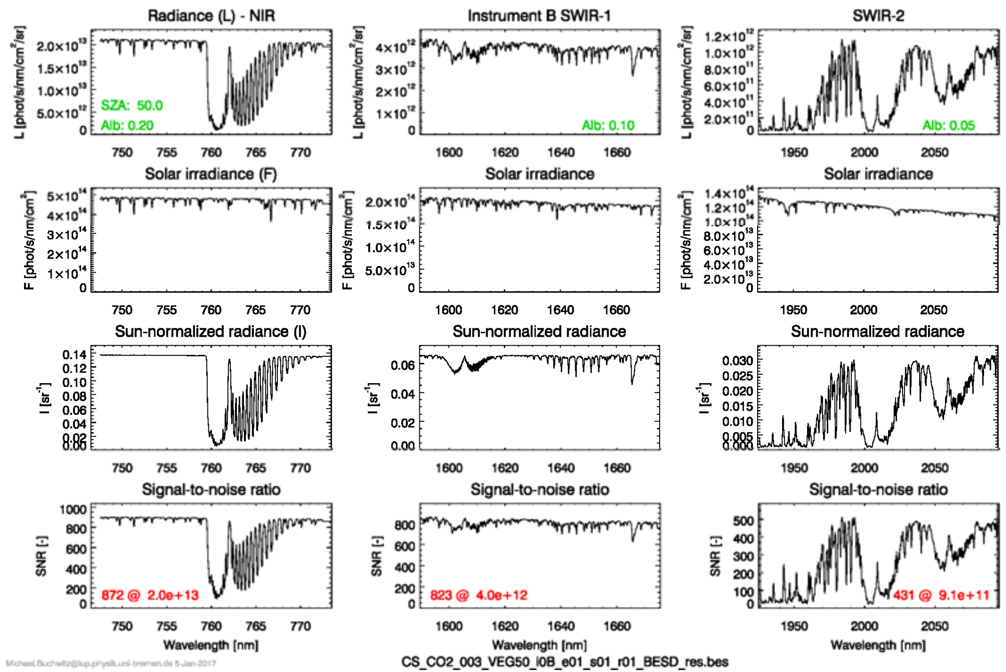

Figure 5: Simulated nadir radiance (top), solar irradiance (2nd row), sun-normalized radiance (3rd row) and signal-to-noise ratio (bottom) spectra for vegetation albedo and a Solar Zenith Angle (SZA) of 50°. Here the SSP corresponds to instrument B. The scenario is s01 (details are given below).

4. Geophysical Scenarios

4.1. Overview

For the purpose of this study we use the 15 geophysical scenarios as defined and used also in the past to optimize the SSP of CarbonSat **/Bovensmann et al., 2014/**. They are described in **/Bovensmann et al., 2014/** but also in the following sub-sections.

Key parameters which are varied and which define the used geophysical scenarios are:

- CO_2 (and CH_4) vertical profiles
- SIF
- Aerosol profile
- Aerosol type
- Cirrus optical depth (COD)
- Cirrus altitude

The focus is on simulations for vegetation surface albedo (VEG) and a solar zenith angle (SZA) of 50°. If other conditions have been used, then this is explicitly mentioned in the following.

4.2. GHG vertical profiles

Two sets of CO_2 and CH_4 vertical profiles have been used. They are shown in **Figure 6** (see also **Table 1**). One set (shown in black) corresponds to the *a priori* (= first guess) profiles as used for the retrieval. The other set (green) has been used for most of the simulated satellite observations presented in this report. It corresponds to a typical northern mid-latitude summer (MLS) scenario, where lower atmospheric CO_2 (especially in the boundary layer) is lower than average due to CO_2 uptake by growing vegetation (plant uptake) and CH_4 is higher primarily due to wetland emissions (note that the same profiles have been used for the assessments presented in **/Bovensmann et al., 2010/**). As can be seen from **Figure 6**, XCO_2 is 390 ppm for the *a priori* profile and 386.27 ppm for the MLS profile, i.e., XCO_2 is 3.7 ppm ppm lower for the MLS scenario.

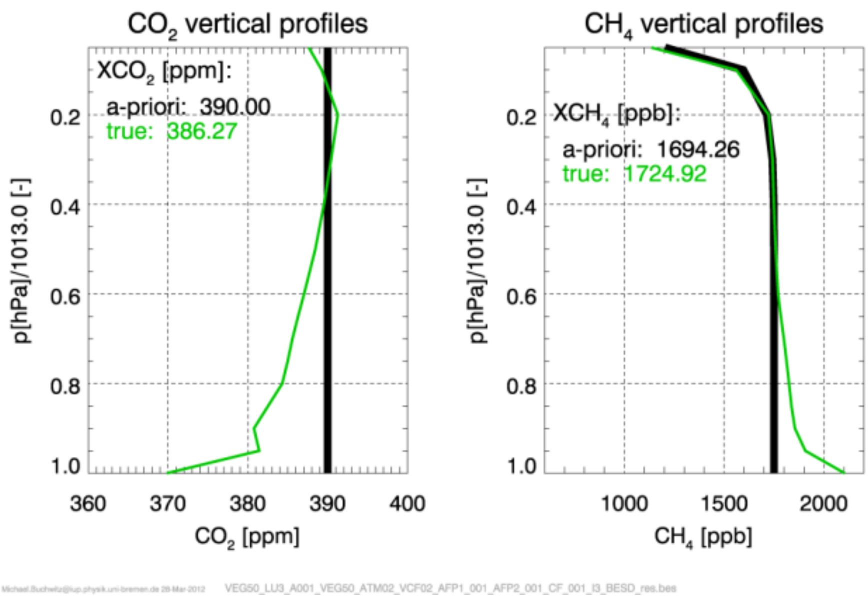

Figure 6: The two sets of CO_2 and CH_4 vertical profiles used for the assessments described in this document (black: *a priori* profiles; green: northern mid-latitude summer (MLS) profiles as used for most of the simulated satellite observations presented in this document).

Greenhouse Gas (CO_2 and CH_4) vertical profiles		
No.	**Type**	**Comment**
1	*A priori*	-
2	Perturbed	Northern hemispheric mid-latitude summer (MLS) conditions, see also **/Bovensmann et al., 2010/**

Table 1: The two sets of CO_2 and CH_4 vertical profiles used in this study. See also **Figure 6**.

4.3. Sun-Induced Fluorescence (SIF)

Four different Sun-Induced Fluorescence (SIF) / Vegetation Chlorophyll Fluorescence (VCF) emission spectra have been used for this study. They are shown in **Figure 7** (see also **Table 2**).

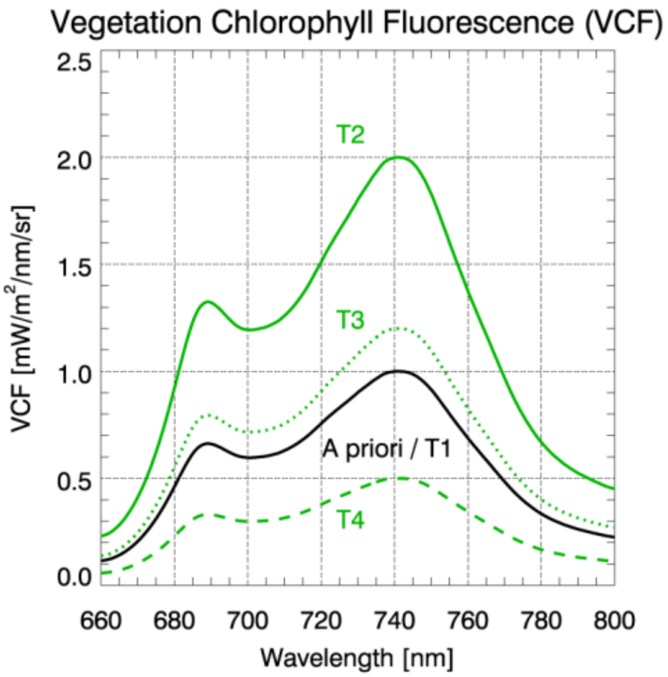

Figure 7: The four SIF/VCF emission spectra used in this study (from **/Rascher et al., 2009/**). See also **Table 2**.

Sun-Induced Fluorescence (SIF) / Vegetation Chlorophyll Fluorescence (VCF) emission spectra		
No.	**Type**	**Comment**
1	*A priori*	Peak emission: 1 mW/m^2/nm/sr @ 740 nm = 0.8 mW/m^2/nm/sr @ 755 nm
2	Perturbed (x2)	As 1 but scaled with x 2.0
3	Perturbed (x1.2)	As 1 but scaled with x 1.2
4	Perturbed (x0.5)	As 1 but scaled with x 0.5

Table 2: The four SIF/VCF emission spectra used in this study. See also **Figure 7**.

4.4. Aerosols

Five different aerosol types based on OPAC **/Hess et al., 1998/** have been used. They are summarised in **Table 3**. Note that they differ somewhat from the scenarios listed in Tab. 6 of **/Bovensmann et al., 2014/**. The main reason is that the latest version of the BESD/C retrieval algorithm use "OPAC continental average, 70% humidity" (here: No. 0) as *a priori* aerosol type.

Aerosol types		
No.	**Type**	**Comment**
0	*A priori*: OPAC continental average, 70% humidity (CA70)	Mixture: • 46% water soluble • 54% soot Humidity troposphere: 90%
1	OPAC continental clean (CC)	Mixture: • 100% water soluble Humidity troposphere: 70%
2	OPAC continental average, 90% humidity (CA90=CA)	Mixture: • 46% water soluble • 54% soot Humidity troposphere: 90%
3	OPAC continental polluted (CP)	Mixture: • 31% water soluble • 69% soot Humidity troposphere: 90%
4	OPAC desert (DE)	Mixture: • 87% water soluble • 12% mineral (nucleation mode) • 1% mineral (accumulation mode) Humidity troposphere: 70%

Table 3: The five aerosol types used in this study based on OPAC **/Hess et al., 1998/**.

Five different aerosol extinction profiles have been used and are summarised in **Table 4**. Note that the extinction profiles are only valid for 550 nm as the wavelength dependence of the extinction profiles depends on aerosol type. Note that the AODs differ somewhat from the values listed in Tab. 6 of **/Bovensmann et al., 2014/**. The main reason is that the *a priori* profile as used in the latest version of the BESD/C retrieval algorithm has changed.

Aerosol extinction vertical profiles (550 nm)		
No.	**Type**	**Comment**
1	*A priori*	AOD: 0.200
2	Enhanced in BL: x2.0 in 0-2 km	AOD: 0.305
3	Enhanced in BL: x1.5 in 0-2 km	AOD: 0.252
4	Reduced in BL: x0.5 in 0-2 km	AOD: 0.174
5	Reduced in BL: x0.2 in 0-2 km	AOD: 0.111

Table 4: The five aerosol extinction profiles and corresponding AODs (at 550 nm) as used in this study. BL = Boundary Layer.

4.5. Cirrus clouds

Six different cirrus clouds have been defined for this study and they are summarised in **Table 5** shown below.

Cirrus clouds		
No.	**Cloud Optical Depth (COD) [-]**	**Cloud Top Height (CTH) [km]**
1	*A priori*: 0.05	*A priori*: 10.0
2	0.10	10.0
3	0.20	10.0
4	0.20	8.0
5	0.02	12.0
6	0.05	9.0

Table 5: The six cirrus clouds defined for this study.

4.6. Summary geophysical scenarios

Fifteen different geophysical scenarios have been defined using different combinations of the parameters described in the previous sub-sections. They are presented in **Table 6**.

Note that XCO_2 is 390.00 ppm for GHG vertical profile No. 1 (XCH_4: 1694.26 ppb) and 386.27 ppm for No. 2 (XCH_4: 1724.92) (see **Figure 6**).

Overview Geophysical Scenarios					
No.	**GHG vertical profiles**	**VCF**	**Aerosol type**	**Aerosol extinction**	**Cirrus**
1	1 (~constant)	1	1 (clean, CC)	1	1 (COD 0.05 / 10 km)
2	2 (mid-lat.summer)	1	1	1	1
3	2	2 (x2.0)	1	1	1
4	1	2	1	1	1
5	2	3 (x1.2)	1	1	1
6	2	3	1	2 (x2.0)	1
7	2	3	1	2	2 (0.1)
8	2	3	1	2	3 (0.2)
9	2	3	1	2	4 (0.2 / 8 km)
10	2	3	2 (average, CA90)	2	4
11	2	3	3 (polluted, CP)	2	4
12	2	3	4 (desert, DE))	3 (x1.5)	5 (0.02 / 12 km)
13	2	4 (x0.5)	4	4 (x0.5)	5
14	2	1	1	5 (x0.2)	1
15	2	1	1	4	6 (9 km)

Table 6: The 15 geophysical scenarios defined for this study.

5. Instrument configurations

An overview of the 4 instrument configurations A, B, C and D, which have been investigated in this study, is given in **Table 7.**

Spectra for instrument B for scenario s01 are shown in **Figure 5**. The corresponding spectra for instruments A, C, and D are shown in **Figure 8**, **Figure 9**, and **Figure 10**, respectively.

Radiance ratios for all scenarios w.r.t. one reference scenario (s01) are shown in **Figure 11** (instrument A) to **Figure 14** (instrument D).

Instrument concept	Band	Spectral range [nm]	Spectral resolution FWHM [nm]	Continuum SNR [-]	SSR (per FWHM)	Comment
A	NIR SW1 SW2	756-773 1559-1675 2043-2095	0.045 0.3 0.13	622 949 167	2.5 2.5 2.5	Similar as CS MRDv1.0 except SNR
B	NIR SW1 SW2	747-773 1590-1675 1925-2095	0.1 0.3 0.55	872 823 431	3.1 3.1 3.3	Similar as CS MRDv1.2 except SNR
C	NIR SW1 SW2	758-772 1591-1621 2042-2081	0.042 0.076 0.097	405 385 170	2.5 2.5 2.5	Similar as OCO-2
D	NIR SW1 SW2	758-769 1597-1619 2023-2051	0.032 0.067 0.085	190 160 61	2.9 2.9 2.9	Similar as MicroCarb

Table 7: The four instrument configurations investigated w.r.t. XCO_2 data quality. SSR is the Spectral Sampling Ratio = FWHM/SSI, where FWHM is the “Full Width Half Maximum” of the satellite Instrument Spectral Response Function (ISRF). The Signal-to-Noise Ratios (SNRs) are valid for the following radiances (given in photons/s/cm^2/nm/sr): NIR: 2x10^{13}, SW1: 4x10^{12}, SW2: 9.1x10^{11}. The instrument parameters are from **/Landgraf et al., 2017b/**.

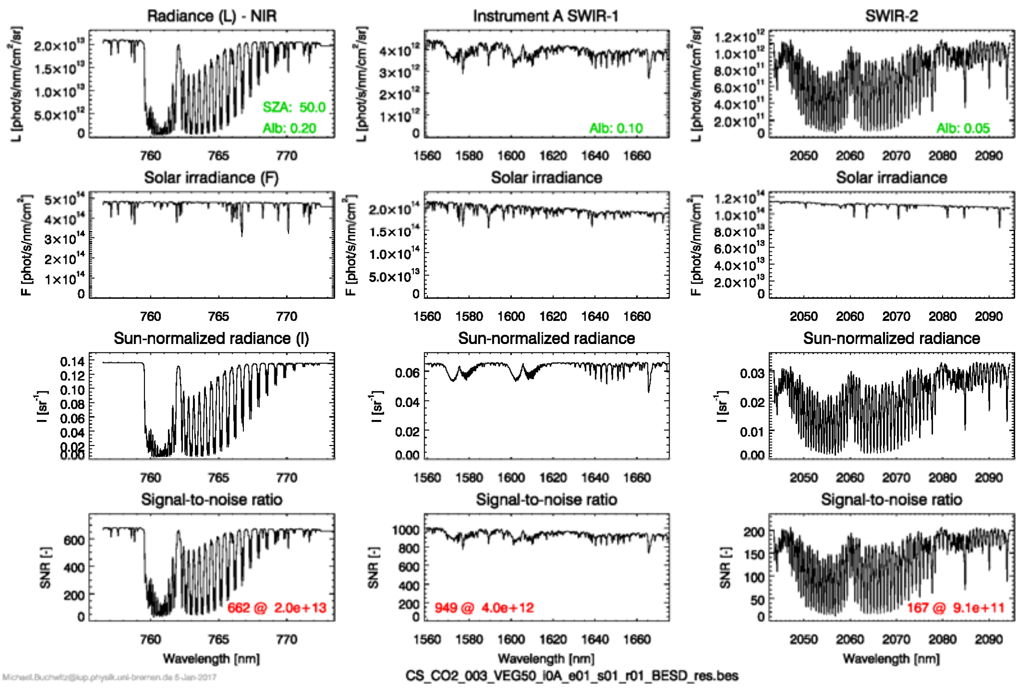

Figure 8: As **Figure 5** but for instrument A.

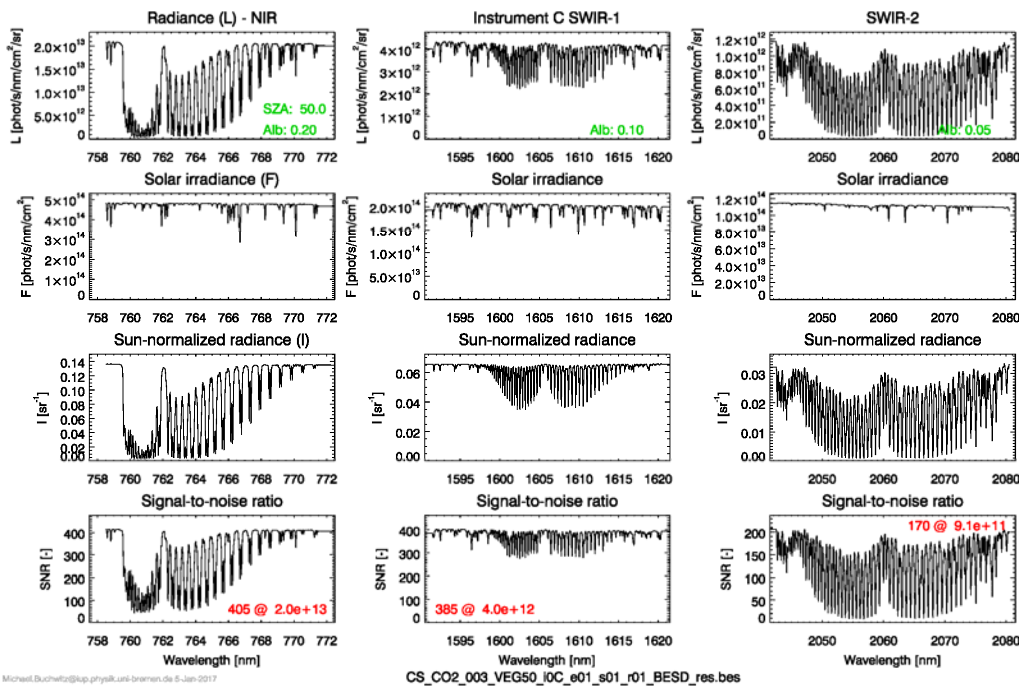

Figure 9: As **Figure 5** but for instrument C.

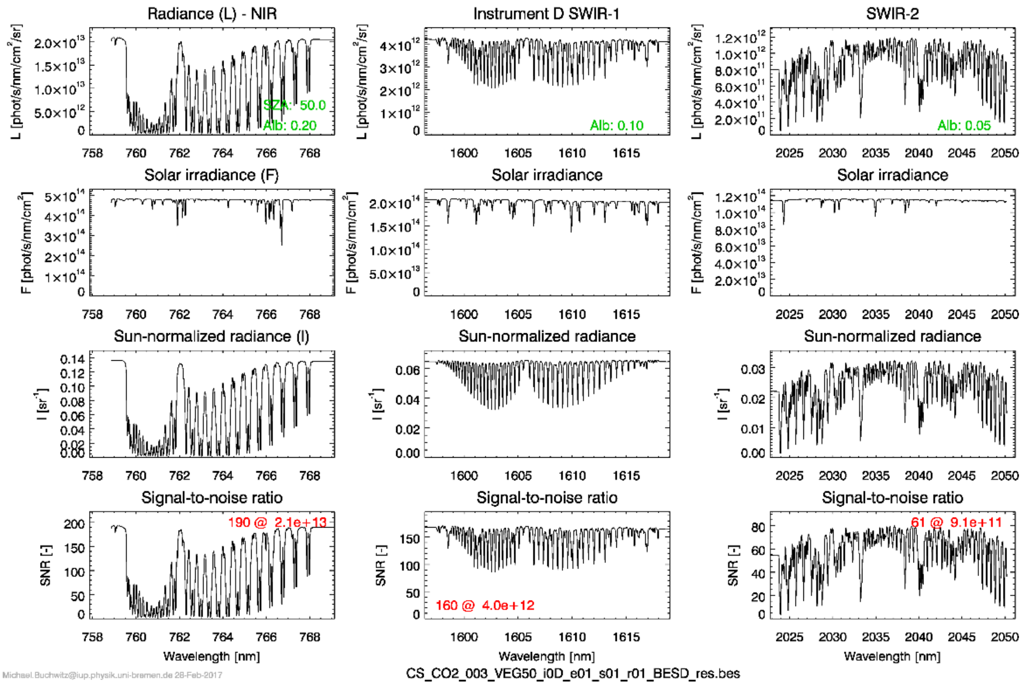

Figure 10: As **Figure 5** but for instrument D.

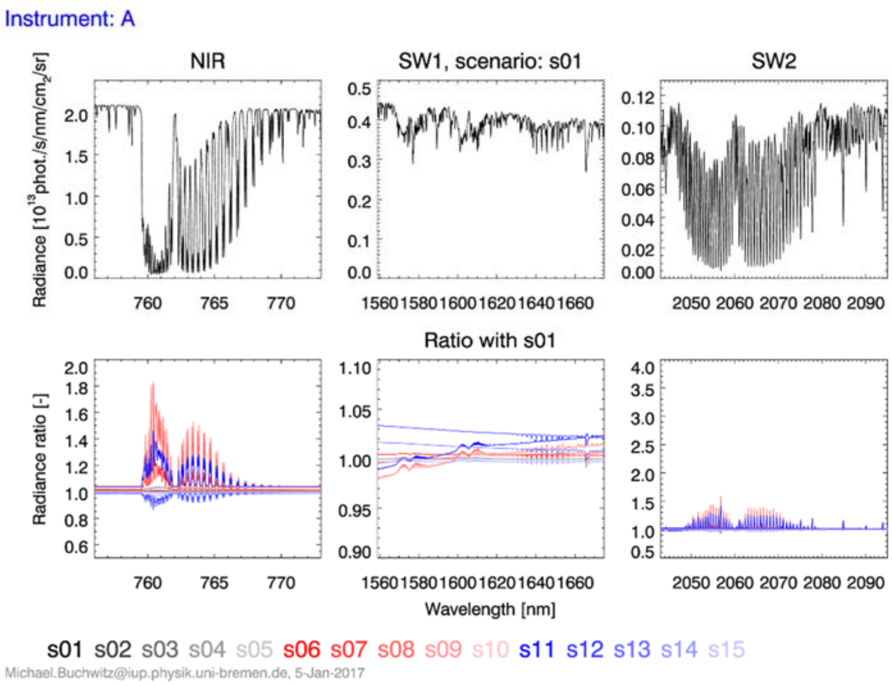

Figure 11: Radiance of scenario s01 for instrument A (top) and radiance ratios of scenarios s02 to s15 w.r.t. s01 (bottom).

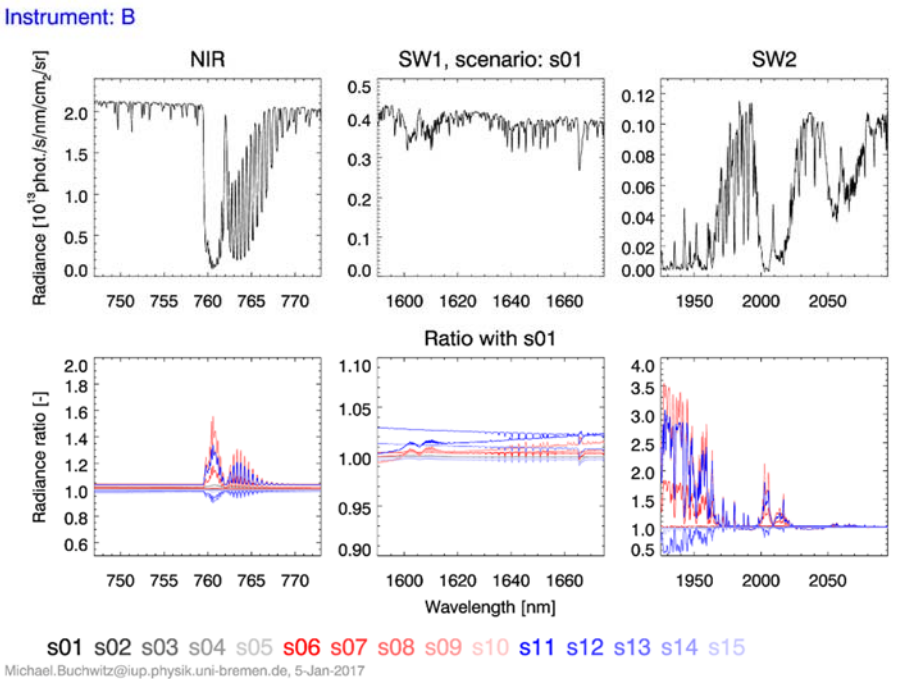

Figure 12: As **Figure 11** but for instrument B.

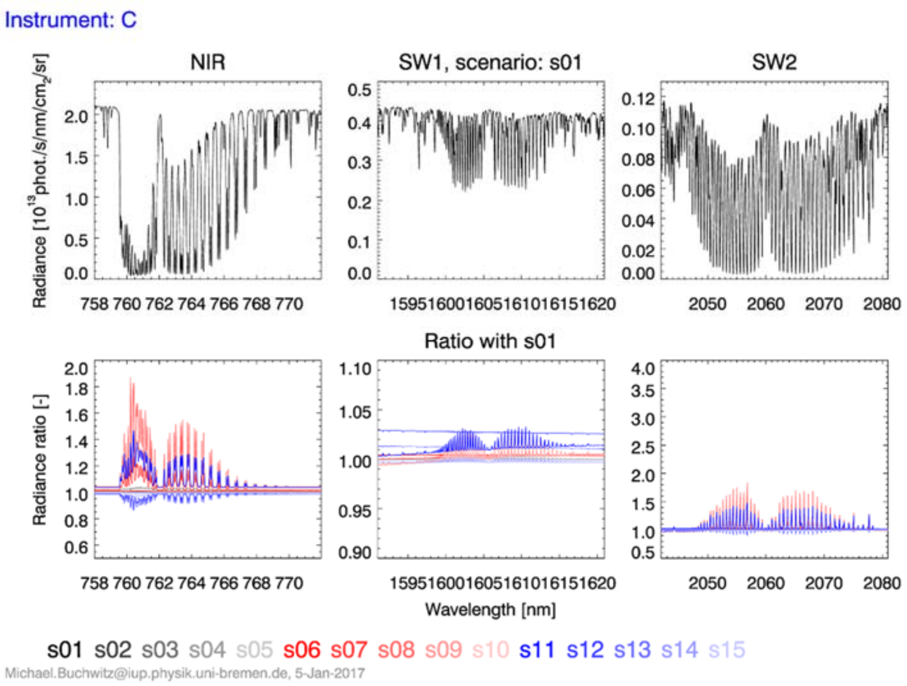

Figure 13: As **Figure 11** but for instrument C.

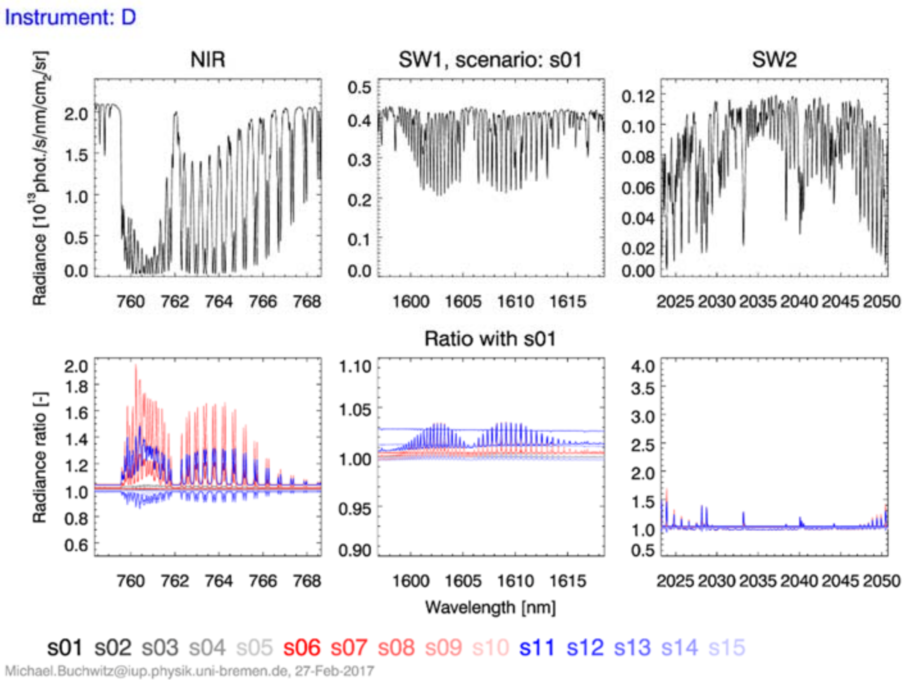

Figure 14: As **Figure 11** but for instrument D.

6. XCO_2 retrieval results ("Iterative abs.")

In this section, the XCO_2 retrieval results are presented for the described 4 instruments (= 4 different spectral sizing points). For each instrument the XCO_2 random and systematic retrieval error has been determined by applying the BESD/C retrieval algorithm to simulated radiances corresponding to the 15 selected scenarios.

The assessment method and results as presented in this section are referred to as **"Iterative abs."** in this document (i.e., absolute XCO_2 biases are presented and discussed originating from application of the iterative BESD/C algorithms to radiance spectra "with errors").

Additional assessment results are presented and explained in Sect. 7, which are referred to as "Iterative diff." and "Linearization" in this document.

6.1. Error source: Instrument noise and geophysical error (GEO)

In this section XCO_2 systematic and random errors are shown for the four instruments (= four spectral sizing points) assuming no systematic instrument related radiance errors.

The single measurement XCO_2 random error - or 1-sigma retrieval precision due to instrument noise - has been computed via the BESD/C retrieval method essentially by mapping the random error of the radiance (i.e., the noise) onto the random error (uncertainty, scatter) of the retrieved XCO_2. This error depends primarily on the radiance noise but to some extent also on the retrieval algorithm.

The retrieved XCO_2 also (typically) has a systematic error or bias. This error is computed as "retrieved – true". Note that the retrieval algorithm is typically not able to provide error free XCO_2 retrievals especially if the scenario used for the generation of the simulated observation does not correspond to the *a priori* assumptions used for the retrieval algorithm (e.g., w.r.t. aerosol type). Note that this is the case for all 15 scenarios (i.e., at least one parameter chosen for the selected scenarios differs from the retrieval assumptions). This source of systematic error – which is present even for error-free radiance spectra - is referred to as "geophysical error" in this document. Note that the bias would typically differ from zero even if the simulated observation would be fully consistent with the *a priori* assumption as some bias typically also originates from the pre-processing algorithms (e.g., surface albedo retrieval).

Before the error analysis results are shown and discussed the BESD/C Jabobian matrix is shown in
Figure 15 for instrument A, in
Figure 16 for instrument B, in
Figure 17 for instrument C and in
Figure 18 for instrument D.

The Jacobians show the change of the radiance due to a change of a retrieval state vector element. The state vector elements are (from bottom to top); CO_2 (3 layers), CH_4 (3 layers), surface pressure (PRE), Vegetation Chlorophyll Fluorescence (VCF or SIF), temperature (TEM), H_20, 2 aerosol parameters, one water cloud parameter (WOD), two cirrus clouds parameters, albedo (3 parameters), low order polynomial coefficients (9 parameter), spectral squeeze (3 parameters), spectral shift (3 parameters) and zero level offset (3 parameters).

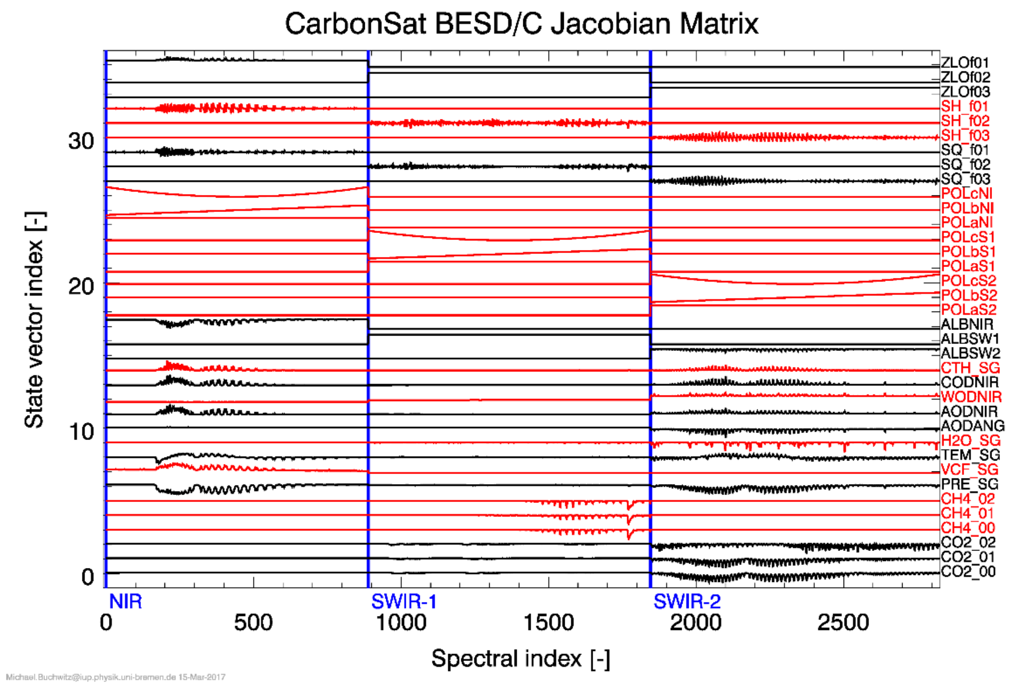

Figure 15: BESD/C Jabobian matrix for instrument A.

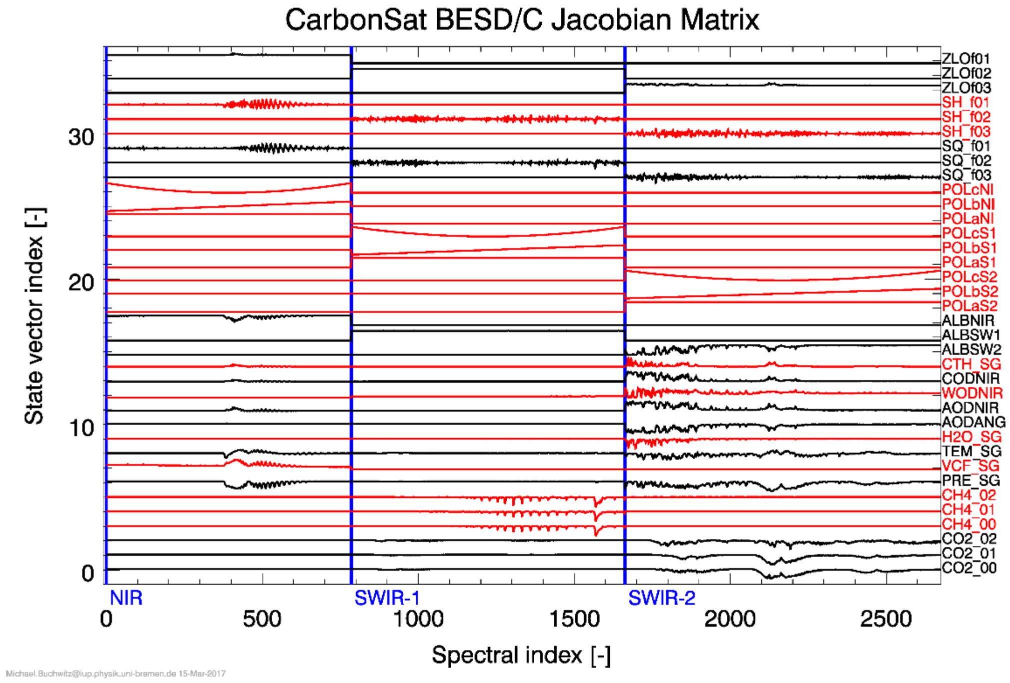

Figure 16: BESD/C Jabobian matrix for instrument B.

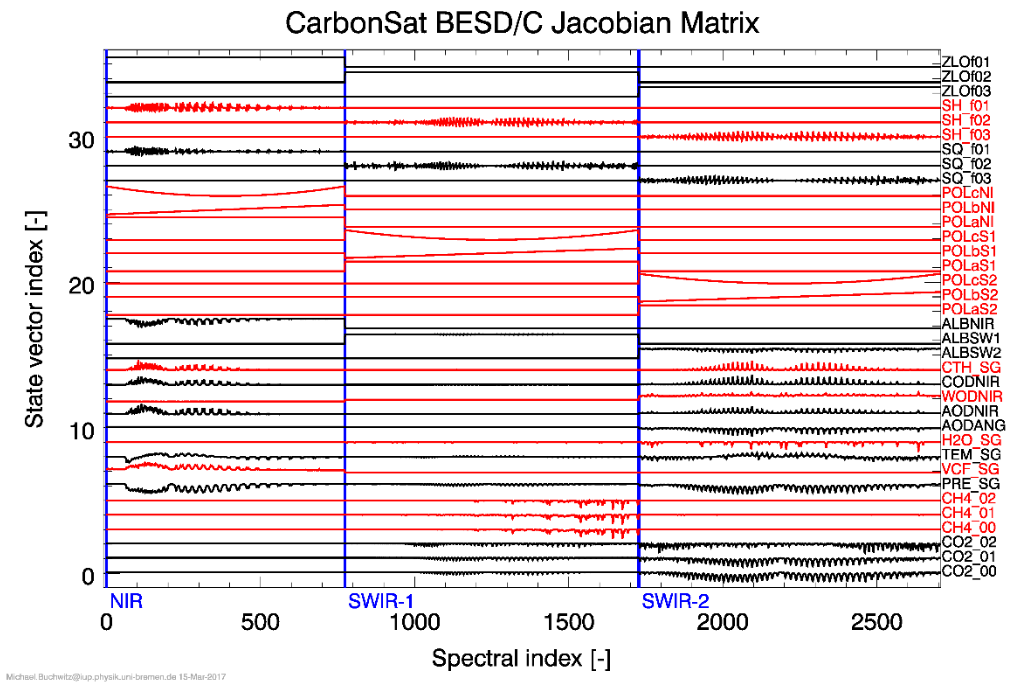

Figure 17: BESD/C Jabobian matrix for instrument C.

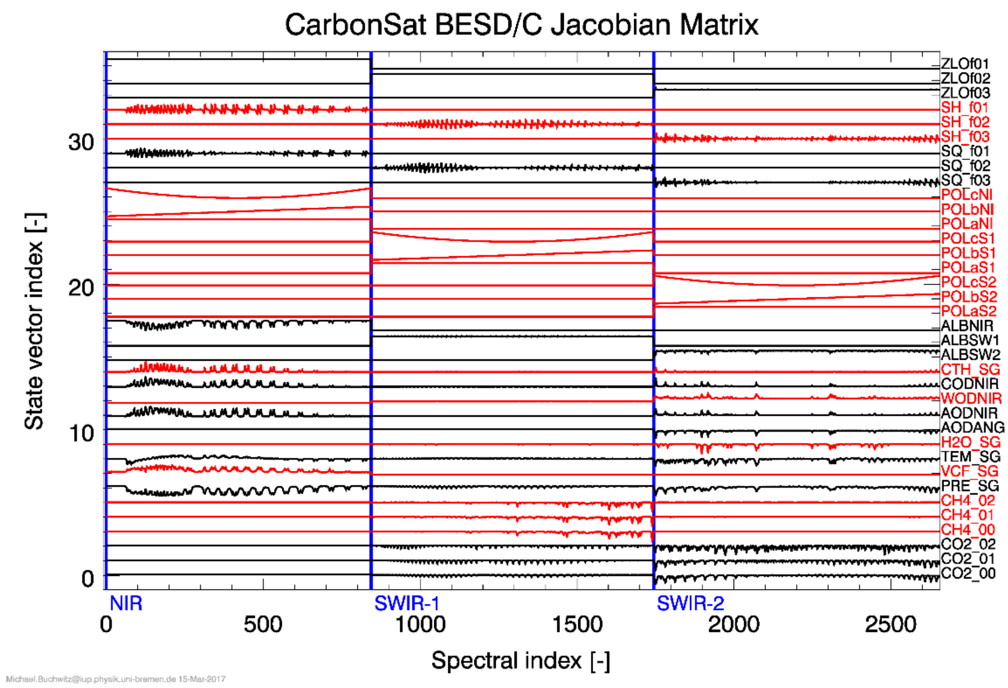

Figure 18: BESD/C Jabobian matrix for instrument D.

Figure 19 shows the error analysis results. As can be seen (top panel), the systematic XCO_2 error depends on the scenario and on the instrument, as expected.

For each instrument three numbers have been computed to characterise systematic errors, namely the mean error (mean bias), the standard deviation of the bias and the root mean square error (RMSE) (or root mean square bias), and the corresponding values are shown on the right hand side.

As can also be seen, instrument B has the smallest XCO_2 bias (in terms of all three metrics) and the smallest XCO_2 random error (i.e., the best precision).

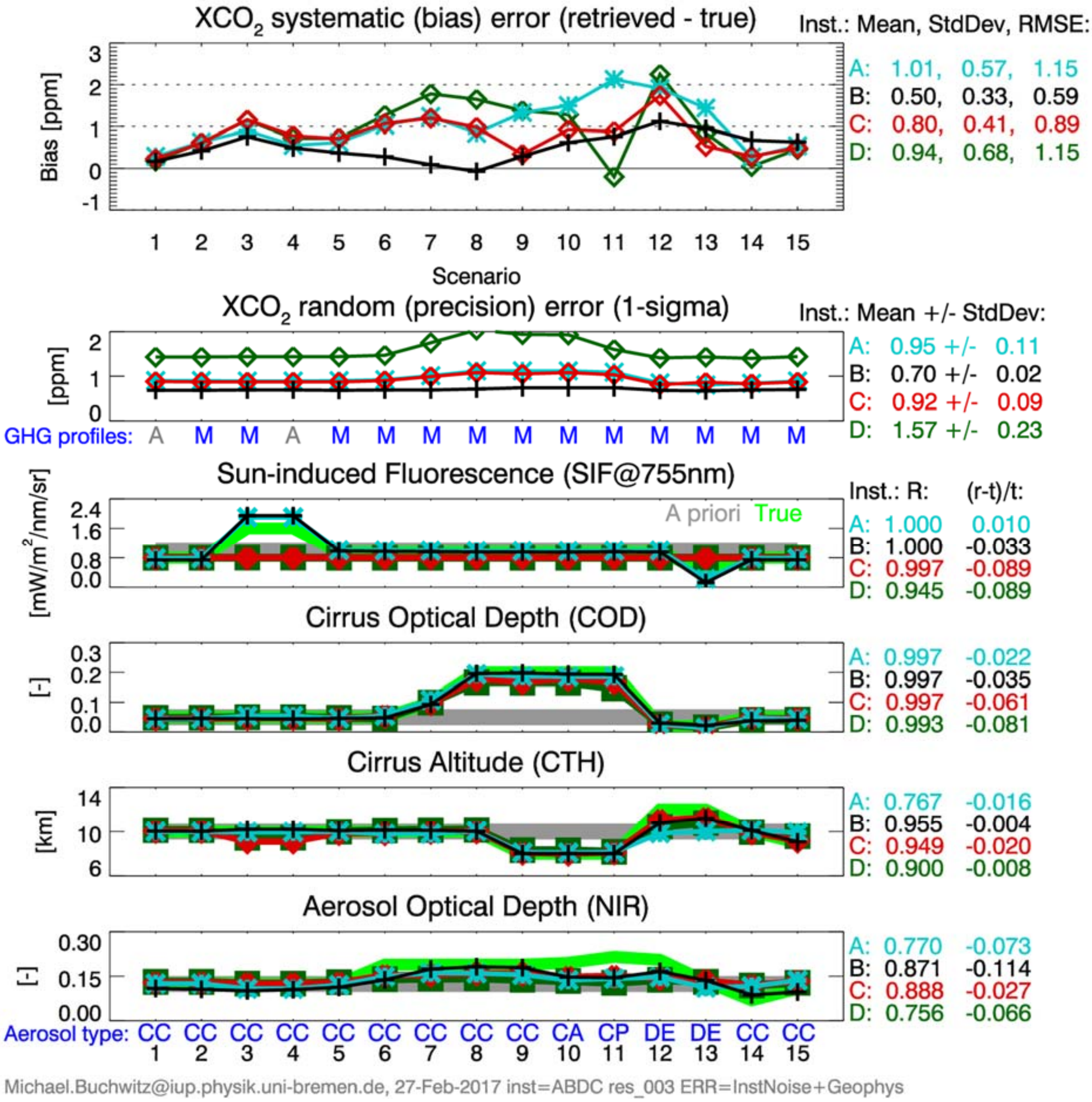

Figure 19: Top panel: XCO_2 systematic error as a function of scenario for the four instruments. In the line below it is listed which GHG profiles have been used (A = *a priori*; M = mid-latitude summer (MLS)). Listed on the right is the mean bias, the standard deviation of the bias and the root-mean-square-error (RMSE). Panel below: As top panel but for XCO_2 random error. Listed on the right is the mean precision and its standard deviation. Following 4 panels: A priori values (grey), true values (green) and retrieved values (for the 4 instruments) for the following 4 parameters: SIF, COD, CTH, AOD(NIR). Listed on the right is the linear correlation coefficient between the retrieved and the true parameters and the mean value of the relative difference ((retrieved-true)/true). At the bottom it is shown which aerosol type has been used for each scenario (note that the *a priori* type is Continental Average (CA)).

6.1. Additional error source: Zero-level-offset (ZLO)

In this section error source “Zero-Level-Offset” (ZLO) has been investigated by adding to each spectral channel the following radiances (see Sect. 1.5 of **/Landgraf et al., 2017b/**):

- NIR: 4.2×10^9 photons/s/nm/cm^2/sr
- SW1: 4.3×10^9 photons/s/nm/cm^2/sr
- SW2: 5.3×10^8 photons/s/nm/cm^2/sr

These radiometric offsets have been added to the radiances as computed for each instrument and each scenario for the e01 simulations and the BESD/C retrieval algorithm has been applied to these radiances.

The retrieval results are shown in **Figure 20**.

As can be seen from **Figure 20** (top panel), instrument B has the smallest XCO_2 bias (in terms of all three metrics) and the smallest XCO_2 random error (best precision).

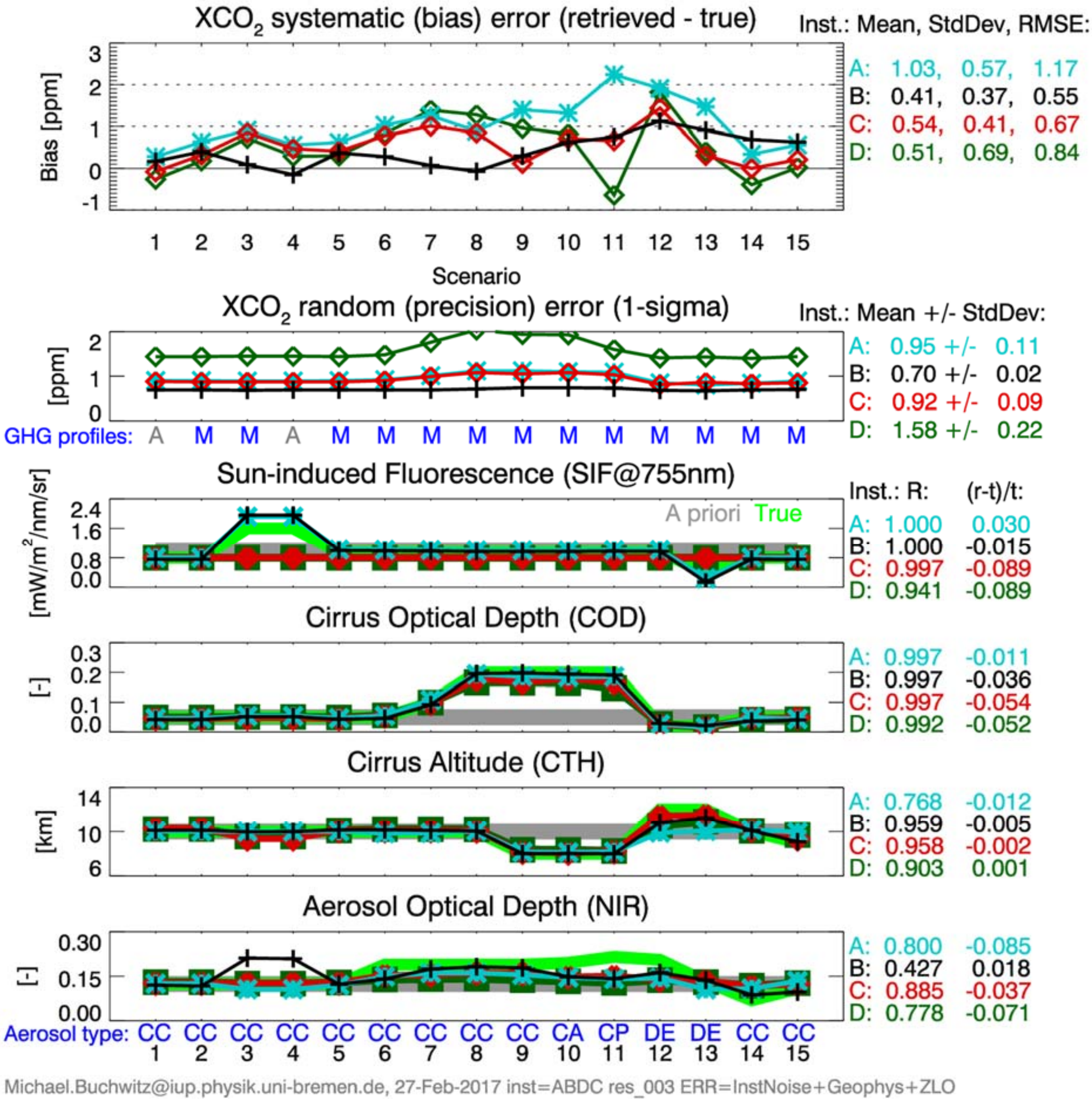

Figure 20: As
Figure 19 but also considering ZLO as an additional error contribution.

6.2. Additional error source: ISRF distortion (ISRF)

In this section error source "Instrument Spectral Response Function distortion" (ISRF distortion) has been investigated by computing simulated radiance observations using ISRF anti-symmetrical distortion No. 3 and symmetrical distortion No. 1 as given in Sect. 1.2 of **/Landgraf et al., 2017b/** (see **Figure 21**).

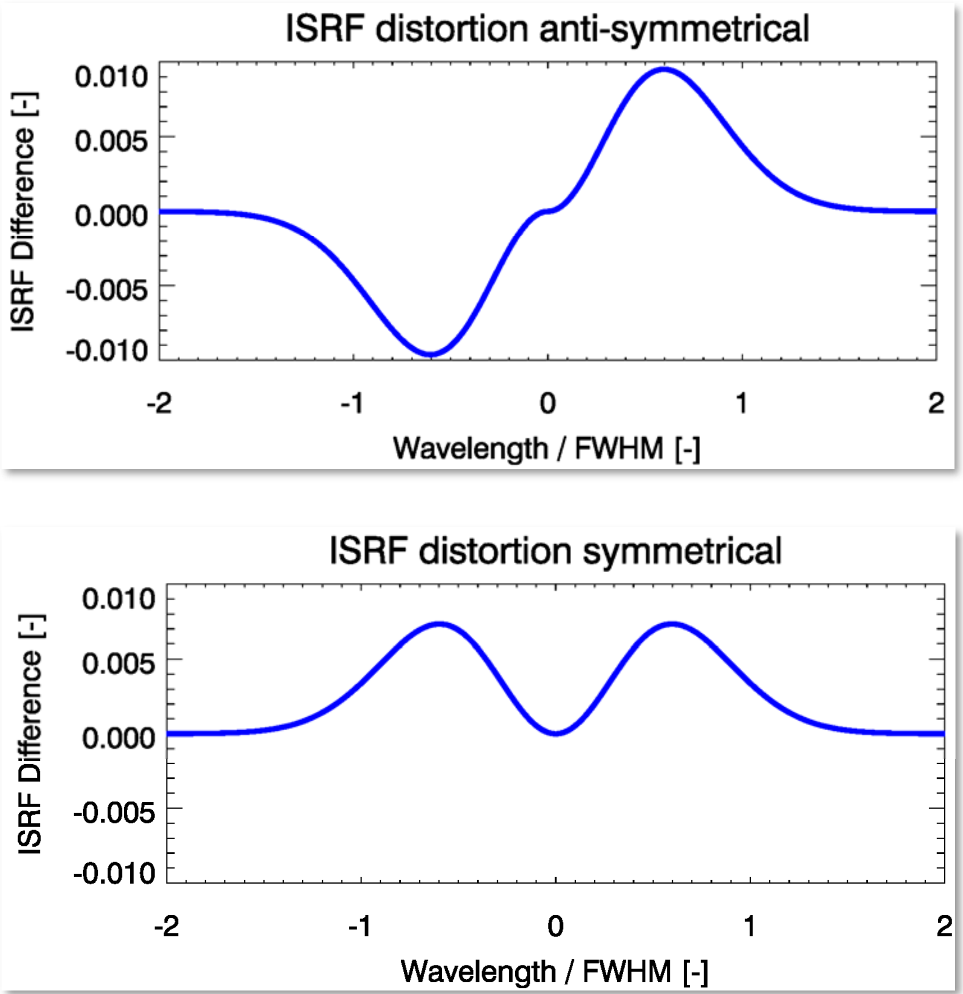

Figure 21: Illustration of ISRF distortion No. 3 (top, anti-symmetrical) and No. 1 (bottom, symmetrical). Source: **/Landgraf et al., 2017b/**.

The retrieval results for the anti-symmetrical ISRF distortion are shown in **Figure 22**. As can be seen from **Figure 22** (top panel), instrument B has the smallest XCO_2 bias (in terms of all three metrics) (but StdDev is identical for instrument A) and the smallest XCO_2 random error (best precision).

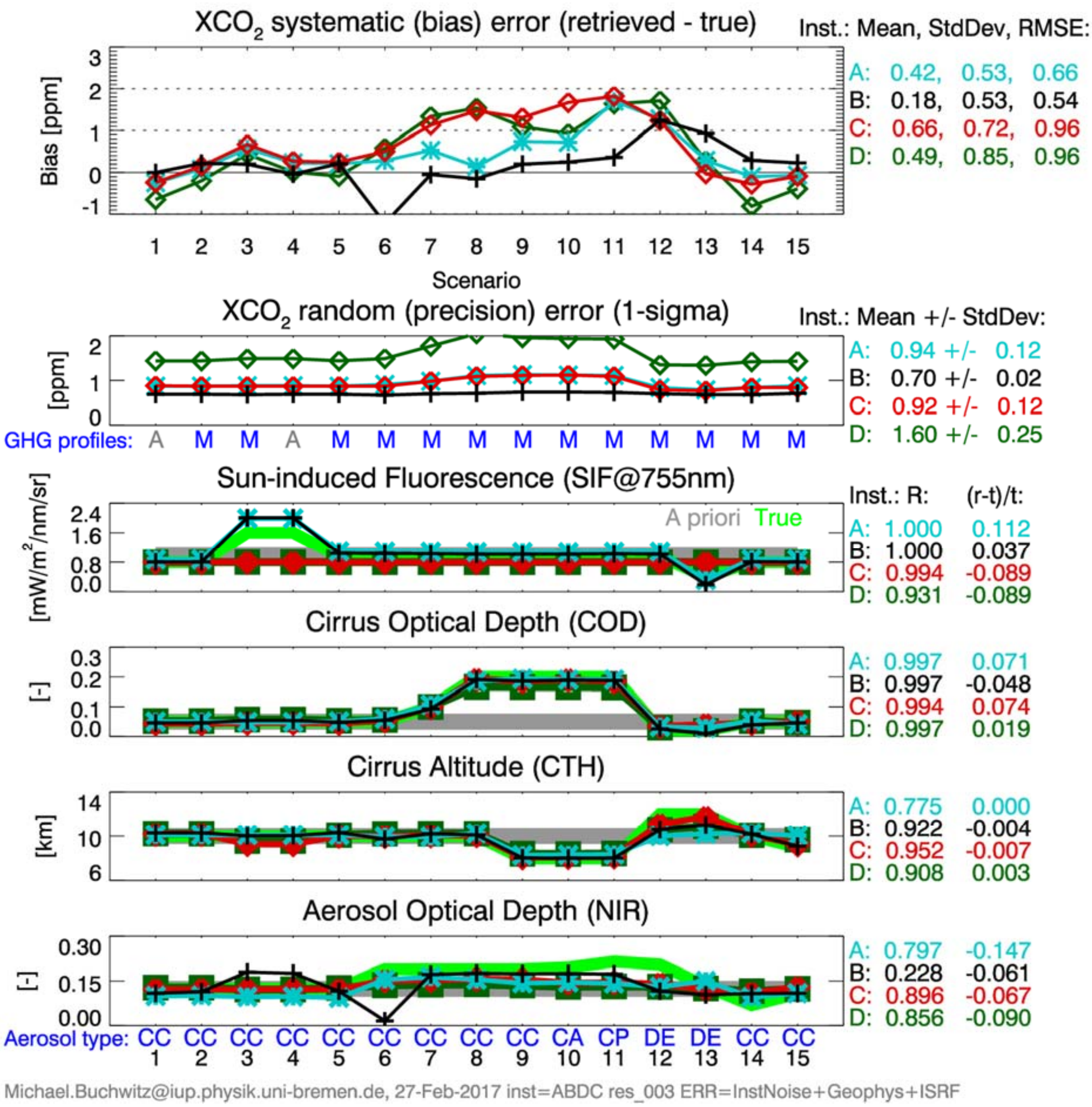

Figure 22: As
Figure 19 but also considering anti-symmetrical ISRF distortions as additional error contributions.

The retrieval results for the symmetrical ISRF distortion are shown in **Figure 23**. As can be seen from **Figure 23** (top panel), instrument B has the smallest XCO_2 mean bias and RMSE and instrument A has the smallest standard deviation of the bias. Instrument B has the smallest XCO_2 random error (best precision).

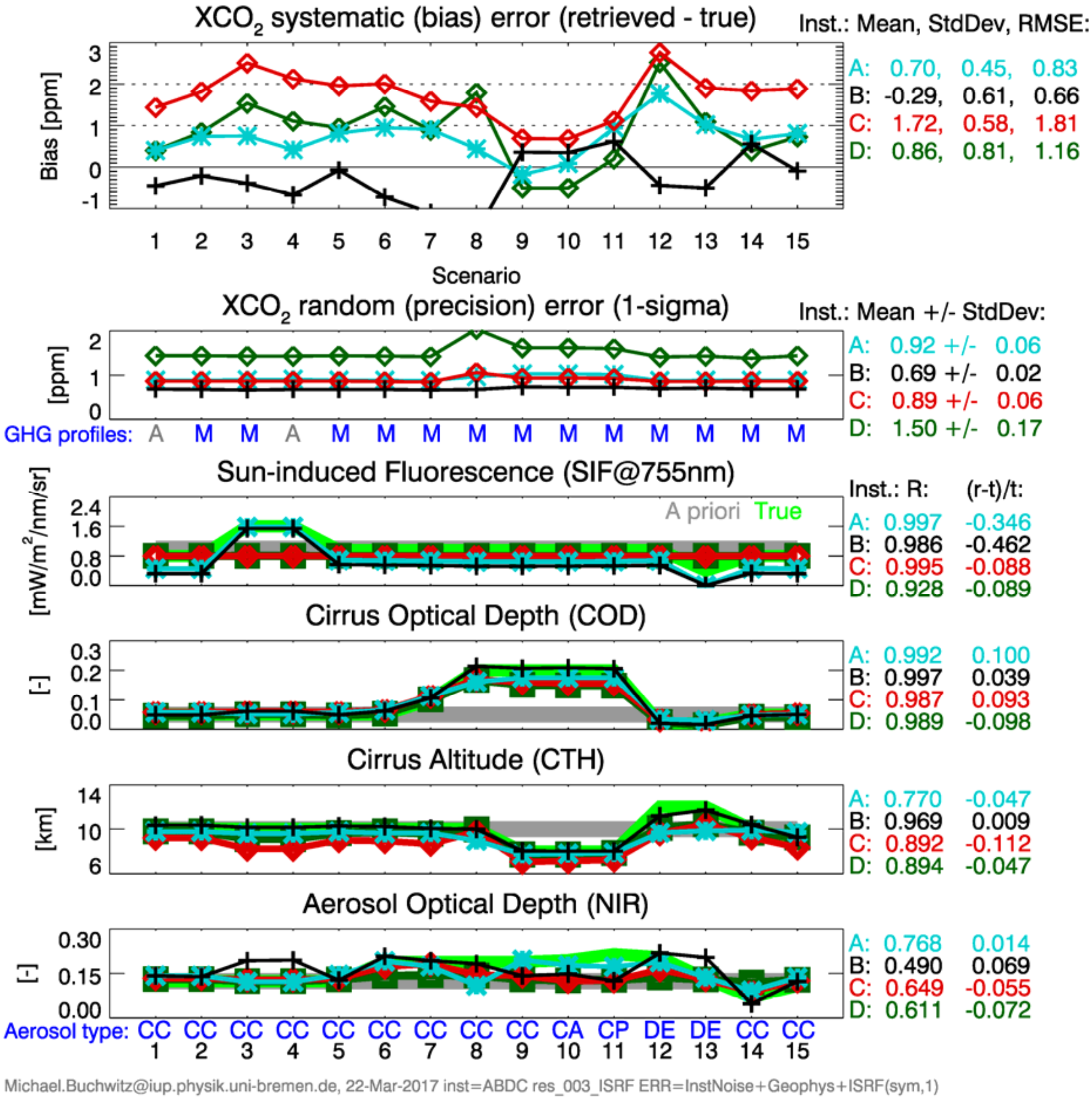

Figure 23: As
Figure 19 but also considering symmetrical ISRF distortions as additional error contributions.

6.3. Additional error source: Detector non-linearity (NL)

In this section error source “Detector non-linearity” (NL) has been considered for the simulated retrievals by using the radiance dependent systematic errors as specified in **/Landgraf et al., 2017b/** (see **Figure 24**).

(a) Detector non-linearity for SWIR-1 and instruments A and B

(b) Detector non-linearity for SWIR-2 and instruments A and B

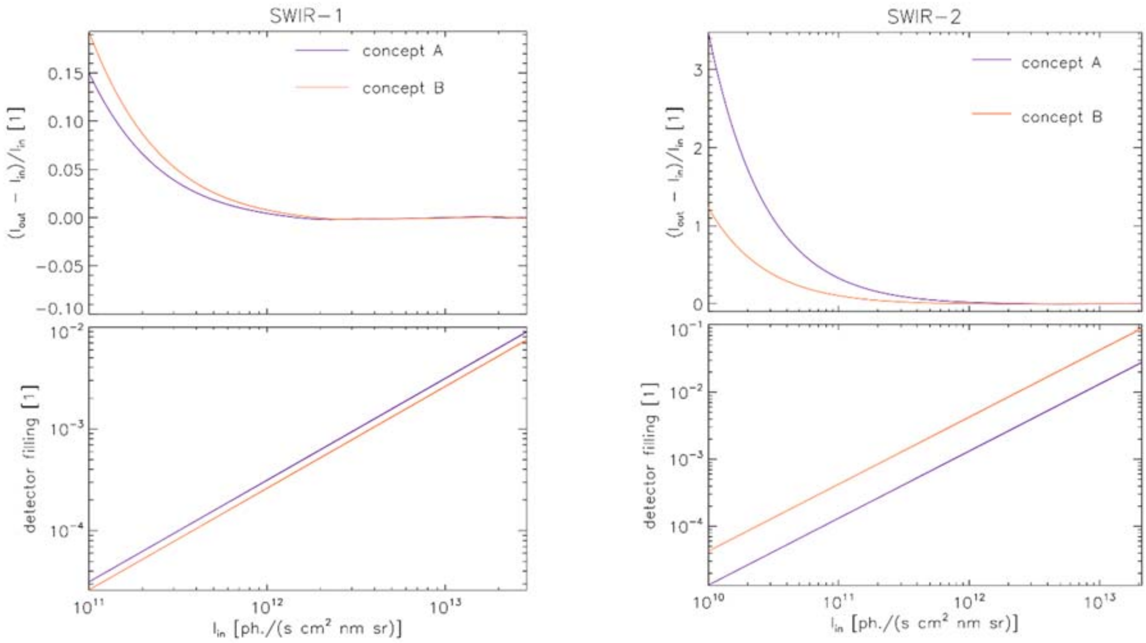

Figure 24: Detector non-linearity for the SWIR-1 (a) and SWIR-2 (b) bands for instruments A and B (source: **/Landgraf et al., 2017b/**).

These errors have been used to modify the radiances as computed for each instrument and each scenario for the e01 simulations and the BESD/C retrieval algorithm has been applied to these radiances.

The spectral dependence of the error is shown in **Figure 25**.

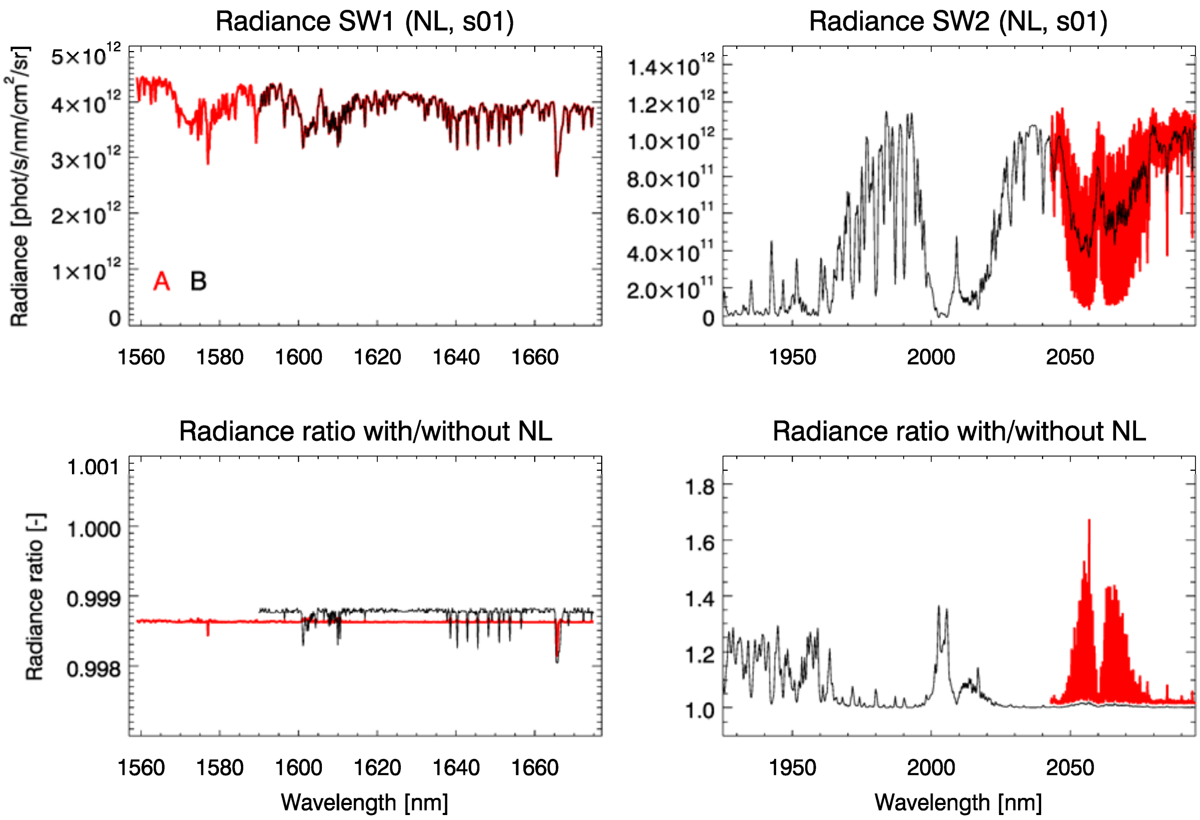

Figure 25: Radiance spectra (top) and radiance ratios (bottom) for the SWIR-1 (left) and SWIR-2 (right) bands for instrument A (red) and B (black), where ratio is the radiance ratio for a radiance with and without non-linearity error.

The retrieval results are shown in
Figure 26.

As can be seen from
Figure 26 (top panel), instrument B has the smallest XCO_2 bias (in terms of all three metrics) and the smallest XCO_2 random error (best precision).

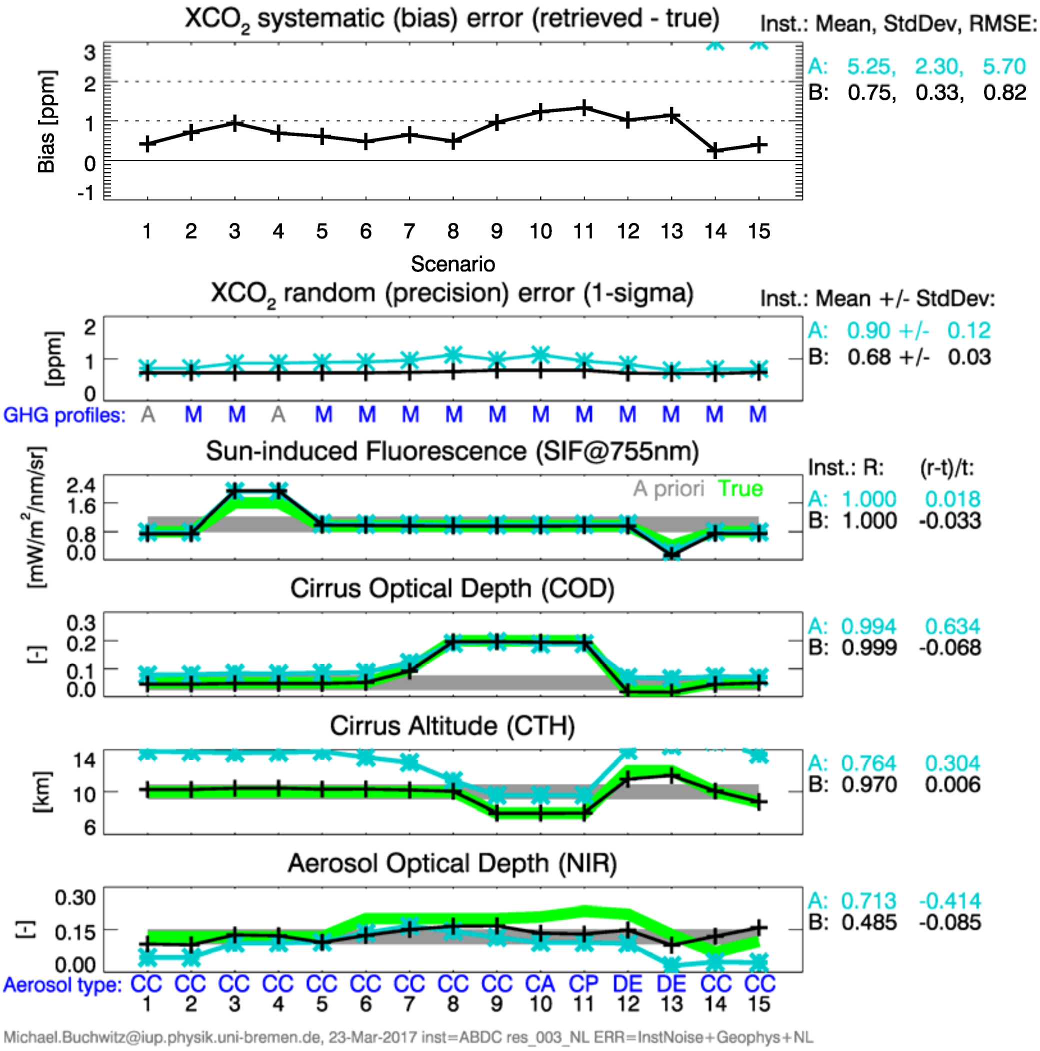

Figure 26: As
Figure 19 but also considering detector non-linearity as an additional error contribution.

6.4. Additional error source: Polarization (POL)

In this section error source “Polarization” (POL) has been considered for the simulated retrievals by using the radiance dependent systematic errors as specified in **/Landgraf et al., 2017b/**. Radiance errors *δI* (see **/Landgraf et al., 2017b/**) are assumed to result from an instrument, which is not perfectly polarization insensitive, i.e., from instrument Mueller matrix elements *M01* and *M02*, which are not zero:

$$\delta I = M01/M00 * Q + M02/M00 * U \qquad \text{Eq. 1}$$

Here *M01, M00* and *M02* are wavelength dependent instrument Mueller Matrix elements (see **Figure 27**) and *Q* and *U* are radiance Stokes vector elements (i.e., differences of radiance spectra). For the results shown in this section radiances *Q*, *U* and *I* have been calculated with the radiative transfer model SCIATRAN (version 3.4) **/Rozanov et al., 2014/** assuming a polarizing vegetation surface. The Mueller matrix elements correspond to parameters ACT field = 8.584° and ALT field = 0.208°.

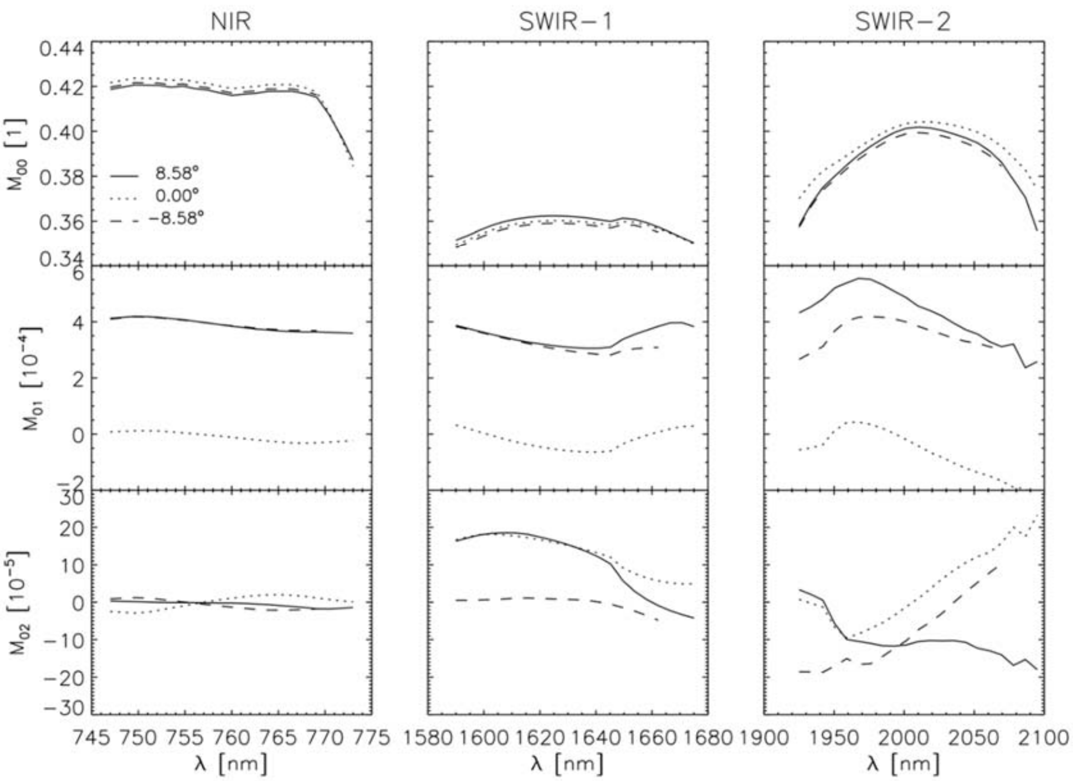

Figure 27: Instrument Mueller matrix elements (source: **/Landgraf et al., 2017b/**).

The polarization related errors have been used to modify the radiances as computed for each instrument and each scenario for the e01 simulations and the BESD/C retrieval algorithm has been applied to these radiances.

The spectral dependence of the radiance error is shown in
Figure 28 -
Figure 30 for the three bands. It can be seen that - as expected (see **Figure 27**) - the radiance errors are very small, on the order of 10^{-4} for the NIR band, essentially zero for the SWIR-1 band and on the order of 10^{-3} for the blue part of the SWIR-2 band.

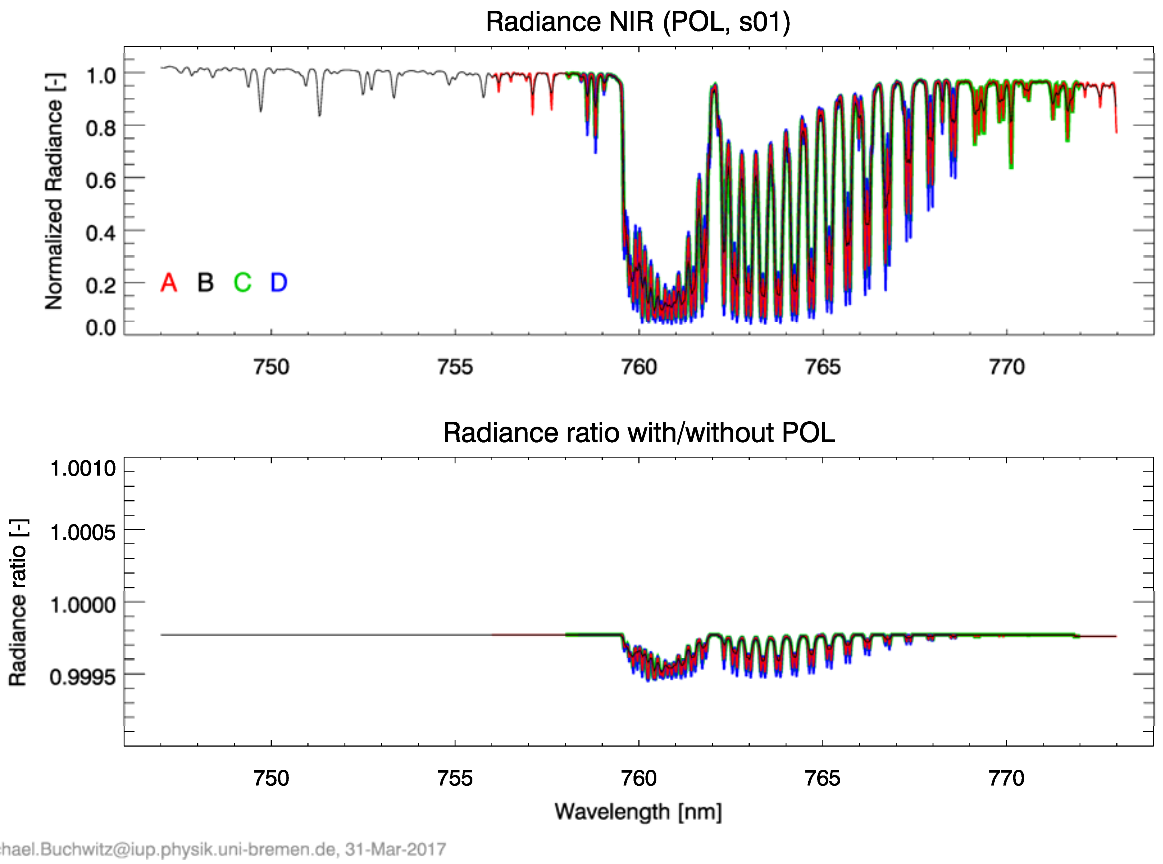

Figure 28: Radiance spectra in the NIR band of all four instruments (top) and ratios of radiance spectra (bottom) for radiances with and without adding radiance polarization error *δI* (see Eq. 1).

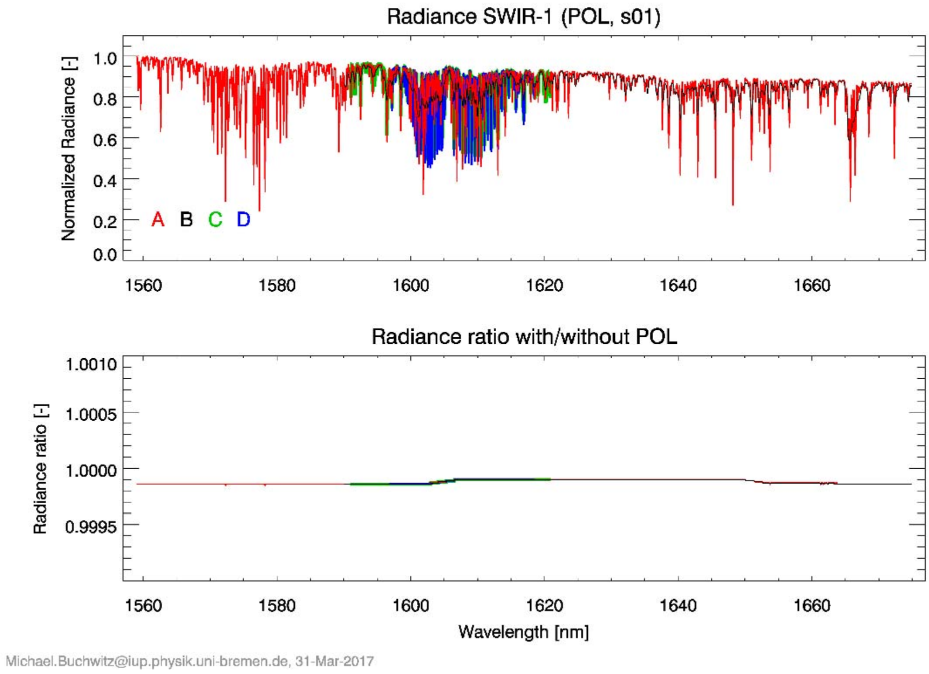

Figure 29: As
Figure 28 but for the SWIR-1 band.

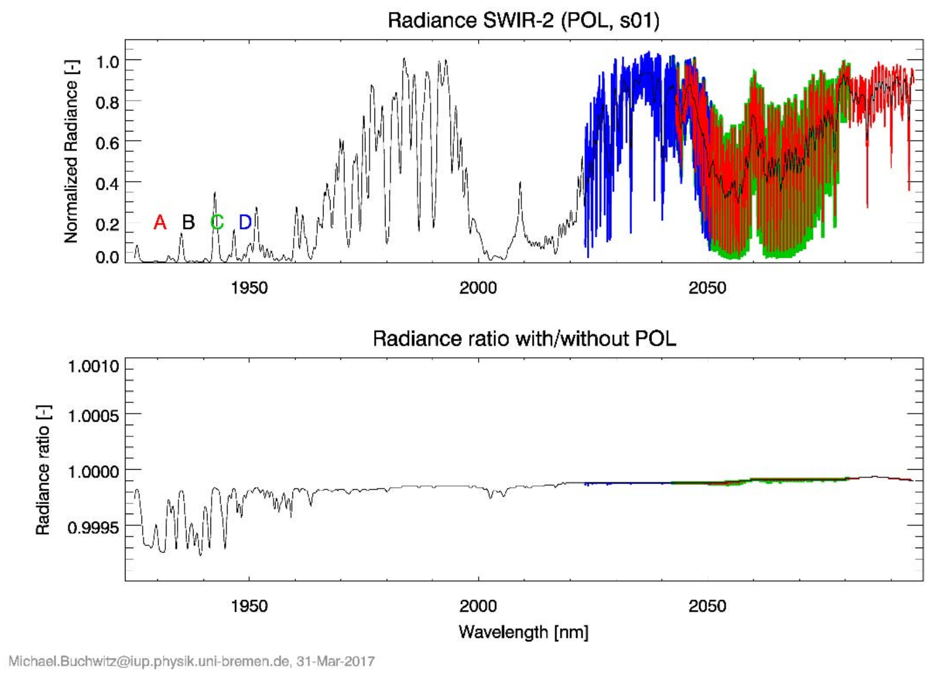

Figure 30: As
Figure 28 but for the SWIR-2 band.

The retrieval results are shown in
Figure 31.

As can be seen from
Figure 31 (top panel), instrument B has the smallest XCO_2 bias (in terms of all three metrics) and the smallest XCO_2 random error (best precision).

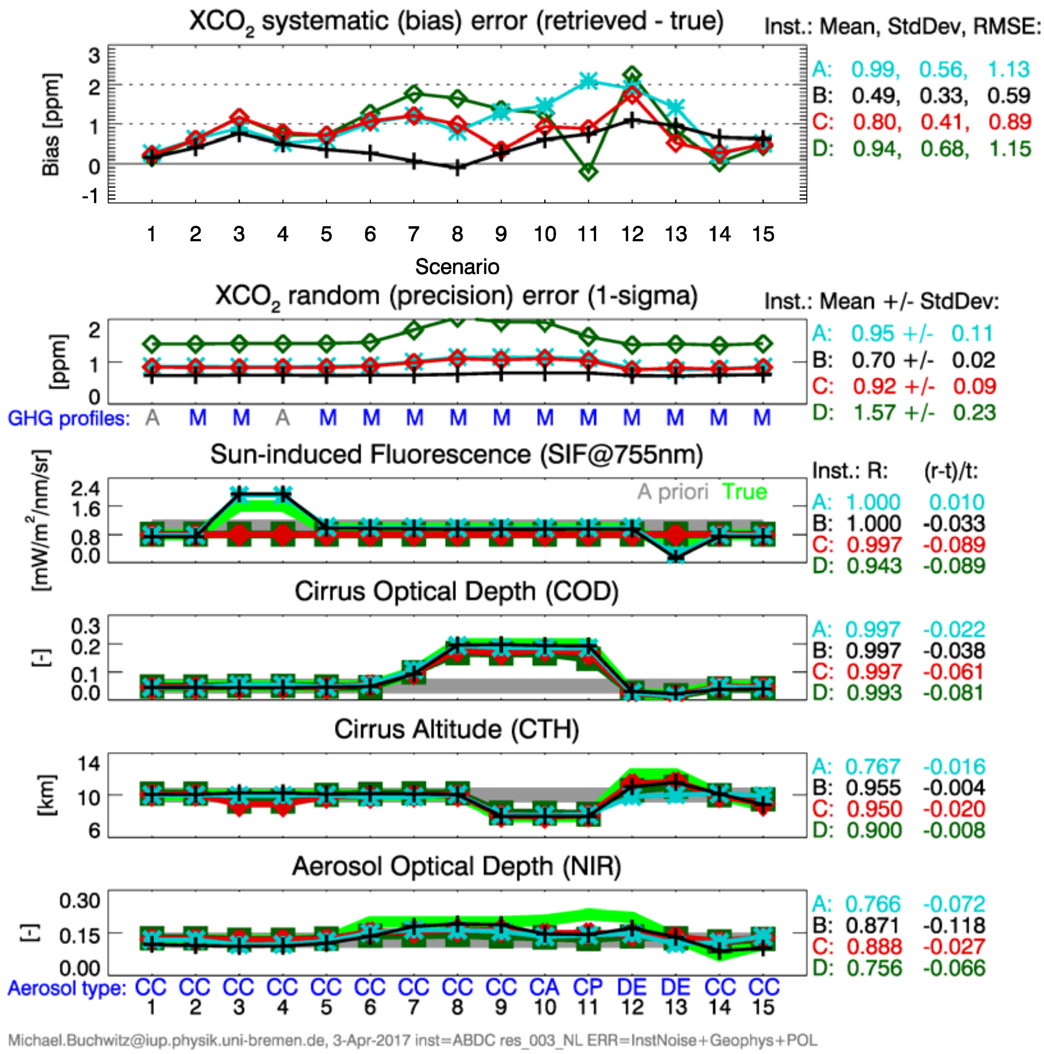

Figure 31: As
Figure 19 but also considering polarization as an additional error contribution.

6.5. Additional error source: Straylight (STRAY)

In this section error source "Straylight" has been considered for the simulated retrievals by using straylight as specified in **/Landgraf et al., 2017b/** using a scaling (straylight correction) factor of *a* = 1/5 (see **/Landgraf et al., 2017b/** for details). The radiance of the observed scene is contaminated from spectral straylight and from spatial straylight according to the straylight kernel (see **/Landgraf et al., 2017b/**). The observed scene is located close (5 SSD away) to a bright scene (on one side) corresponding to a desert scene with much higher albedo, which is 0.6 in all three bands. The bright scene is therefore approximately a factor of 3 (= 0.6/0.2) brighter in the NIR, a factor of 6 (=0.6/0.1) brighter in the SWIR-1 and a factor of 12 (0.6/0.05) brighter in the SWIR-2 band.

The following modifications (i.e., differences w.r.t. to the description given in **/Landgraf et al., 2017b/**) have been applied based on information from ESA (e-mail B. Sierk, 18-June-2017):

- Instrument independent straylight kernels have been used (by setting factors $\Delta\lambda_B/\Delta\lambda$ and $\Delta x_B/\Delta x$ in Formula (13) to 1.0)
- The straylight kernels have been normalized to "Total Intensity Scatter" (TIS) 0.9% for the NIR bands, 0.7% for the SWIR-1 bands and 0.5% for the SWIR-2 bands.

The resulting straylight spectra of the three bands are shown in **Figure 32 - Figure 34** for scene s01.

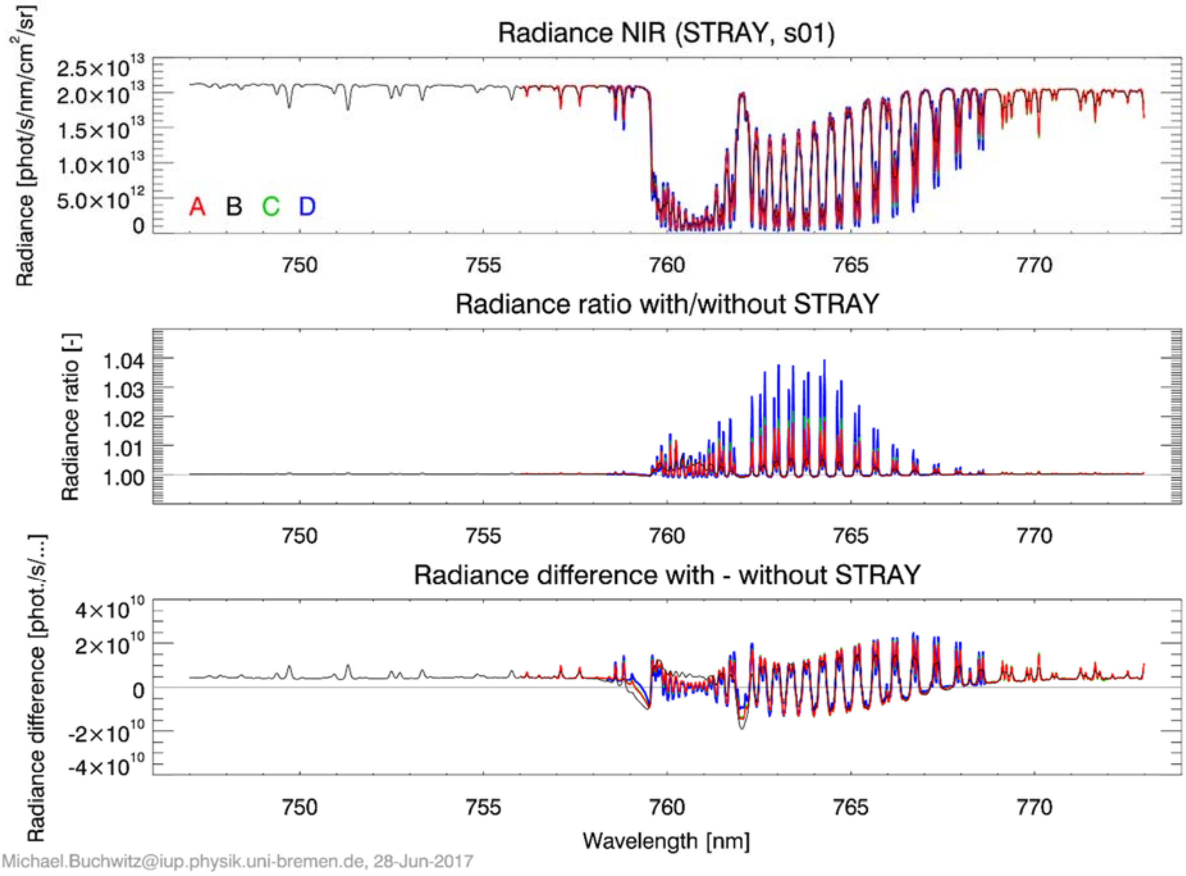

Figure 32: Radiance spectra of all four instruments (top) and corresponding straylight spectra (bottom) for the NIR bands.

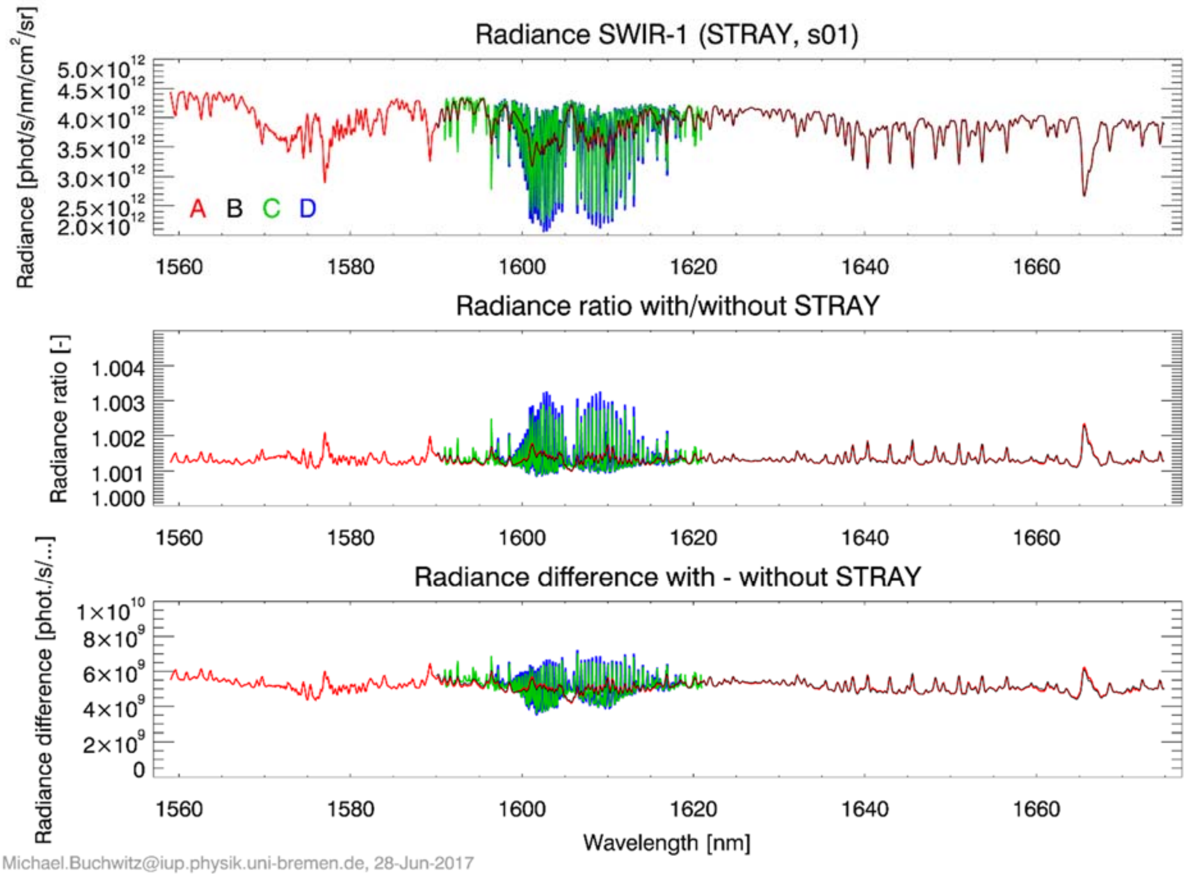

Figure 33: As
Figure 32 but for the SWIR-1 bands.

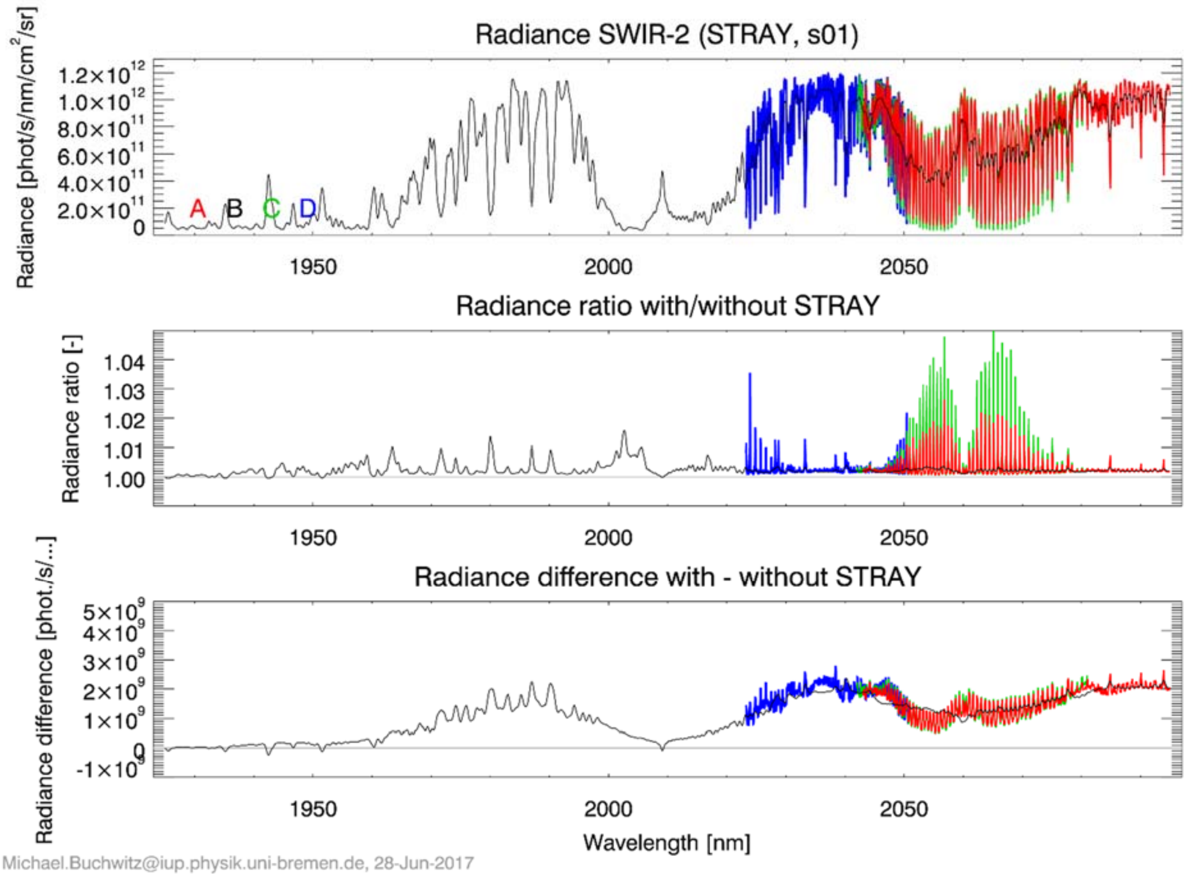

Figure 34: As
Figure 32 but for the SWIR-2 bands.

Simulated retrievals have been performed using the straylight contaminated radiance spectra as observations. The results are shown in
Figure 35.

As can be seen from
Figure 35 (top panel), instrument D has the smallest XCO_2 mean bias, instrument B has the smallest standard deviation of the bias, and instrument D has the smallest root-mean-square-error. As can also be seen, instrument B has the smallest XCO_2 random error (best precision).

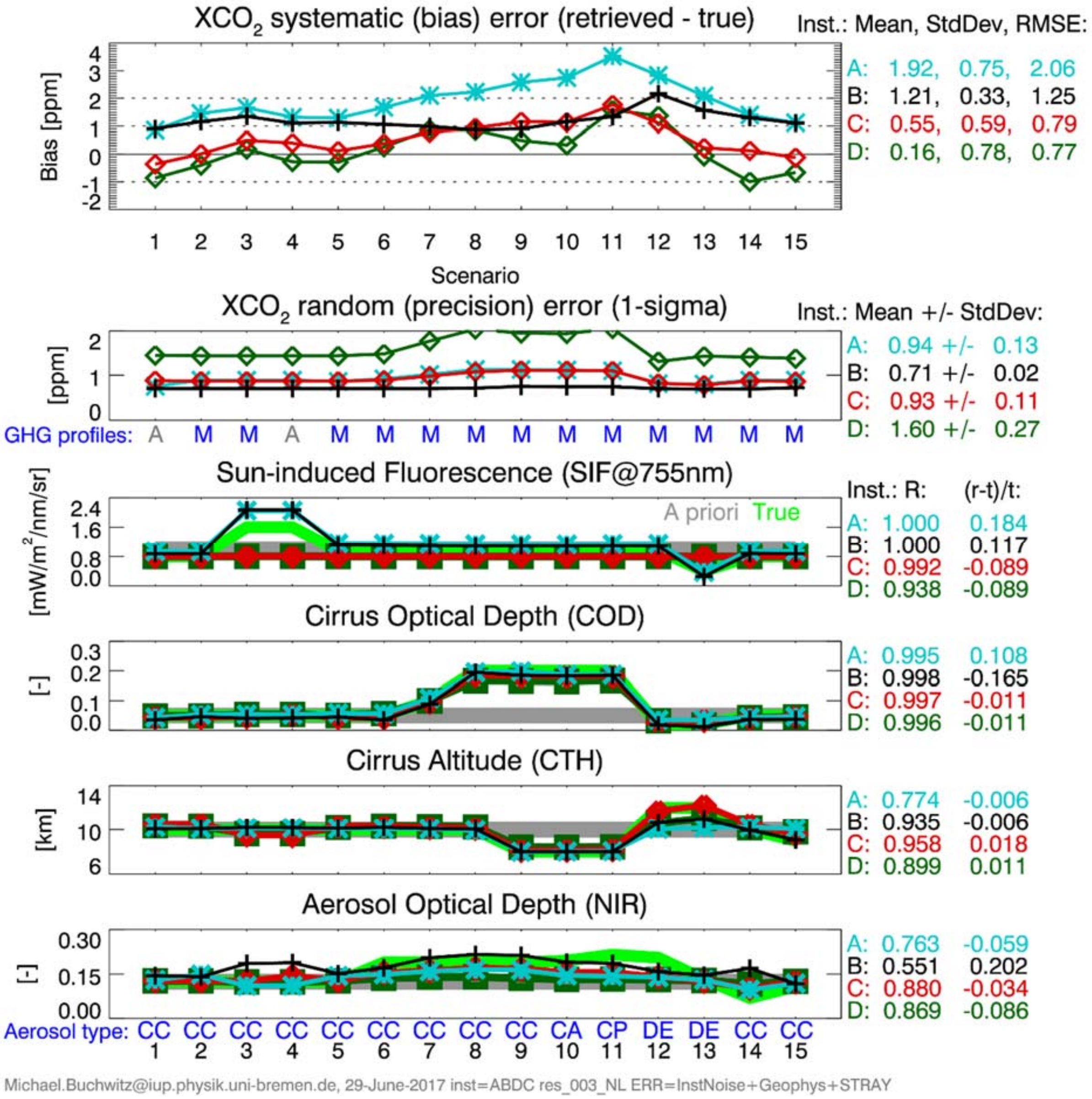

Figure 35: As
Figure 19 but also considering straylight as an additional error contribution.

6.6. Summary of "Iterative abs." results

The results presented in the previous sub-sections, which are summarized in **Figure 36**, show that instrument B has smallest XCO_2 random error ("best precision", green bars in **Figure 36**) for all investigated cases and the smallest XCO_2 systematic error for nearly all investigated cases (red bars in **Figure 36**).

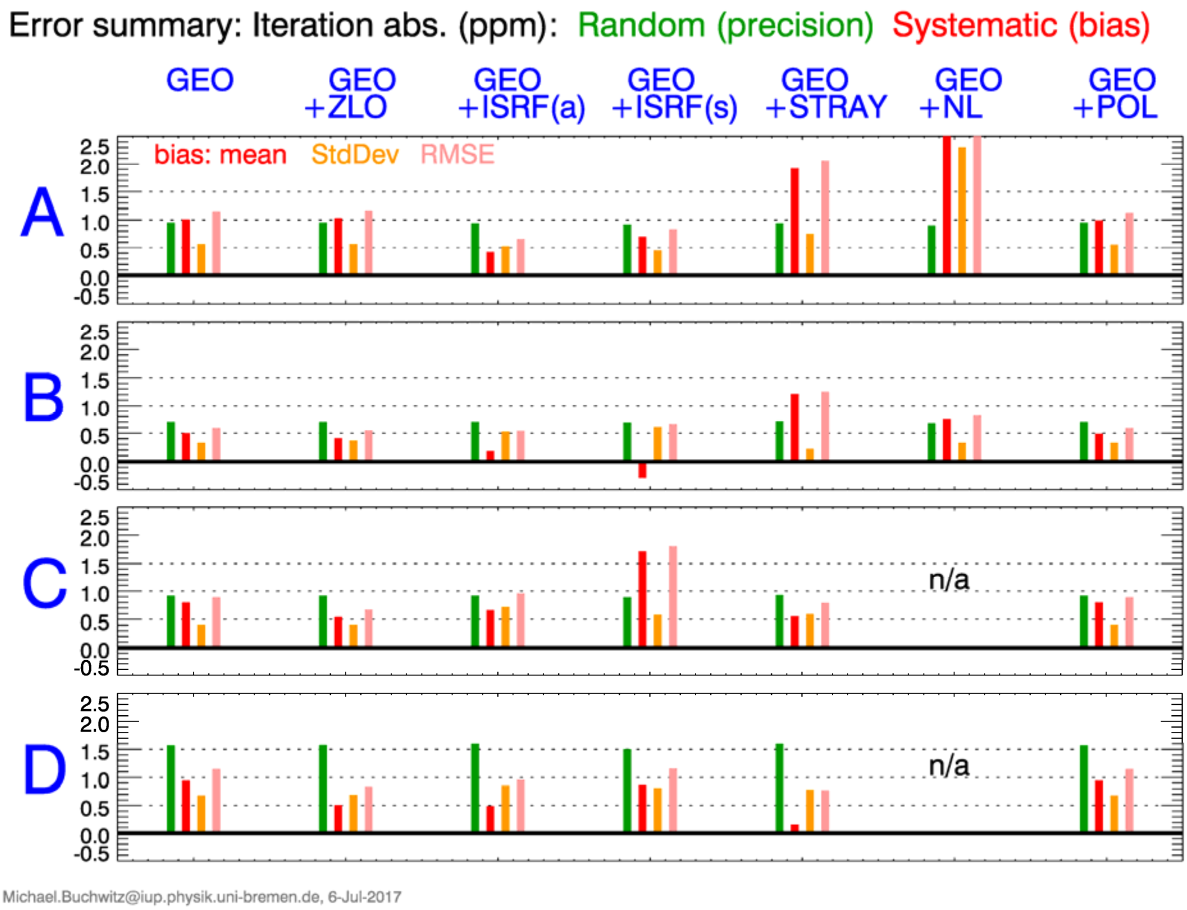

Figure 36: Summary of the "Iterative abs." error analysis results for instruments A, B, C, D (from top to bottom) and all investigated error sources, which are (from left to right): geophysical (Geo), i.e., errors due aerosols, clouds, etc., and the following additional instrument/calibration related error sources: zero level offset (ZLO), Instrument Spectral Response Function (ISRF) anti-symmetrical ("a") and symmetrical ("s") distortions, straylight (stray), detector non-linearity (NL) and polarization (Pol). The XCO_2 random error ("precision") is shown in green, the three metrics for XCO_2 systematic error are shown in red (from left to right: mean bias, standard deviation of bias, root-mean-square-error).

The presented results suggest that instrument B is the preferred instrument concept of the four instrument concepts, which have been investigated in this study.

However, it needs to be noted that concepts C and D seem somewhat less sensitive to straylight than concept B (assuming that the approach to consider straylight related errors is realistic).

Nevertheless, before drawing any final conclusions - it may be worthwhile to carry out some additional investigations and these are described in the following section.

7. Additional error analysis

As shown in the previous section, instrument B has smallest random error ("best precision") compared to the other three instruments. This is a robust finding as (typically) the random error is dominated by the instrument signal-to-noise performance and not so much by the retrieval algorithm (at least if a "good" algorithm is used).

For XCO_2 biases this is less clear as biases critically depend on the used retrieval algorithm. This means that it is less clear (compared to random errors) if the systematic errors shown in the previous section are primarily due to the different instrument concepts or due to the retrieval algorithm. For example it could be that the BESD/C algorithm as used to generate the results shown in the previous section is somehow "better" to better deal with (pre-defined) "GEO scenarios" (see **Sect. 6.1**) for instrument B compared to the other three instruments. If this would be the case than instrument B would be the "winner" for GEO errors. If in addition the additional instrument related errors are relatively small (compared to GEO related errors) than instrument B would also be the winner for all instrument related errors, i.e., instrument B would be the overall winner.

It therefore seems important to aim at disentangling instrument/calibration related errors from GEO errors, i.e., from errors due to aerosols and clouds, etc. This can be achieved by

(i) computing the difference of the ("absolute") XCO_2 biases shown in the previous section w.r.t. the GEO biases (i.e., "GEO + instrument error" minus "GEO error" = "instrument error"). These bias differences are called "Iterative diff." results in this document and these results are obtained by computing differences of the "Iterative abs." results. The disadvantage of this approach is that the disentangling is far from perfect (due to pre-processing related errors and potential influence of the iterative scheme).

(ii) computing instrument related biases directly by applying the "retrieval Gain matrix" to radiance error spectra. These biases are called "Linearization" results in this document. This approach has the advantage that it is independent of the iteration method as implemented for the BESD/C retrieval method and the results do not suffer from pre-processing related errors. Arguably, this is the best method to quantify the instrument related errors.

The corresponding results are presented in the following sub-sections.

7.1. Close loop scenario s00

For retrieval studies based on simulations it is always interesting (or even mandatory) to perform a “close loop” (CL) test. This means that the retrieval algorithm is applied to synthetic radiance observations which have been computed using a model atmosphere (and other parameters/conditions such as surface reflectivity) which is fully consistent (ideally identical) with the retrieval algorithm assumptions (i.e., “true” = *a priori* for all parameters (CO_2, aerosols, clouds, SIF, …)).

Therefore, an additional “close loop scenario” s00 has been defined, which is identical with the assumptions as used in the BESD/C retrieval.

Note that scenario s01 is nearly identical with scenario s00. The only difference of s00 compared to s01 is the aerosol type. For s00 the aerosol type is “continental average with 70% humidity” (CA70) instead of “continental clean with 90% humidity” (CA90) as used for s01.

The corresponding XCO_2 ZLO-related biases for scenario s00 are shown in **Table 8**.

Row “GEO” lists the XCO_2 biases for all four instruments without any instrument related systematic radiance error. In this case one would ideally expect zero biases for all four instruments. However, as can be seen, the biases are small but not zero. This is because of the pre-processing steps, which typically result in small biases (as, for example, the surface albedo retrieval is not “perfect”). Note that the retrievals have been done as before, i.e., using the BESD/C retrieval program, but without iteration (i.e., the option to iterate has been “switched off”).

Row “ZLO” shows the biases if error source ZLO is added and row “ZLO bias via e02-e01” lists the difference of biases as listed in the first two rows, i.e., the “isolated” ZLO error.

Here the “isolated” ZLO related biases are computed from the difference of two biases but these ZLO related biases can also be estimated “directly” using “gains” as shown in the last row.

The last row “ZLO bias via GMM” shows the ZLO bias as computed with the Gain Matrix Method (GMM) (details are given in the following **Sect. 7.2**).

Comparison of the last two rows shows that the two methods “ZLO bias via e02-e01” and “ZLO bias via gains” give similar but not exactly identical results (because of pre-processing related errors present in “ZLO bias via e02-e01”).

The advantage of the gain method is that it permits "direct" computation of XCO_2 biases from instrument/calibration specific radiance errors without introducing "additional errors", e.g., due to pre-processing.

The gain method is explained and applied in the following sub-sections and the resulting "Linearization" method biases are compared with "Iterative diff." biases.

XCO_2 ZLO-related biases for Close Loop scenario					
Error source	**A**	**B**	**C**	**D**	**Comment**
GEO (e01)	0.03	-0.14	0.00	-0.04	Close loop
GEO+ZLO (e02)	0.04	-0.13	-0.23	-0.48	
ZLO bias via e02-e01	0.01	0.01	-0.23	-0.44	
ZLO bias via GMM	0.04	0.07	-0.35	-0.44	

Table 8: XCO_2 ZLO related biases for Close Loop (CL) scenario s00 (see main text for details).

7.2. Linearization via Gain Matrix Method (GMM)

The Gain Matrix Method (GMM) as used here is described and used also in **/Buchwitz et al., 2015/**.

Using a Gain Matrix (GM), G, the relative error of the reflectance spectrum, Δy (a vector), can be mapped onto the error of a geophysical parameter of interest, Δx:

$$\Delta x = G\ \Delta y$$

Here, Δy (which is dimensionless) is the multiplicative reflectance (or radiance) relative error spectrum (i.e., a value of 0.01 corresponds to a +1% error) or the ratio of a spectrum with error divided by the error-free spectrum (in this case a +1% error corresponds to 1.01).

To illustrate how Δy is defined, here some examples, using reflectance (or radiance) ratios:

- If Δy = 1.0 (for certain wavelengths), the reflectance has no (systematic) error (at these wavelength).
- If Δy = +1.001 (for certain wavelengths), the reflectance has a (systematic) error of +0.1% (at these wavelengths).
- If Δy = +0.999 (for certain wavelengths), the reflectance has a (systematic) error of -0.1% (at these wavelengths).

Matrix G is defined by the following three G row or gain vectors G0, G1 and G2:

- G0 is the "Normalized CO_2 vertical column" "G"; G0 is a (1-dimensional) vector with number of elements = number of spectral samples of all three CarbonSat bands (concatenated).
- G1: same as G0 but for methane (CH_4).
- G2: same as G0 but for Surface Pressure (PRE) or, equivalent, the normalized (dry) air (AIR) column.

Recipe how to use the three gain vectors

For each of the three G row vectors (i.e., G0, G1, G2), compute the following three numbers (scalars) by computing the scalar product ($<|>$) of each G row vector with the reflectance error spectrum (vector) Δy as follows (the sum extends over all elements of the vectors = number of elements of vector Δy):

- $\Delta x0 = <G0 \mid \Delta y> := \Sigma_i\ G0_i \times \Delta y_i$
- $\Delta x1 = <G1 \mid \Delta y> := \Sigma_i\ G1_i \times \Delta y_i$ (not used here)
- $\Delta x2 = <G2 \mid \Delta y> := \Sigma_i\ G2_i \times \Delta y_i$

These three numbers can be interpreted as follows:

- Δx0 is the relative error of the CO_2 vertical column (i.e., if Δx0 = +0.01, the retrieved CO_2 column would have a systematic error of +1%)
- Δx1: as Δx0 but for methane (not used here)
- Δx2: as Δx0 but for the surface pressure / air column (e.g., if Δx2 = -0.01 the retrieved surface pressure / air column would have a systematic error of -1%)

Computation of the XCO_2 bias:

- B^{XCO2} := XCO_2 bias in ppm = ((1+Δx0)/(1+ Δx2) -1)

A GMM overview is shown in **Figure 37**.

For illustration, **Figure 38** to **Figure 41** show BESD/C gain vectors for instruments A to D.

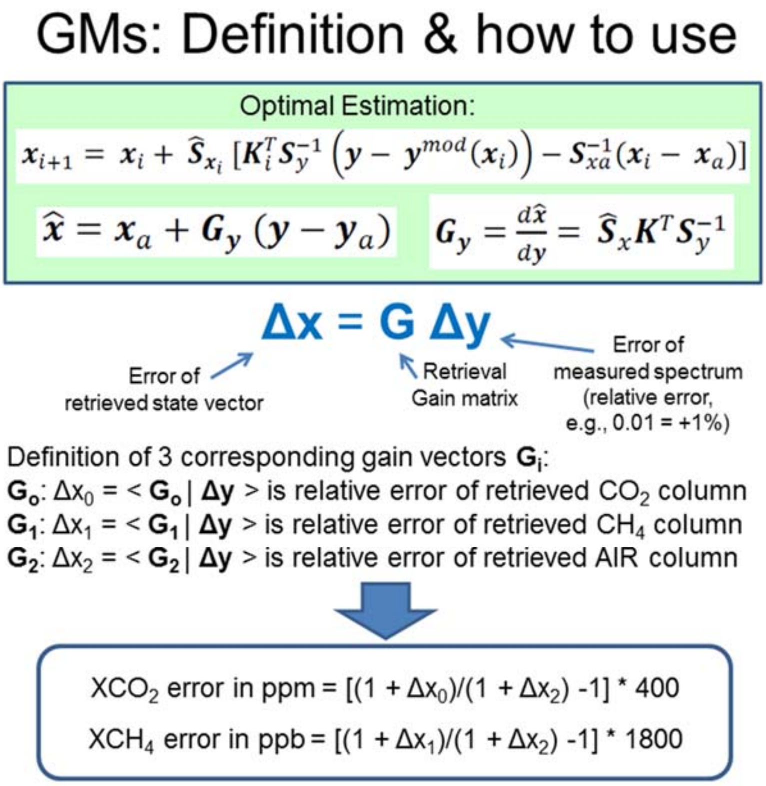

Figure 37: Gain Matrices (GMs): Definition and how to use.

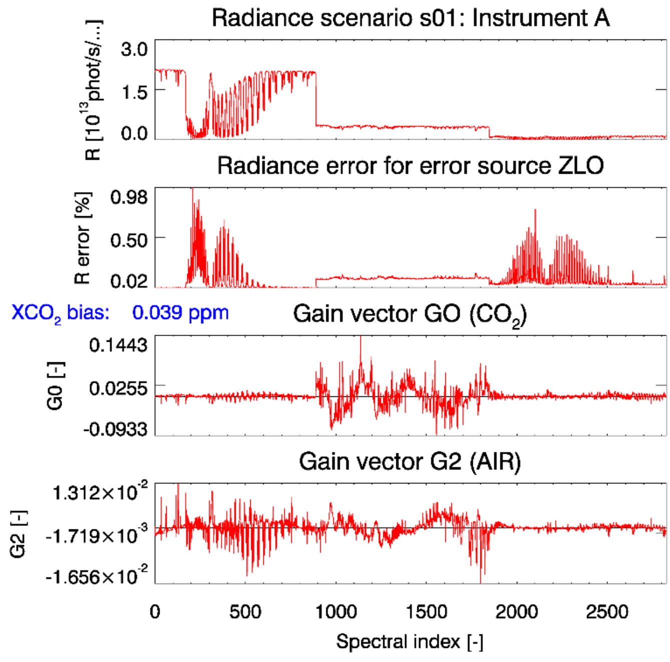

Figure 38: Radiance (top), ZLO radiance error (2nd row), and the gain vectors G0 for the CO_2 column (3rd row) and G2 for surface pressure or dry air column (bottom) for instrument A.

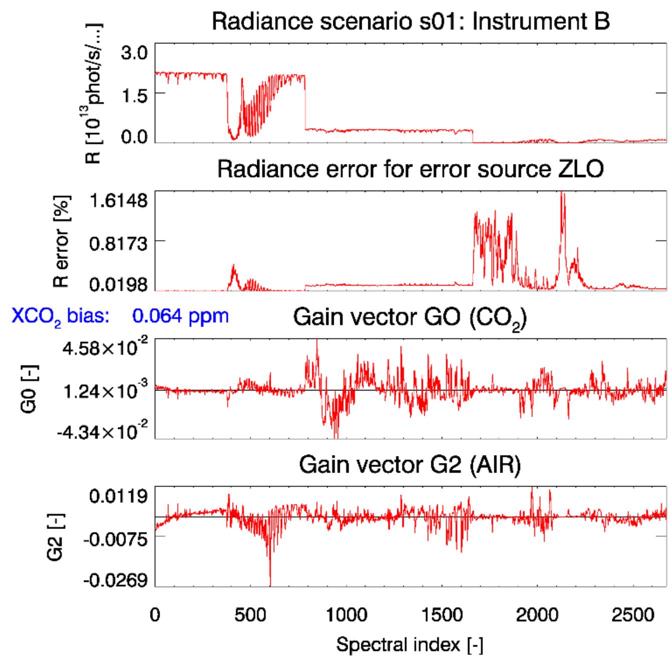

Figure 39: As **Figure 38** but for instrument B.

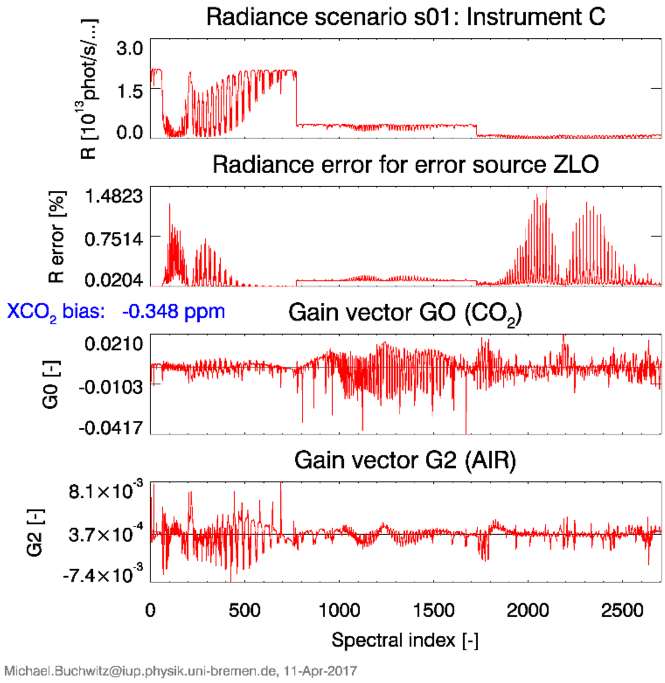

Figure 40: As **Figure 38** but for instrument C.

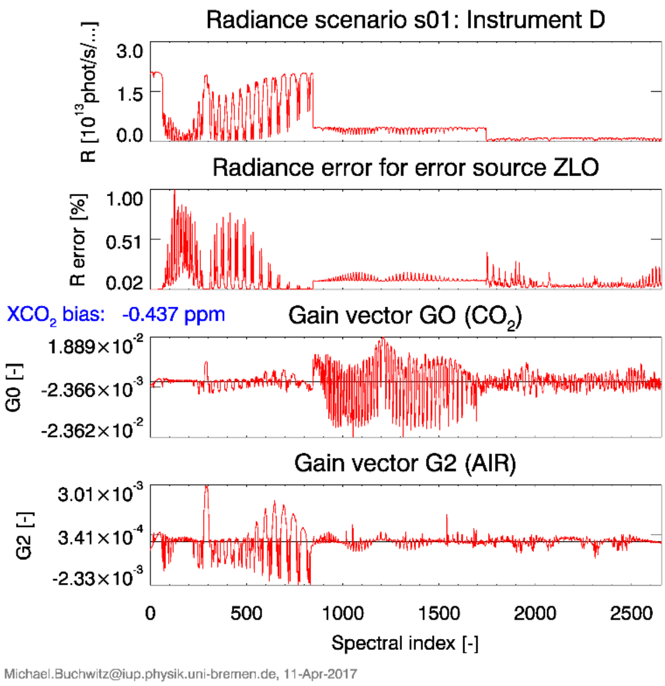

Figure 41: As **Figure 38** but for instrument D.

7.3. Additional error analysis results via Linearization and „Iterative diff.“

Figure 42 shows ZLO-related XCO_2 biases computed via gains (top), i.e., using linearization, and via the “Iterative diff.” method (bottom). The results for the latter method have been computed using the “Iterative abs.” results shown in **Sect. 6**.

Specifically, the results shown in
Figure 42 bottom have been computed as the difference of the biases for “GEO+ZLO” (**Figure 20**) minus the GEO-biases (**Figure 14**). As can be seen, the “Iterative diff.” biases exhibit significantly more scenario dependence compared to the linearized results. This is because the “Iterative diff.” results have been computed using full iterative BESD/C retrievals including pre-processing (as needed to obtain first guess and *a priori* values for surface albedo and other parameters) whereas for the linearized results it is essentially assumed that only one error source (here ZLO) exists. As can also be seen, instrument D shows by far the largest scenario dependence for the “Iterative diff.” results. It is not clear, why this is the case.

As already explained earlier, the “Iterative diff.” approach to isolate the XCO_2 biases originating from specific instrument/calibration related errors is not optimal. For this purpose, the linearization approach is much better. The linearization approach ensures that the bias is zero if the radiance error is zero, which is not the case for the “Iterative diff.” approach.

Similar results as shown in
Figure 42 are shown in
Figure 43 to
Figure 46 for the other instrument related errors ISRF distortion (anti-symmetrical and symmetrical), straylight, and polarization.

The various bias results are summarized and classified in the following section via “scoring”.

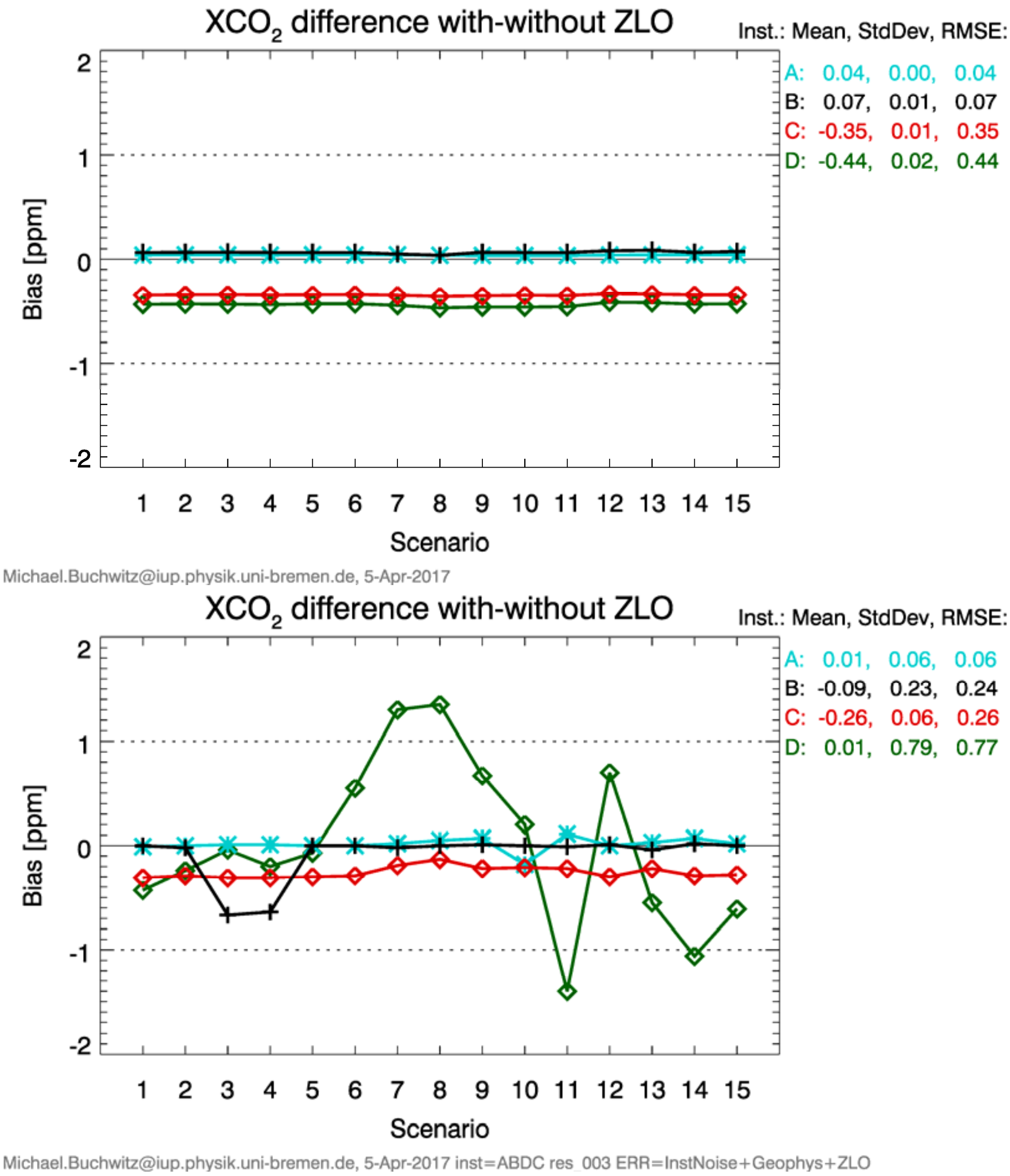

Figure 42: Top: XCO_2 biases for error source ZLO computed with “gains”, i.e., using linearization. Listed are three figures of merit to characterize the biases: (i) mean bias, (ii) standard deviation of bias and (iii) root-mean-square error (RMSE). Bottom: As top panel but using the “Iterative diff.” method.

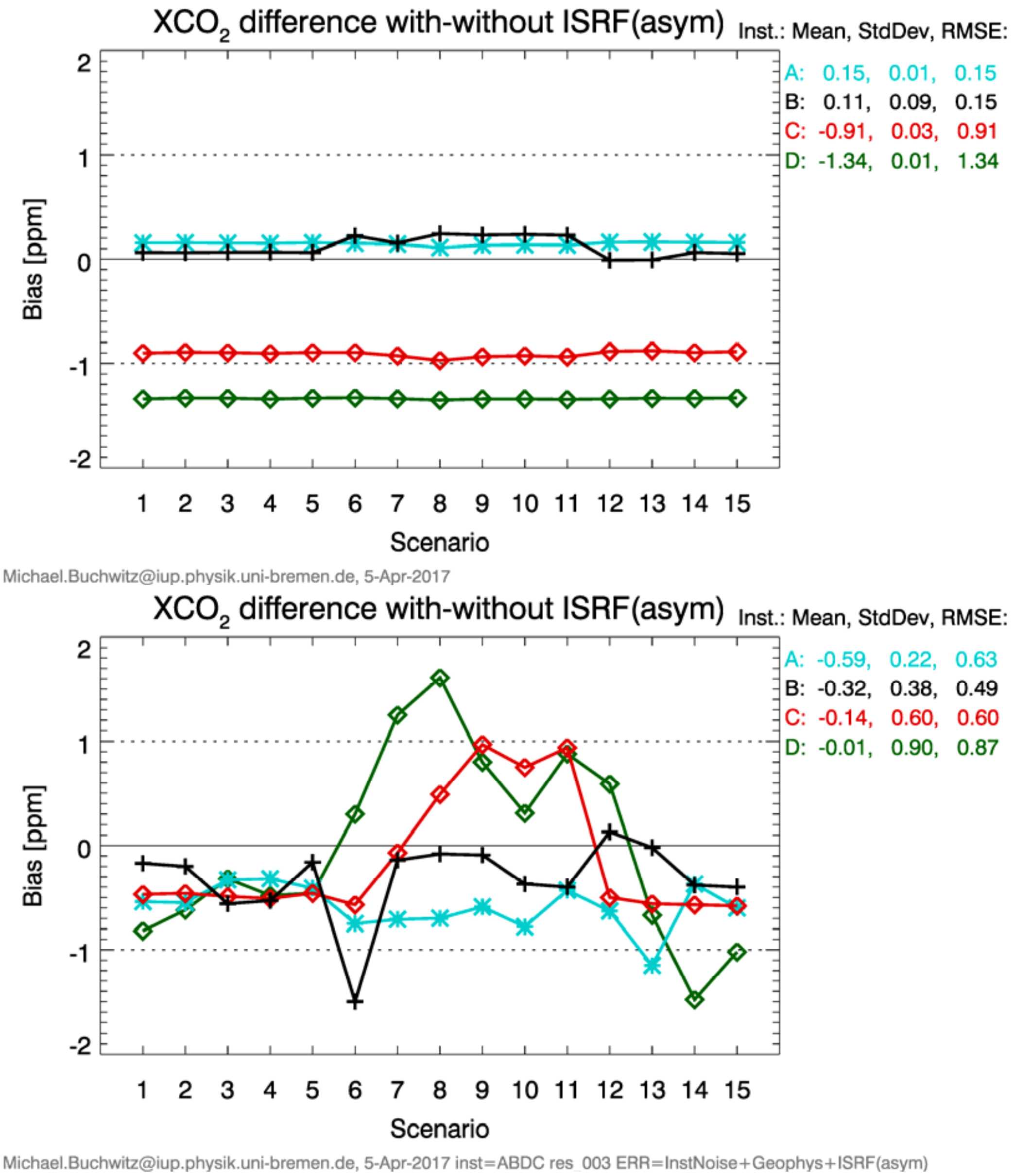

Figure 43: As
Figure 42 but for error source asymmetrical ISRF.

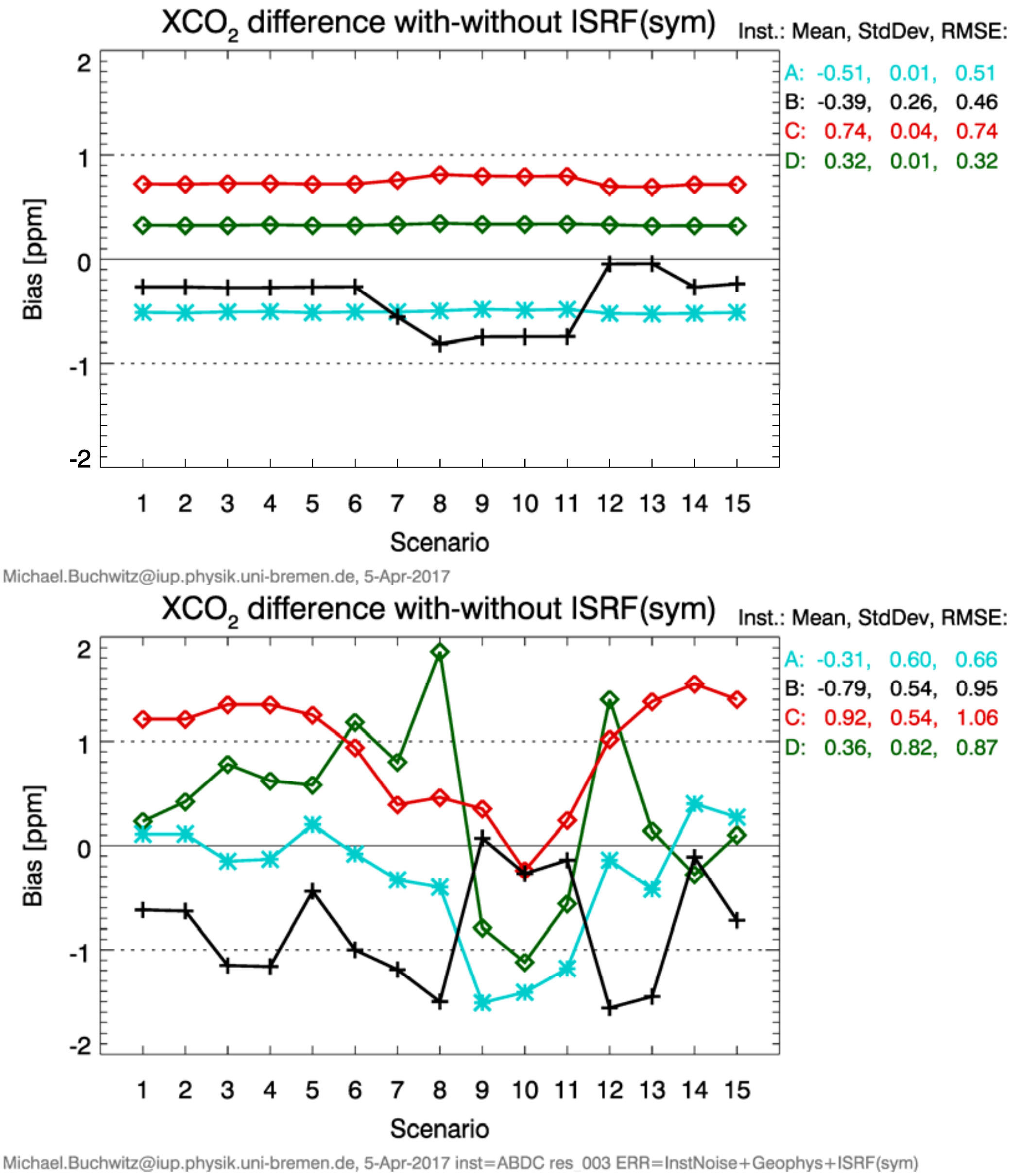

Figure 44: As
Figure 42 but for error source symmetrical ISRF.

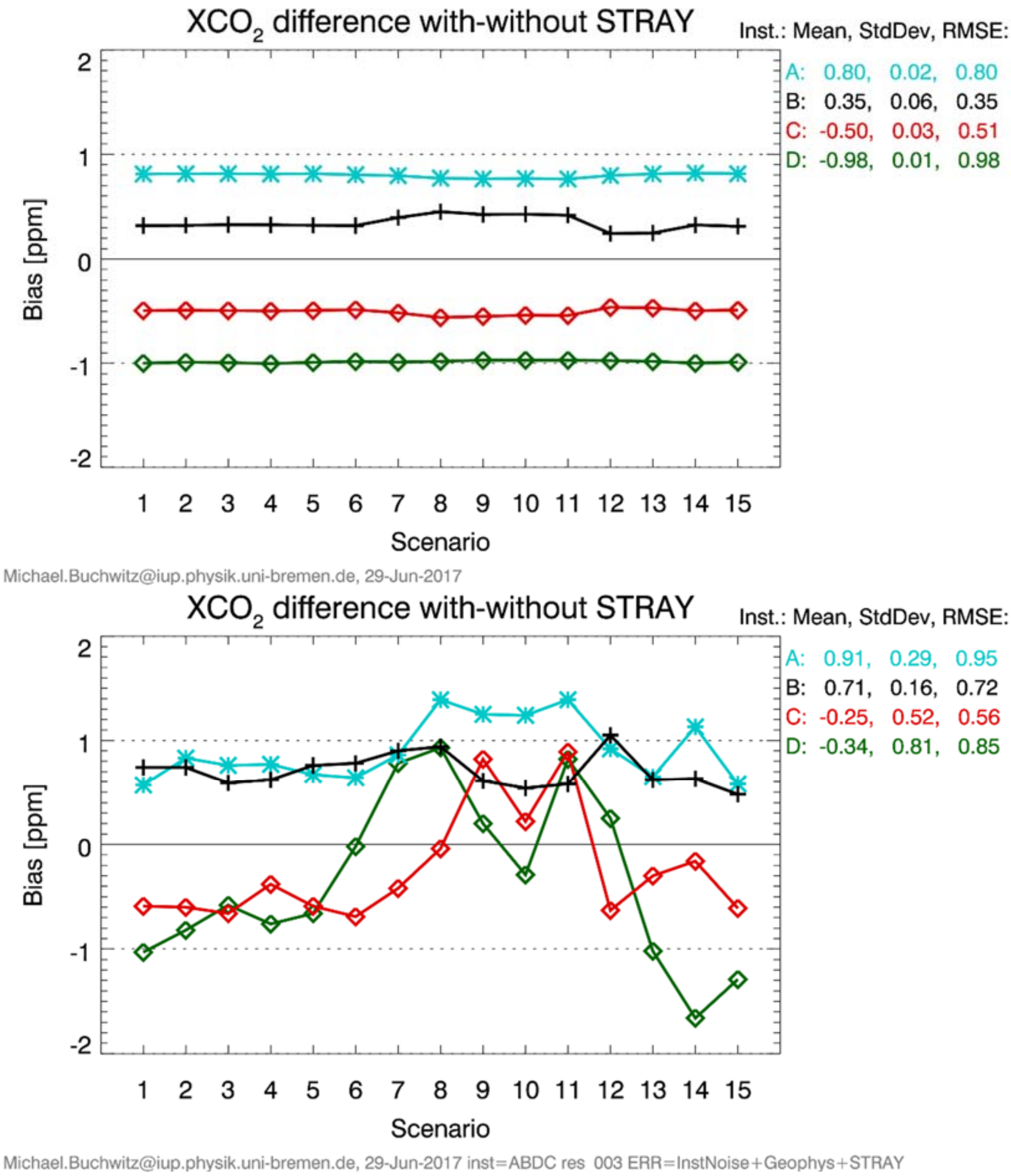

Figure 45: As
Figure 42 but for error source straylight.

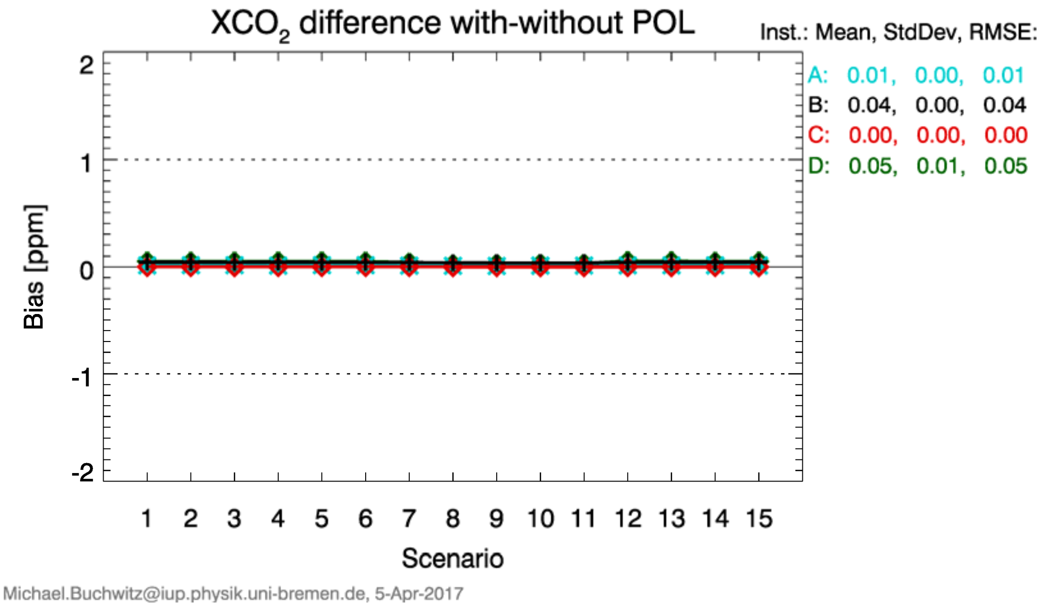

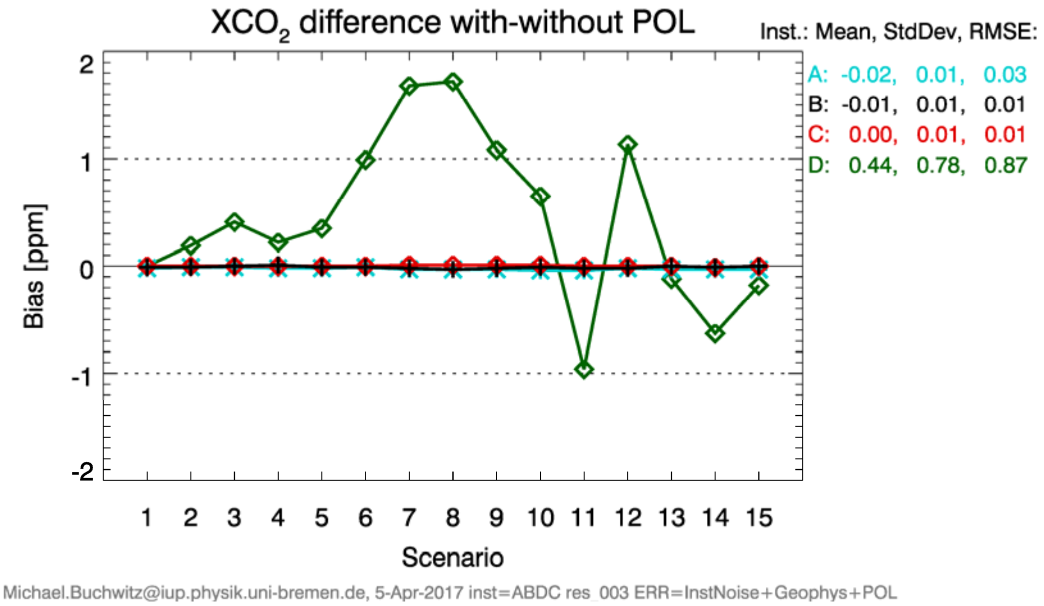

Figure 46: As
Figure 42 but for error source polarization.

Figure 47 summarizes the results of the linear error analysis. As can be seen, these results do not confirm that concept D has smallest sensitivity to straylight in contrast to the “Iterative abs” analysis shown earlier in this document. According to linear error analysis results instrument B has the smallest sensitivity to straylight.

This indicates that overall not strong conclusions can be drawn w.r.t. the best instrument concept in terms of smallest straylight related biases.

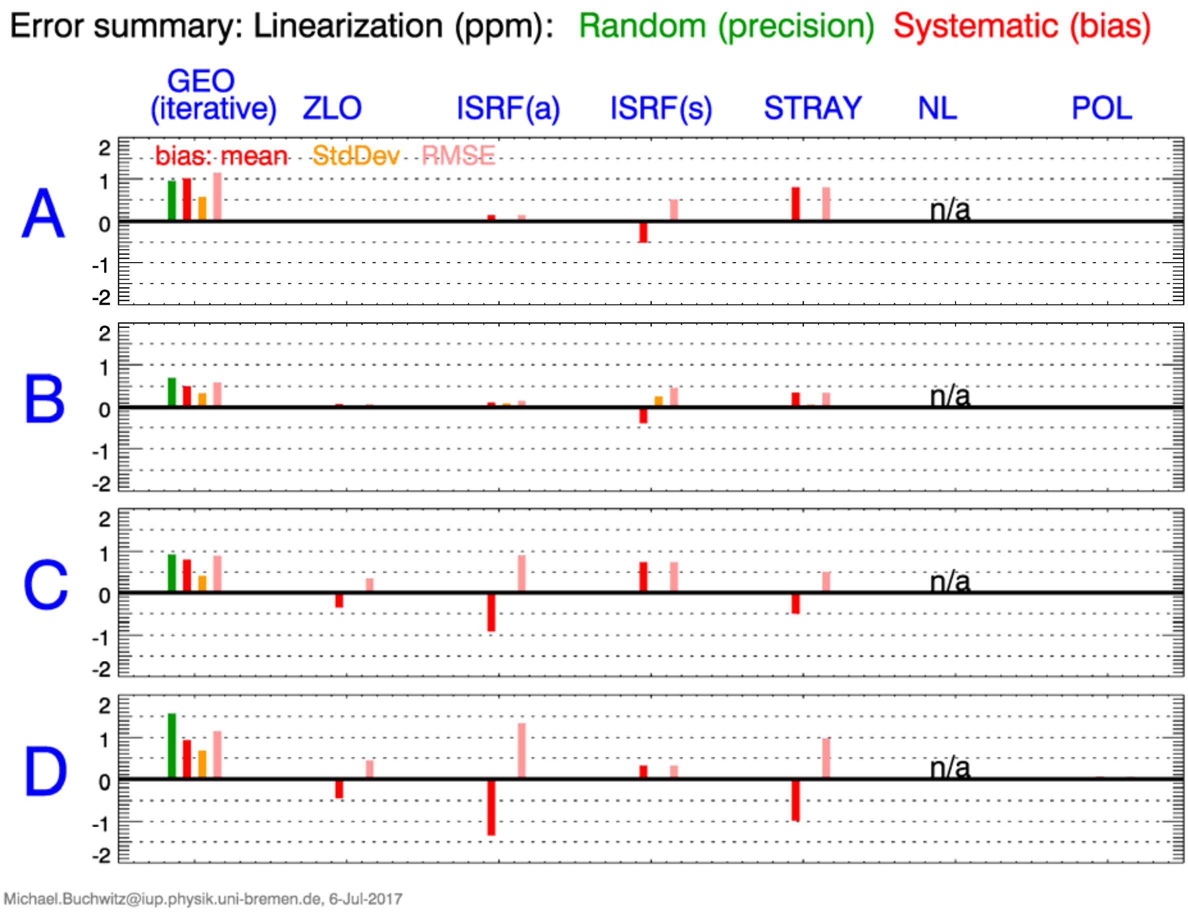

Figure 47: Summary of linear error analysis results. Note that for error “GEO” the “Iterative abs.” results are shown including random error and that the “POL” errors have also been added but are too small to be visible.

8. Summary of all instrument A-D results

In **Sect. 6** various XCO_2 bias results are shown for method “Iterative abs.” and in **Sect. 7** the corresponding biases as obtained for the “Iterative diff.” and “Linearization” methods are presented.

To get an overview about all results in a clear and condensed way a simple scoring scheme has been defined and applied to the various bias results. This scheme and its results are presented in the following sub-section.

8.1. Scoring

8.1.1. Scoring method

The scoring scheme is defined and applied only to the various XCO_2 biases.

For the XCO_2 random error scoring is not needed as it is obvious from the results shown in **Sect. 6** that instrument B has smallest random error („best precision“) for all scenarios.

The scoring scheme for biases is as follows:

- Score = 0 for all instruments except if:
  - +1 if the mean bias is smallest (for a given comparison of the four instruments)
  - -1 if the mean bias is largest
  - +1 if the standard deviation of the bias is smallest
  - -1 if the standard deviation of the bias is largest
- If more than one instrument is the winner (looser) for a given error source than all “equivalent” winners (looser) get +1 (-1)

Note:

- The RMSE is not used as this quantity is redundant
- Only the „mean bias“ is used for the linearization results as here the scenario dependence is typically very small (the standard deviation of the biases are typically close to zero as can be seen from the figures shown in **Sect. 7.3**)

The scoring results are shown in the following section.

8.1.2. Scoring results

The XCO_2 bias scoring results are shown in **Table 9** to **Table 11** for the three used methods. The overall scoring results are shown in **Figure 48**.

The higher the score, the lower the biases, i.e., the better the instrument.

As can be seen from **Figure 48**, instrument B has by far the highest score for method “Iterative abs.” (see detailed results in **Sect. 6**). For “Linearized” instruments A, B and C are essentially equally good (see detailed results in **Sect. 7.3**).

Instrument A has the highest score for method “Iterative diff.” followed by B and C (identical scores). However, as already explained, method “Iterative diff.” is not appropriate to determine “which instrument is better” in terms of instrument related biases.

Instrument D has lowest score for all three methods.

Following the explanations given earlier, namely that method “Linearized” is the best of the used methods to quantify instrument/calibration related XCO_2 biases, it is concluded from the results shown here that instrument B seems to be as good as instruments A and C. In terms of random errors instrument B is the winner.

In summary, the results of this study show that there is no indication that instrument B is worse than any of the other three instruments.

Error source	Mean bias	StdDev bias
GEO	+1: B -1: A	+1: B -1: D
GEO+ZLO	+1: B -1: A	+1: B -1: D
GEO+ISRF(asym)	+1: B -1: C	+1: AB -1: D
GEO+ISRF(sym)	+1: B -1: C	+1: A -1: D
GEO+STRAY	+1: D -1: A	+1: B -1: D
GEO+POL	+1: B -1: A	+1: B -1: D

Table 9: Scores for method “Iterative abs.”. Result: A: -1; B: 11; C: -2; D: -7.

Error source	Mean bias	StdDev bias
ZLO	+1: AD -1: C	+1: AC -1: D
ISRF(asym)	+1: D -1: A	+1: A -1: D
ISRF(sym)	+1: A -1: C	+1: BC -1: D
STRAY	+1: C -1: A	+1: A -1: D
POL	+1: C -1: D	+1: ABC -1: D

Table 10: Scores for method “Iterative diff.”. Result: A: 6; B: 2; C: 2; D: -5.

Error source	Mean bias
ZLO	+1: A -1: D
ISRF(asym)	+1: B -1: D
ISRF(sym)	+1: D -1: C
STRAY	+1: B -1: D
POL	+1: C -1: D

Table 11: Scores for method "Linearization". Result: A: 1; B: 2; C: 0; D: -3.

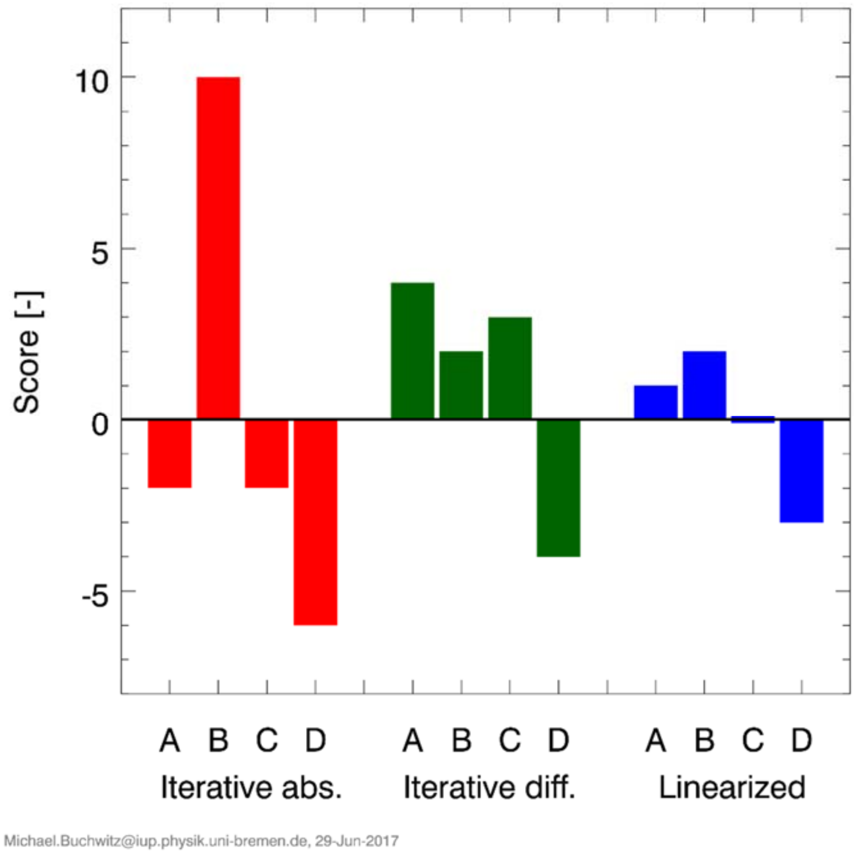

Figure 48: Scoring results for instruments A-D for the three methods "Iterative abs." (red), "Iterative diff." (dark green) and linearization (blue). The higher the score, the better the performance in terms of XCO_2 biases.

8.2. Overall summary and context

As shown in this document, instrument B has the smallest XCO_2 random error (see **Sect. 6**) of all four investigated instrument concepts.

Concerning XCO_2 systematic errors the situation is less clear and the findings can be summarized as follows: Overall, instrument B often has the smallest biases for the investigated scenarios as concluded from applying the full iterative BESD/C retrieval algorithm (with pre-processing) to simulated radiance spectra with various types of geophysical and instrument/calibration related errors present (see **Sect. 6**). As this approach is not optimal to "isolate" instrument/calibration related biases from other ("geophysical") biases also a linearized error analysis has been conducted (see **Sect. 7**). According to the linear error analysis instrument B shows good performance in terms of XCO_2 biases (see also **Sect. 8.1.2**) but here the differences to the other instrument concepts is much less pronounced compared to full iterative retrievals (in fact, instruments A, B and C have very similar performance).

Instrument B has the lowest spectral resolution but the highest signal-to-noise ratio (SNR) and covers the largest spectral range in the NIR (around 760 nm) and SWIR-2 (around 2000 nm) spectral regions.

Spectral resolution cannot be seen in isolation as a higher spectral resolution spectrum does not contain more information if much noisier. Therefore, also other aspects such as signal-to-noise performance and spectral coverage need to be considered. The findings of this study are therefore not necessarily a surprise. This study confirms results obtained in previous studies (see in particular the Final Reports of the two CarbonSat L1L2 studies (**/Bovenmann et al., 2014, 2015/**)). As shown in **/Bovenmann et al., 2014/**, simulated retrievals for several instrument configurations have been performed and it has been found that an instrument with lower spectral resolution can give superior performance in terms of XCO_2 random and systematic errors if the signal-to-noise ratio is high enough and spectral coverage is appropriately selected. These conclusions have been drawn by applying independently two different retrieval algorithms (the one from Univ. Bremen and the one from Univ. Leicester).

In **/Bovenmann et al., 2014/** also results from SRON are shown based on an analysis of real GOSAT data which were later also published in a peer-reviewed publication (**/Galli et al., 2014/**). Here the following has been concluded **/Galli et al., 2014/**: "For GOSAT spectra, the most notable effect on CO_2 retrieval accuracy is the increase of the standard deviation of retrieval errors from 0.7 to 1.0 % when the spectral resolution is reduced by a factor of six. The retrieval biases against atmospheric water abundance and air mass become stronger with decreasing resolution. The error scatter increase for CH_4 columns is less pronounced. … . For both GOSAT and synthetic measurements, retrieval accuracy decreases with lower spectral resolution for a given signal-to-noise ratio, suggesting increasing interference errors. … A countermeasure for instruments with a lower spectral resolution than GOSAT is to aim at a higher SNR. …". A limitation has been highlighted in **/Bovenmann et al., 2014/**: "The GOSAT data have a SNR of 300 at continuum level for an SZA of 30 degress and an albedo of 0.3. In this report, we did not test whether the increase of error scatter caused by spectral degradation can be mitigated if the SNR for CarbonSat were better than for GOSAT. For this purpose, a representative global ensemble of synthetic spectra, combined with exact CarbonSat instrument settings would be necessary".

Very strong evidence that high spectral resolution is not mandatory for precise and accurate XCO_2 retrieval is provided by a comparison of the XCO_2 performance as obtained for XCO_2 retrieval from SCIAMACHY compared to GOSAT (using real satellite data). As can be seen from **Table 12**, similar random (around 2 ppm) and systematic (around 0.5 ppm) errors have been obtained for SCIAMACHY and for GOSAT XCO_2 although the spectral resolution of SCIAMACHY is much worse compared to GOSAT - and also significantly worse compared to instrument B investigated in this study by a factor of 4-5 in the NIR and SWIR-1 bands.

GHG-CCI: Estimates of achieved data quality (#): CRDP#4 XCO_2

Sensor	Algorithm	Random error [ppm]	Systematic error [ppm]	Stability [ppm/year]		Details (section)
				Long-term drift	Year-to-year	
SCIAMACHY on ENVISAT	BESD v02.01.02	1.9 1.9 2.0 1.9	0.37 - 0.56 0.38 – 0.40 0.39 – 0.43 0.4 – 0.8	-0.03 +/- 0.06 (*) -0.13 +/- 0.28 (?) -0.02 +/- 0.33 (?) -0.01 +/- 0.08 (*)	0.32 +/- 0.08 0.34 (?) 0.23 (?) 1.68 +/- 2.03 (*)	VAL (Sect. 3) DP (6.1.1) EMMA (6.1.5) QA/QC (7.1)
SCIAMACHY on ENVISAT	WFMD V4.0	2.7 2.6 2.9 3.0 2.7	0.57 – 0.71 0.48 – 0.52 0.60 – 0.75 0.60 – 0.63 0.5 – 1.0	-0.03 +/- 0.10 (*) [0.00, 0.04] (?) 0.14 +/- 0.21 (?) 0.23 +/- 0.42 (?) -0.04 +/- 0.09 (*)	0.31 +/- 0.11 0.21 (?) 0.46 (?) 0.33 (?) 1.86 +/- 2.41 (*)	VAL (3) DP (6.1.2) DP (6.1.1) EMMA (6.1.5) QA/QC (7.1)
TANSO on GOSAT	OCFP v7.0 (UoL-FP)	1.8 1.9 1.8 1.7	0.36 - 0.58 0.47 0.36 – 0.42 0.3 – 0.5	-0.07 +/- 0.07 (*) 0.11 (?) -0.15 +/- 0.11 (?) -0.09 +/- 0.08	0.29 +/- 0.06 0.9 (?) 0.23 (?) 1.48 +/- 2.06 (*)	VAL (3) DP (6.1.3) EMMA (6.1.5) QA/QC (7.1)
TANSO on GOSAT	SRFP v2.3.8 (RemoTeC)	2.0 1.9 2.1 1.9	0.36 - 0.51 0.43 0.28 – 0.48 0.4 – 0.5	0.02 +/- 0.04 (*) -0.05 +/- 0.12 (*) 0.00 +/- 0.16 (?) -0.06 +/- 0.11 (*)	0.27 +/- 0.12 0.34 +/- 0.12 0.24 (?) 1.30 +/- 2.11 (*)	VAL (3) DP (6.1.4) EMMA (6.1.5) QA/QC (7.1)
SCIAMACHY & GOSAT	EMMA v2.2a	2.0 2.4	0.37 - 0.45 0.47 – 0.54	0.08 +/- 0.22 (*) -0.30 +/- 0.64 (?)	0.18 +/- 0.12 0.25 (?)	VAL (3) EMMA (6.1.5)
SCIAMACHY & GOSAT	EMMA v2.2b	1.7 1.8	0.29 - 0.38 0.32 – 0.40	-0.08 +/- 0.20 (*) -0.13 +/- 0.42 (?)	0.16 +/- 0.11 0.20 (?)	VAL (3) EMMA (6.1.5)
TANSO on GOSAT	EMMA v2.2c	1.7 1.8	0.30 - 0.39 0.24 – 0.44	-0.14 +/- 0.20 (*) -0.04 +/- 0.16 (?)	0.16 +/- 0.12 0.26 (?)	VAL (3) EMMA (6.1.5)
Required	G / B / T	< 1 / 3 / 8	< 0.2 / 0.3 / 0.5	< 0.2 / 0.3 / 0.5		**/URD GHG-CCI v2.1/**
Required	Target	< 0.5 ppm (uncertainty; 1-sigma)		< 0.15 ppm/year		***/GCOS-200/***
(#) As estimated (mostly) by comparison with ground-based TCCON observations neglecting TCCON accuracy (1-sigma) of 0.4 ppm (*) NOT significant; (?) Significance unclear Green numbers: at least URDv2.1 threshold requirement met; single values random and systematic errors are 1-sigma						

Table 12: Comparison of SCIAMACHY and GOSAT XCO_2 data quality (source: **/Buchwitz et al., 2017/**).

9. Additional sizing points: Instruments B2 and B3

ESA has defined additional sizing points and the corresponding results are provided in this section.

The corresponding instrument concepts are in this document referred to as:

- B2c1: Instrument B2 from “industrial consortium 1”
- B2c2: Instrument B2 from “industrial consortium 2”
- B3c1: Instrument B3 from “industrial consortium 1”
- B3c2: Instrument B3 from “industrial consortium 2”

The differences of the B2 sizing points to instrument B (see previous sections) are:

- SWIR-2 starts at 2043 nm (instead of 1925 nm).
- The spectral sampling ratios (SSR) are 3.0 pixel/FWHM in all three bands (instead of 3.x nm, see **Table 7**).
- New SNR A and B coefficients (as provided by ESA).

All other parameters are identical (for instruments B, B2 and B3) including the spectral resolution, which is 0.1 nm in the NIR, 0.3 nm in the SWIR-1 and 0.55 nm in the SWIR-2.

The only difference between instruments B3 and B2 are:

- B3: SWIR-2 starts at 1990 nm (instead of 2043 nm for B2)

Radiances, solar irradiances and SNR spectra for these instruments (including instrument B) are shown in **Figure 49 - Figure 53**. The scenario is s00 for VEG50. The s00 scenario is identical to s01 (see previous sections, e.g., XCO_2: 390 ppm, H_2O column: 4.8×10^{22}, AOD@550 nm: 0.2, cirrus at 10 km with COD=0.05) with the following exception:

- The aerosol type is “continental average” (CA, also used as *a priori* aerosol type in BESD/C) and not “continental clean” (CC).

In the captions of **Figure 49 - Figure 53** the corresponding XCO_2 retrieval precisions are listed. The retrieval results have been generated with the same BESD/C algorithm as also used for the instrument B study results shown in previous sections with the following exception:

- No cirrus pre-processing (as the 1939 nm is not available for the B2 instruments)

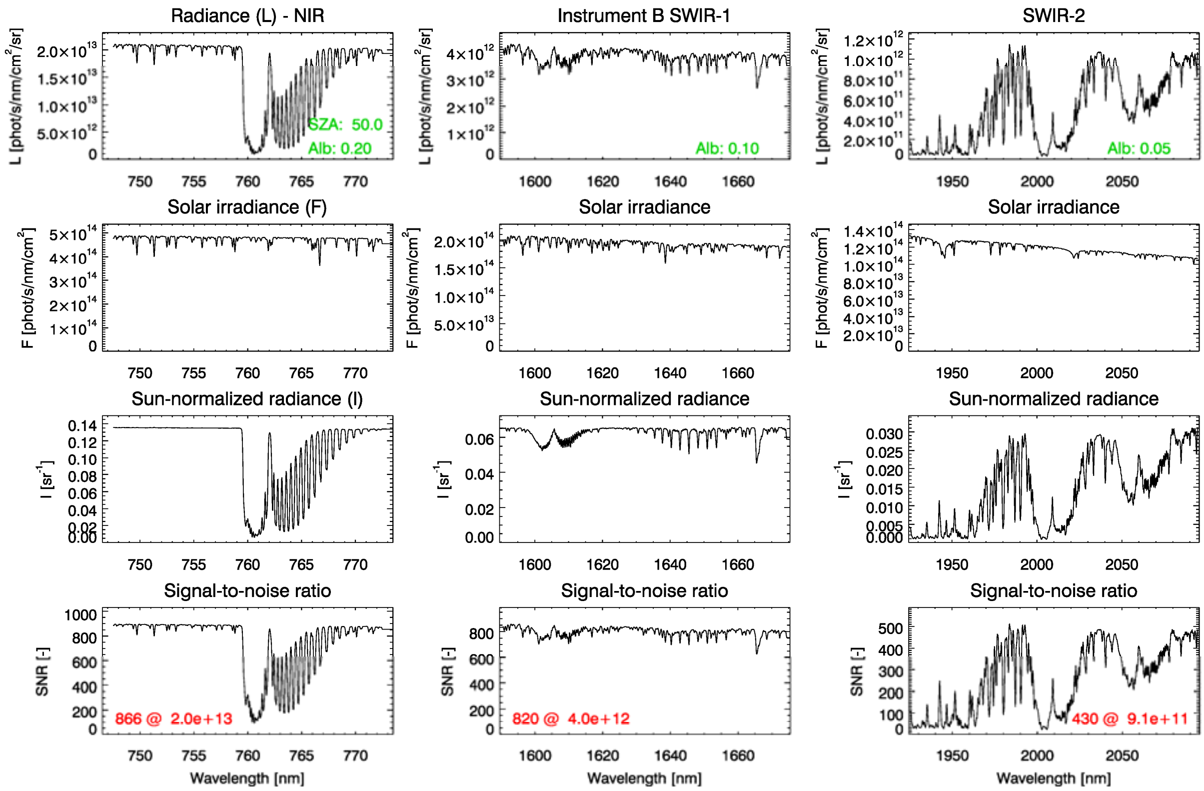

Figure 49: Instrument B spectra (see main text for details). The corresponding BESD/C XCO_2 retrieval precision (total uncertainty, i.e., including smoothing and interference errors): 0.69 ppm.

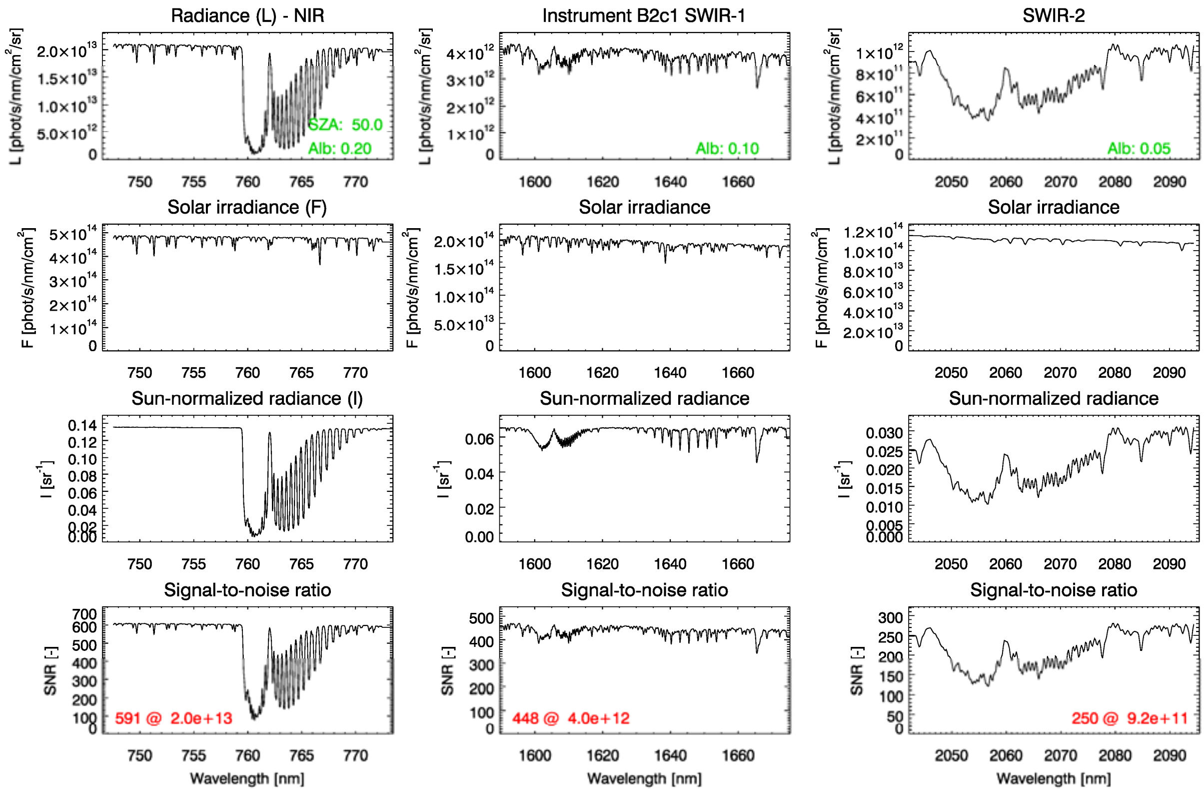

Figure 50: As **Figure 49** but for instrument B2c1. XCO_2 precision: 1.58 ppm.

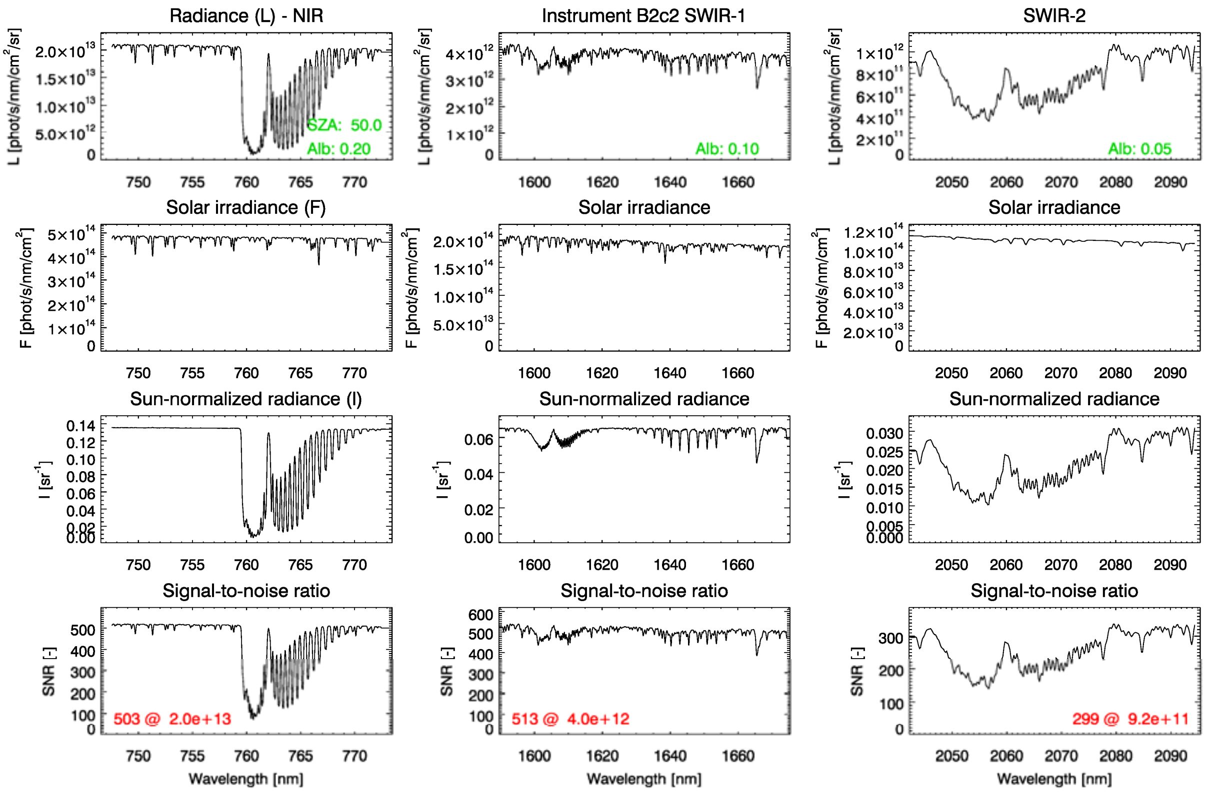

Figure 51: As **Figure 49** but for instrument B2c2. XCO_2 precision: 1.47 ppm.

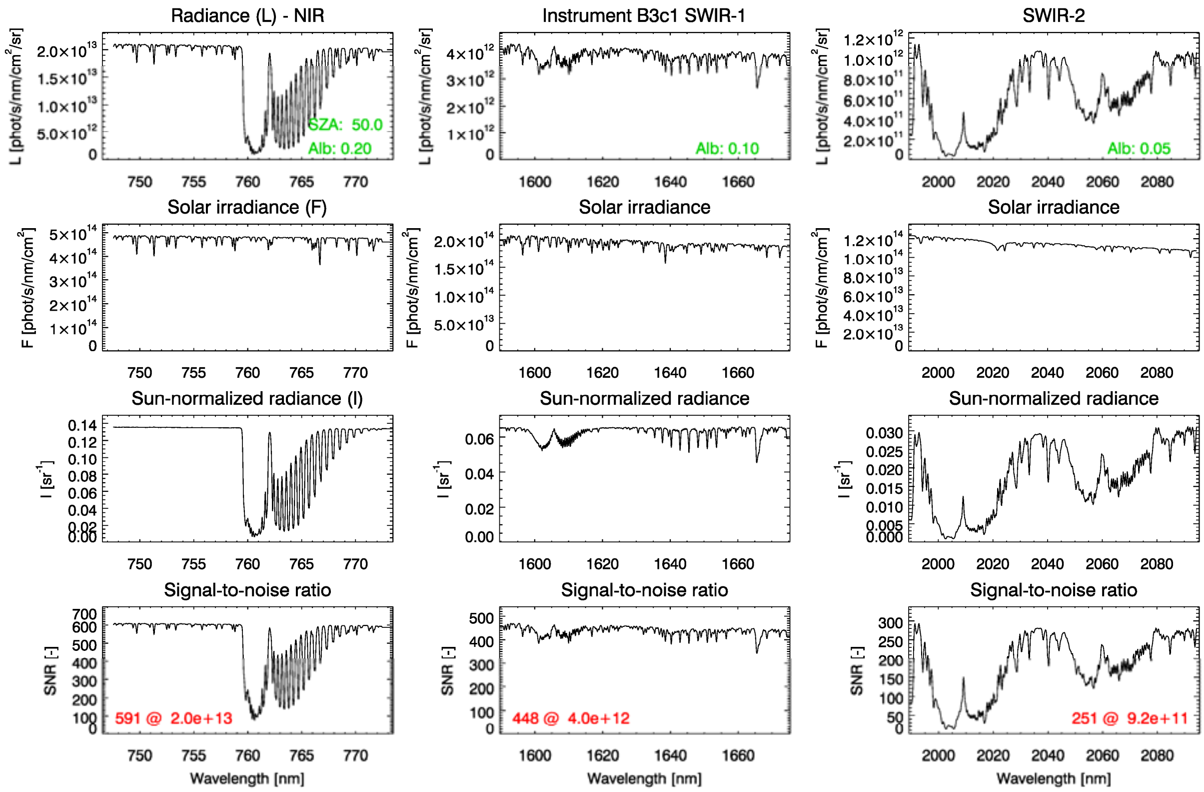

Figure 52: As **Figure 49** but for instrument B3c1. XCO_2 precision: 1.11 ppm.

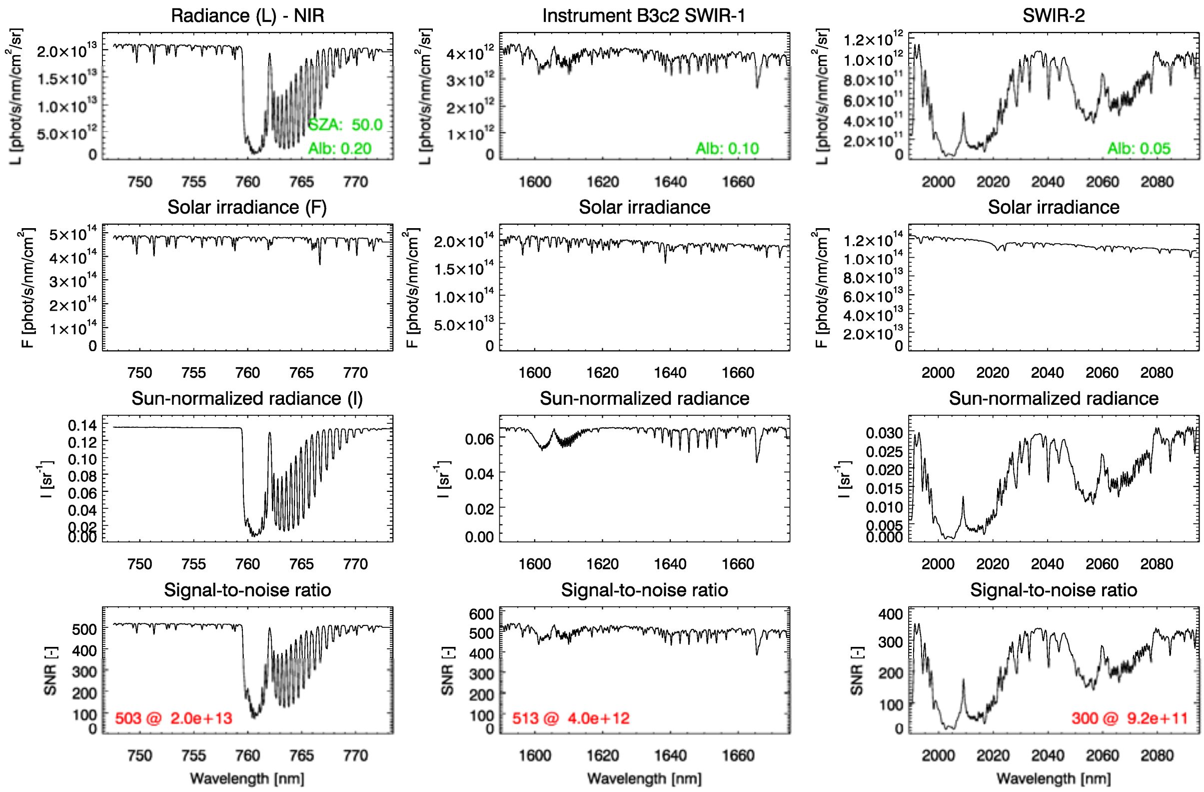

Figure 53: As **Figure 49** but for instrument B3c2. XCO_2 precision: 1.04 ppm.

The “XCO_2 precision” is defined as the overall XCO_2 random error, which has three components (see, e.g., **/Rodgers and Connor, 2003/**):

- Instrument noise (depending on SNR)
- XCO_2 smoothing error (depending on CO_2 and surface pressure state vector elements and their *a priori* uncertainty; note that surface pressure is strongly constrained so that essentially only the uncertainties of the CO_2 state vector elements matter; these are 10% for the lowest layer (lower troposphere) and 0.5% above)
- Interference error (depending on non-CO_2 state vector elements and their *a priori* uncertainty)

How the retrieval precision and the CO_2 column instrument noise errors depends on the BESD/C retrieval settings is shown in **Table 13**. From this the following can be concluded:

- From No. 1-3: Strong dependence on SWIR-2 start wavelength
- From 1, 5-7: Strong dependence on retrieval state vector

No.	BESD/C retrieval settings	XCO_2 precision [ppm]	CO_2 column instrument noise error [%] / [ppm]
1	Instrument B2c1 (SW2 start @ 2040 nm) & BESD/C default settings (= Algorithm Baseline 1 = ABL1)	1.58	0.32% / 1.25
2	As 1 but SW2 start @ 1990 nm	1.11	0.20% / 0.78
3	As 1 but SW2 start @ 1920 nm	0.87	0.15% / 0.59
4	As 1 but BESD/C without ZLO & Sh&Sq	1.20	0.24% / 0.94
5	As 4 but BESD/C without albedo parameters	0.96	0.22% / 0.86
6	As 5 but BESD/C without scattering parameters, TEM, H2O, SIF (remaining: CO_2, CH_4, surface pressure, polynomial)	0.73	0.17% / 0.65
7	As 6 but without polynomial (remaining: CO_2, CH_4, p_s)	0.46	0.10% / 0.32

Table 13: XCO_2 precision and CO_2 column noise error for several BESD/C retrieval settings.

Additional results are shown in **Table 14**. Note that retrieval setting used for No. 1.6 are **“Algorithm Baseline 2” (ABL2)**, which is identical with ABL1 (used in previous sections of this document). For ABL2 the following state vector elements have been removed compared to ABL1: ALB (= albedo; 3 elements, one per band) and ZLO (= zero level offset; 3 elements, one per band).

No.	BESD/C retrieval settings	XCO_2 precision [ppm]	CO_2 column instrument noise error [%] / [ppm]
1.1	For instrument B2c1 with SW2 start wavelength 1990 nm and BESD/C algorithm baseline 1 (ABL1)	1.11	0.20% / 0.80
1.2	As 1.1 but VCF (= SIF) removed from state vector (#)	1.11	0.20% / 0.80
1.3	As 1.2 but albedo (ALB) removed from state vector (#)	0.99	0.21% / 0.82
1.4	As 1.3 but ZLO removed from state vector (*)	0.76	0.16% / 0.64
1.5	As 1.4 but enhanced SNR in NIR / SW1 / SW2: 11% / 0% / 0% 0% / 11% / 0% 0% / 0% / 11% 0% / 11% / 11% 0% / 15% / 15% 0% / 20% / 20%	 0.76 0.73 0.74 0.71 0.70 0.68	 0.16% / 0.64 0.16% / 0.61 0.16% / 0.61 0.15% / 0.58 0.15% / 0.57 0.14% / 0.55
1.6	As 1.4 but VCF (= SIF) added = Algorithm Baseline 2	0.76	0.16% / 0.64
2.1	As 1.4 but with SW2 start wavelength 2043 nm	0.96	0.22% / 0.86
2.2	As 2.1 but enhanced SNR in NIR / SW1 / SW2: 0% / 40% / 40% 0% / 55% / 55% 0% / 60% / 60%	 0.74 0.70 0.67	 0.16% / 0.64 0.15% / 0.59 0.14% / 0.56
2.3	As 2.1 but VCF (= SIF) added	0.96	0.22% / 0.86

Table 14: Additional XCO_2 precision and CO_2 column noise error for several BESD/C retrieval settings. (#) Assumption: Not mandatory as good *a priori* & first guess via pre-processing. (*) Not clear if really needed / if adding ZLO to state vector is the best approach to deal with ZLO related errors.

10. Relevance of SWIR-2a spectral region

The SWIR-2a spectral region (around 1939 nm) covers a strongly absorbing (“saturated”) atmospheric water vapour band, which can be used in BESD/C via a pre-processing step in order to obtain an *a priori* / first guess value of the cirrus optical depth (COD) as input for the subsequent BESD/C 3-band retrieval (see **Sect. 3.2**).

Saturated water bands have been and are used in the context of XCO_2 retrieval from real satellite data: For example, the 1.9 µm spectral region is used for cirrus cloud detection and sub-sequent quality filtering (leading to rejection of the corresponding ground pixel depending on a pre-defined threshold) using a simple threshold technique for BESD XCO_2 retrievals from real GOSAT data **/Heymann et al., 2015/** and for the same reason the 1.4 µm spectral region has been used for WFM-DOAS XCO_2 retrievals from SCIAMACHY **/Heymann et al., 2012/**. As shown in **/Heymann et al., 2012/** the method is sensitive to thin (COD > 0.05) and high (CTH > 4 km) clouds if the water column is > 1.14 g/cm^2 (corresponding to 3.8x10^{22} molecules/cm^2). These findings are consistent with the findings of **/Guerlet et al., 2013/**. They concluded - based on simulated and real GOSAT data - that their detection and filtering method efficiently detects high altitude scattering layers (> 5 km) that are most likely cirrus (or occasionally aerosol volcanic plumes) and is efficient even in the case of relatively dry scenes. In summary, the use of strongly saturated water bands is well established and used in the context of satellite XCO_2 retrievals primarily for the detection and flagging of scenes contaminated with high concentrations of elevated (high altitude) atmospheric scatterers such as cirrus clouds.

Nevertheless, not all satellite XCO_2 retrieval algorithms use saturated water bands for detection and flagging of cirrus contaminated scenes. Examples are **/Reuter et al., 2010/** and **/Reuter et al., 2011/** for SCIAMACHY and all OCO-2 algorithms (e.g., **/Eldering et al., 2017/ /Reuter et al., 2017a/ /Reuter et al., 2017b/**).

Saturated water bands are also used for more general purposes, e.g., the 1.38 µm spectral region is used to generate the Visible Infrared Imaging Radiometer Suite (VIIRS) Cloud Mask data product **/VIIRS Cloud Mask ATBD, 2014/**.

The relevance of the SWIR-2a spectral region for XCO_2 retrieval has been further investigated in this study using simulations and the results are shown in the following.

Figure 54 shows radiance spectra and radiance ratios for several cirrus optical depth (COD). As can be seen, the radiance strongly increases almost linearly with COD, in particular for wavelengths below 1950 nm. The BESD/C retrieval algorithm takes advantage of this by retrieving COD from radiances around 1939 nm using a very simple algorithm, which computes COD from the 1939 nm radiance assuming a linear relationship (more details on this algorithm are given below). The resulting COD values are used as *a priori* and first guess values for the full BESD/C 3-band retrieval (where COD is also a state vector element) as this has the potential to further improve the accuracy of the retrieved COD and therefore also of the retrieved XCO_2.

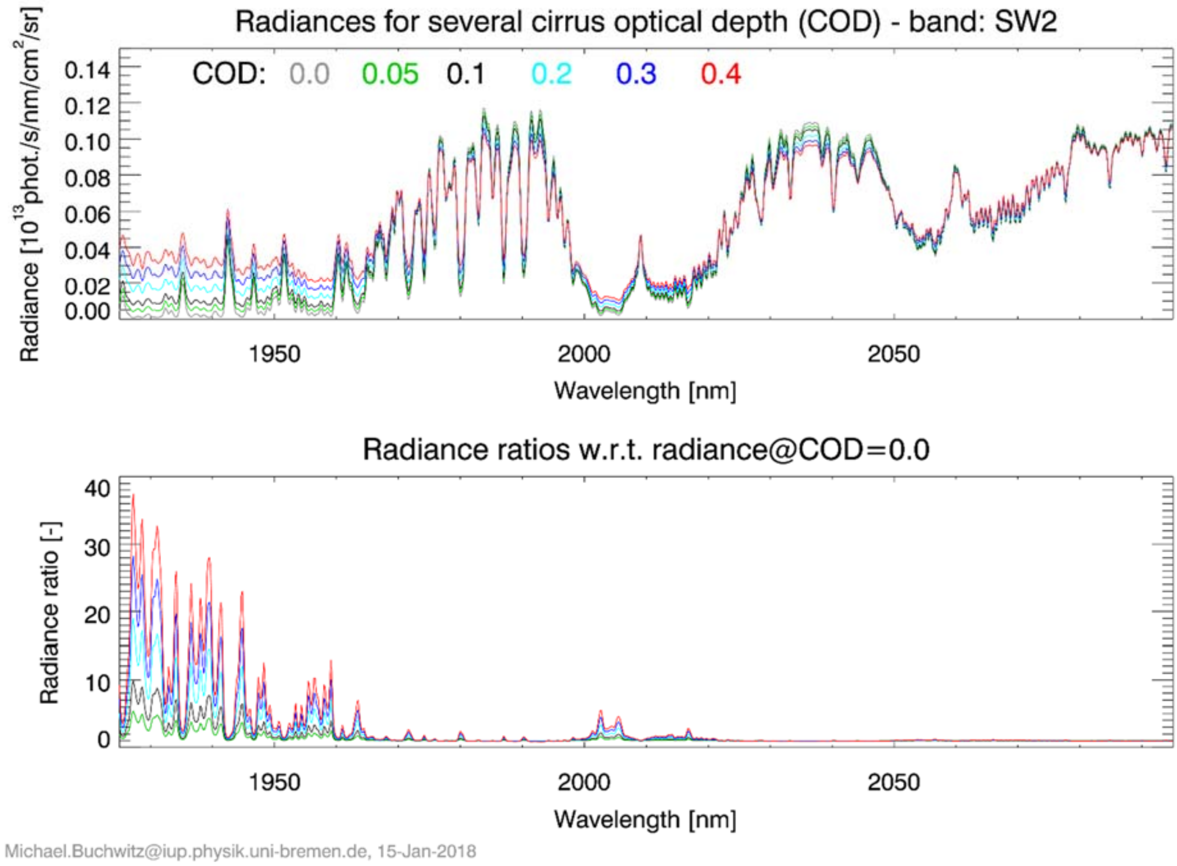

Figure 54: SWIR-2 band radiance spectra and radiance ratios. Top: Radiance spectra (resolution 0.55 nm) for different cirrus optical depths (COD). Other parameters: H_2O column: 4.8×10^{22} molecules/cm^2 (US Standard Atmosphere), SZA 50°, vegetation albedo, cirrus altitude 10 km, default aerosol ("s00": AOD 0.2, type: continental average).

Figure 55 shows a spectral zoom into **Figure 54** including radiance noise error (top) for instrument B2c1 and the corresponding SNR spectra (bottom). As can be seen, the SNR is good enough to distinguish the various radiance levels corresponding to different cirrus optical depths. **Figure 56** shows the corresponding results for the NIR band and **Figure 57** for the SWIR-1 band.

As can be seen, also the NIR band is very sensitive to cirrus but the radiance change is typically less specific compared to the SWIR-2 band as other parameters can lead to similar radiance perturbations. Nevertheless, also the NIR band provides information on cirrus and to what extent this is "good enough" for accurate XCO_2 retrieval if the SWIR-2a spectral region around 1.9 µm is not available has been investigated. The results are presented and discussed in the following.

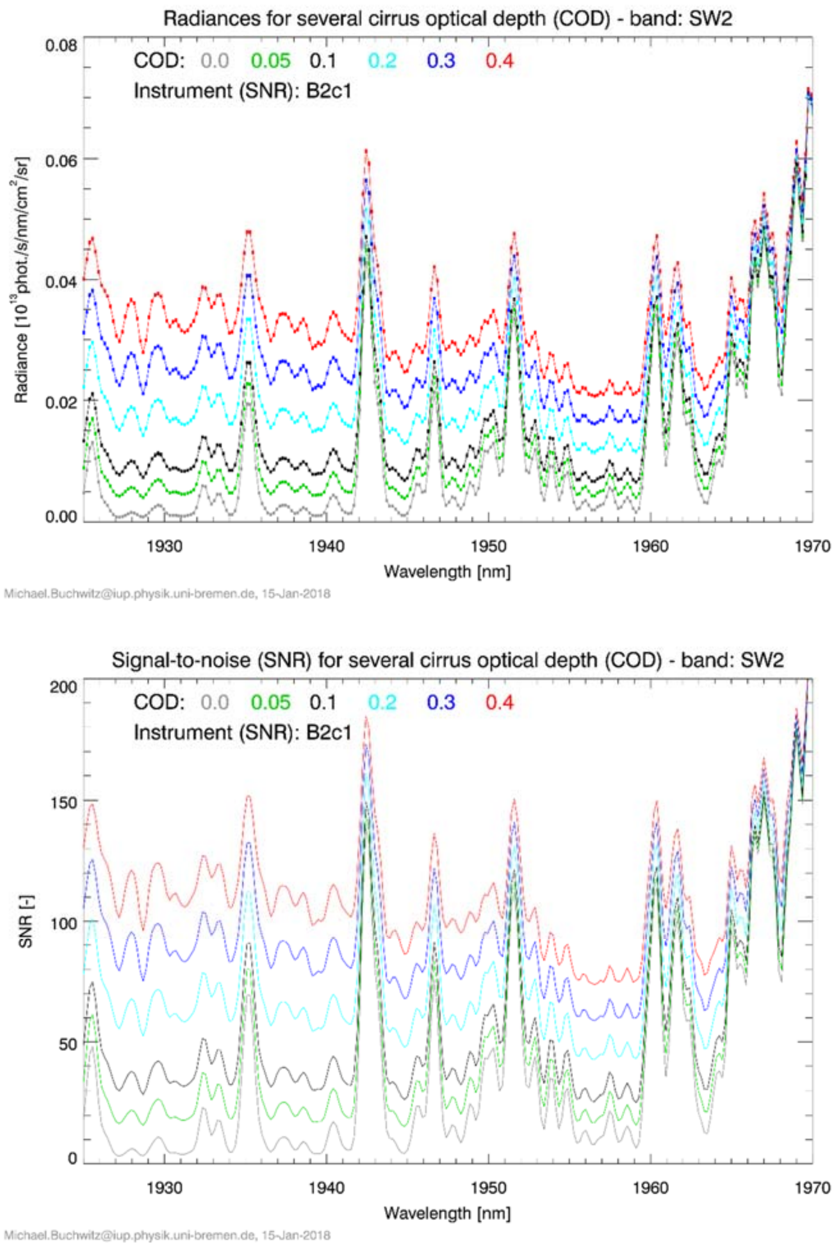

Figure 55: Top: As **Figure 54** but restricted to the first part of the SWIR-2 spectral range and with 1-sigma radiance noise error added. Bottom: Corresponding SNR.

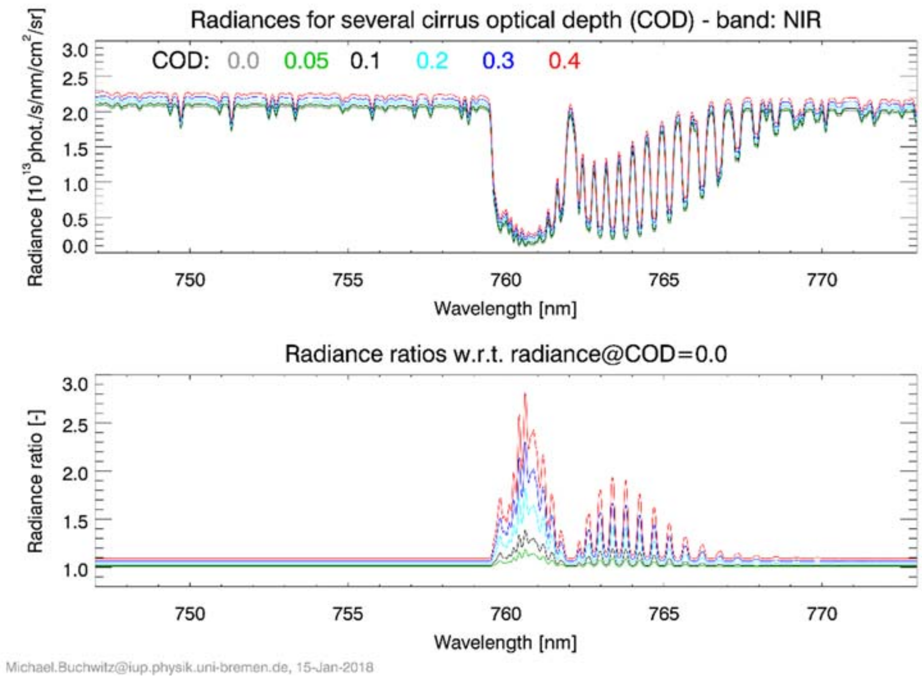

Figure 56: As **Figure 54** but for the NIR band.

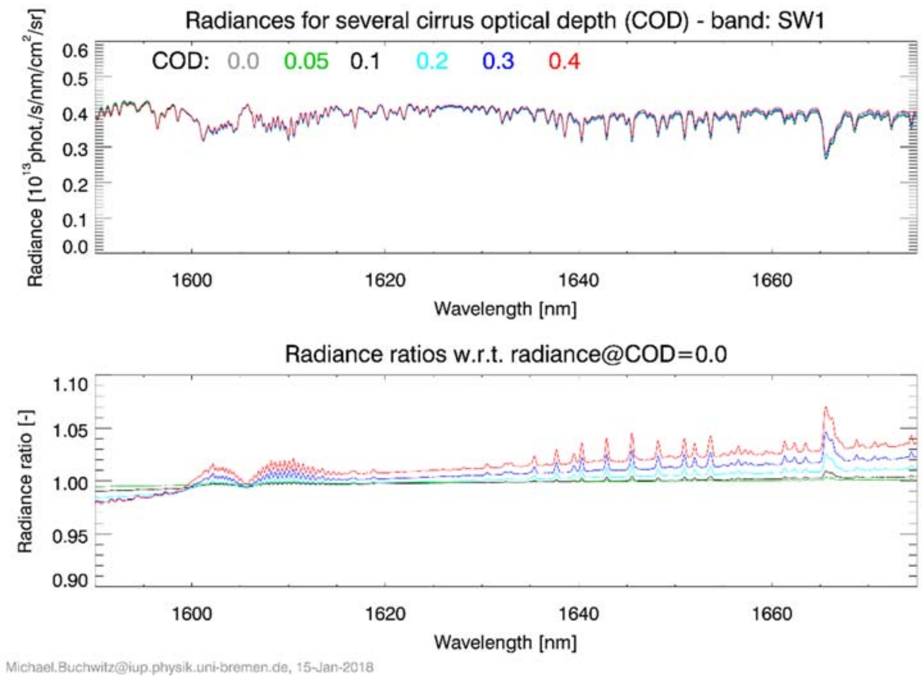

Figure 57: As **Figure 54** but for the SWIR-1 band.

As can be seen from the previous figures, the radiance in the SWIR-2a spectral region increases approximately linearly with COD. BESD/C takes advantage of this by retrieving COD in a pre-processing step from the mean radiance obtained from the 1938 – 1940 nm spectral region according to this equation:

$$COD^a = 0.2 \times RAD / (1.85\ 10^{11})$$

Here RAD is the (mean) radiance given in photons/s/nm/cm^2/sr and COD^a is the dimensionless cirrus optical depth as obtained from the SWIR-2a spectral region.

COD^a can then be used as *a priori* and first guess value for the BESD/C 3-band retrieval instead of the default value of COD, which is 0.05 +/- 0.05, i.e., assuming 100% *a priori* uncertainty (1-sigma).

To investigate if COD^a from SWIR-2a can be used to improve the accuracy of the XCO_2 retrievals and to find out if this likely also helps to increase the yield, i.e., to see if this has the potential to increase the number of ground-pixels where "good" XCO_2 retrievals are possible, the following has been done:

Retrievals have been performed for two cases:

- Case 1: An ideal case where the simulated radiance observations are fully consistent with the retrieval assumptions (same surface and atmospheric conditions except for COD, no measurement errors, etc.)
- Case 2: A nearly ideal case, which differs from Case 1 in only one aspect: Here the cirrus is located at 6 km whereas the retrieval assumes as *a priori* and initial guess that the cirrus is located at 10 km.

To make sure that the resulting XCO_2 bias is only due to COD errors, all other errors have been eliminated. In particular, errors resulting from the (other) pre-processing steps used to obtain initial values for surface albedo and SIF have been eliminated (i.e., it is assumed here that surface albedo and SIF are perfectly known).

The results shown in the following are for the VEG50 scenario (= surface albedo corresponding to vegetation, SZA 50^o) and for instrument B2c1 with the SWIR-2 fitting window starting at 2043 nm. It can however be assumed that the resulting general conclusions (given at the end of this section) are also valid for similar other instruments (e.g., B2c2) and other (shorter) SWIR-2 fitting window start wavelengths.

Figure 58 shows XCO_2 biases as a function of true COD (top panel) for the ideal case (Case 1). As can be seen, use of SWIR-2a results in lower biases (green curve) compared to retrievals, where SWIR-2a has not been used (red curve). **Figure 59** shows results for the same case but with iteration. As can be seen, the iteration reduces the biases for the case where SWIR-2a has not been used (red curve) but does not change the biases for the case where SWIR-2a has been used (as the iteration does not succeed to further reduce the cost function).

As can also be seen from these figures, the SWIR-2a spectral region provides improved *a priori* and first guess values of COD (compare the blue bars with the black bars in the middle and bottom panels). As can also be seen, good COD values can also be obtained if the SWIR-2a band is not used (compare the red bars with the black bars in the middle panels).

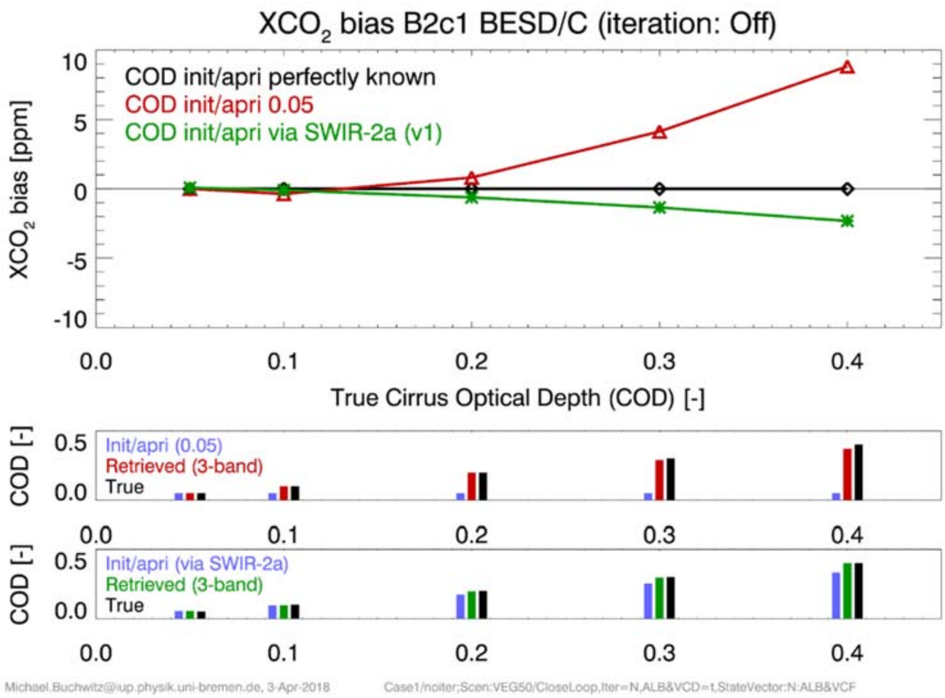

Figure 58: Top: XCO_2 bias versus true COD. The black line corresponds to results obtained with BESD/C 3-band retrievals, where COD is perfectly known. In this case, the resulting XCO_2 biases are all zero, as it should be. The red line shows the XCO_2 biases obtained assuming a default COD *a priori* and initial guess value of 0.05. The green line shows the XCO_2 bias if the SWIR-2a spectral region is used to obtain *a priori* and initial guess values for COD assuming that the COD^a *a priori* uncertainty is 100% (of the retrieved COD^a value). As can be seen, the biases are smaller compared to the case, where the SWIR-2a region has not been used (red curve). Middle panel: COD values for the case where the SWIR-2a region has not been used. Bottom panel: COD values for the case where the SWIR-2a region has been used. The BESD/C retrieval have been performed without iteration.

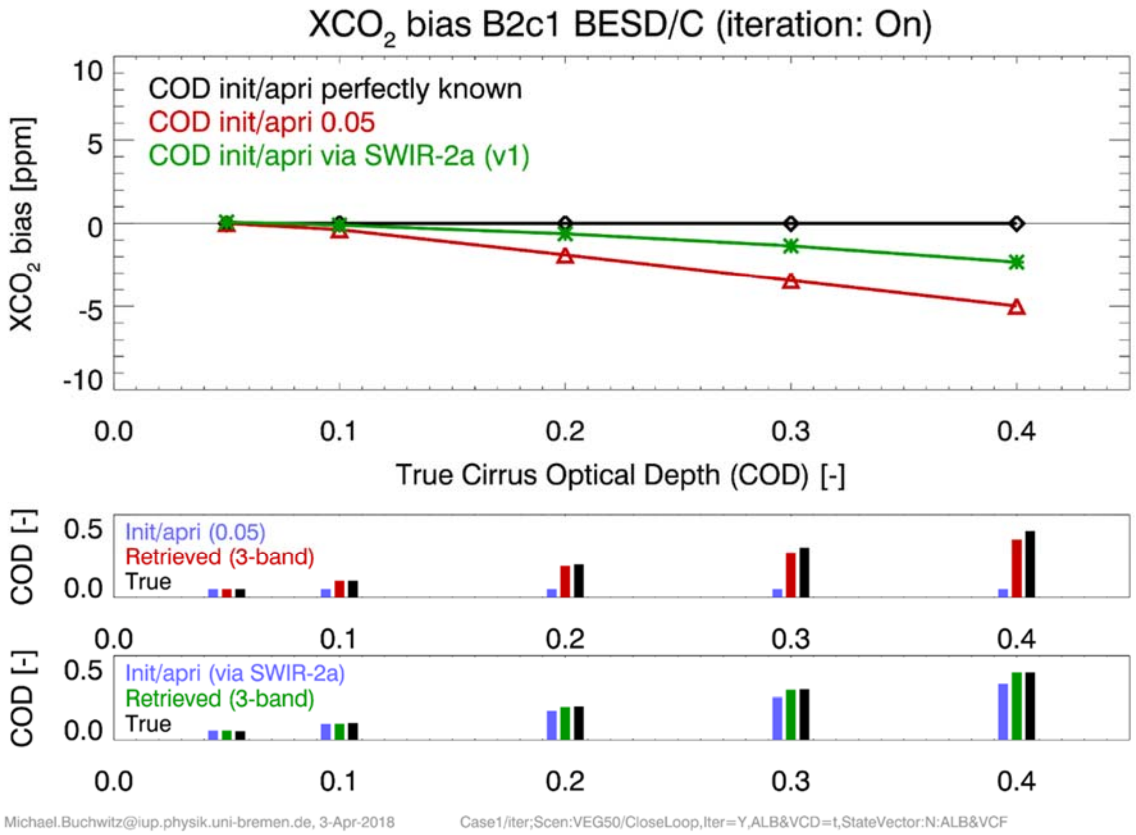

Figure 59: As **Figure 58** but with iteration.

Figure 60 (without iteration) **Figure 61** (with iteration) show the corresponding results for the less ideal case, i.e., for Case 2. As can be seen, even the black curve does not show error zero any more (because the cirrus altitude is not exactly known). As can also be seen, the biases shown by the green curve (use of SWIR-2a) are in this case larger than for the retrievals where SWIR-2a has not been used (red curve). The green curves shown in **Figure 60** and **Figure 61** correspond to retrievals where the assumed *a priori* uncertainty of COD[a] is 100%. **Figure 62** and **Figure 63** show the corresponding results for 30% *a priori* uncertainty. As can be seen, the results are essentially the same, i.e., they do not significantly depend on the assumed *a priori* uncertainty.

It was expected that at least for nearly ideal cases it can be shown that the accuracy can be clearly improved. However, as shown by the results in this section, this is apparently not the case for simulated BESD/C retrievals. It is therefore concluded that the SWIR-2a band is useful for detection and flagging of cirrus contaminated scenes but not to improve the accuracy of the XCO_2 retrieval for individual footprints.

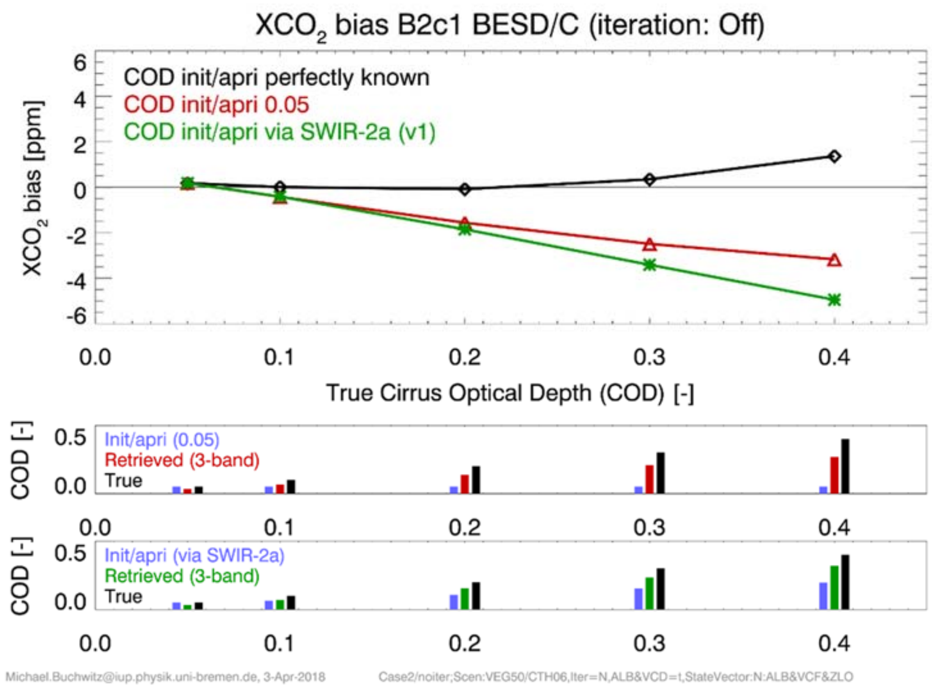

Figure 60: As **Figure 58** but for a slightly less ideal case. Here the cirrus is located at 6 km whereas the retrieval assumes that is it located at 10 km (= BESD/C default value).

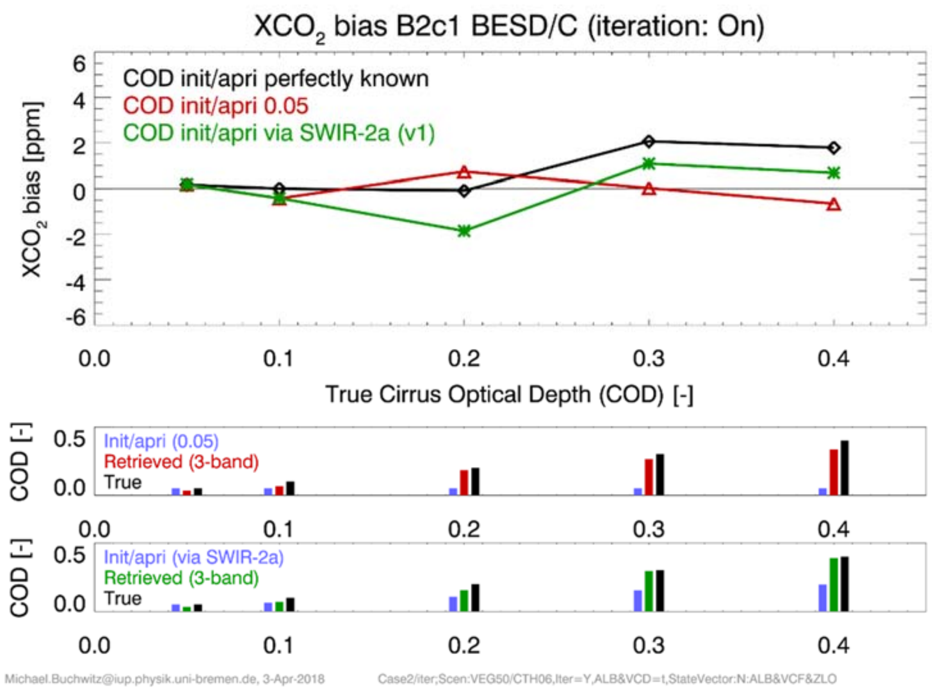

Figure 61: As **Figure 60** but with iteration.

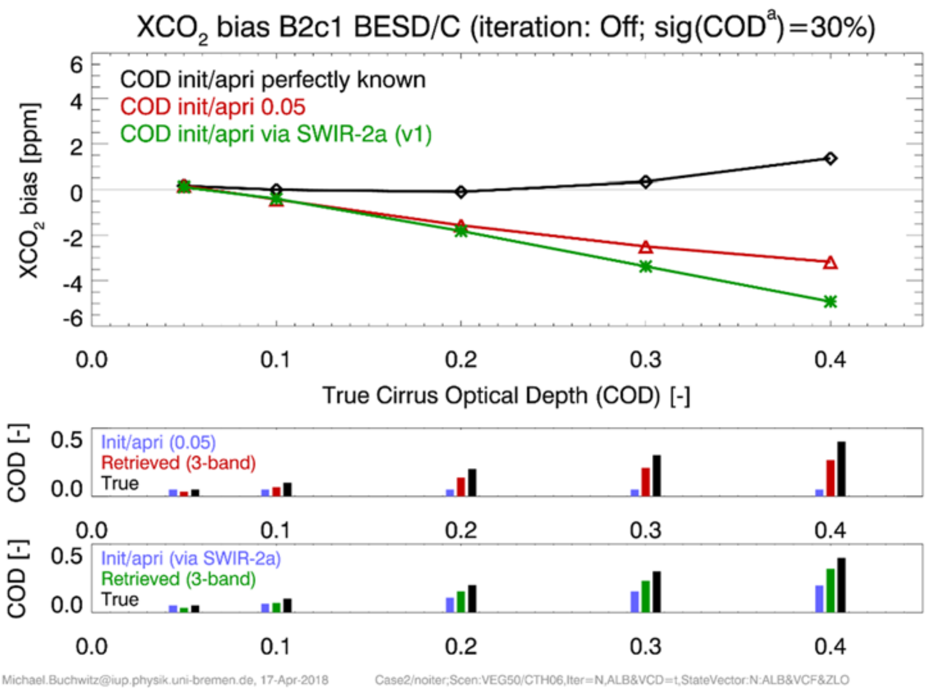

Figure 62: As **Figure 60** but assuming 30% a priori uncertainty for COD[a].

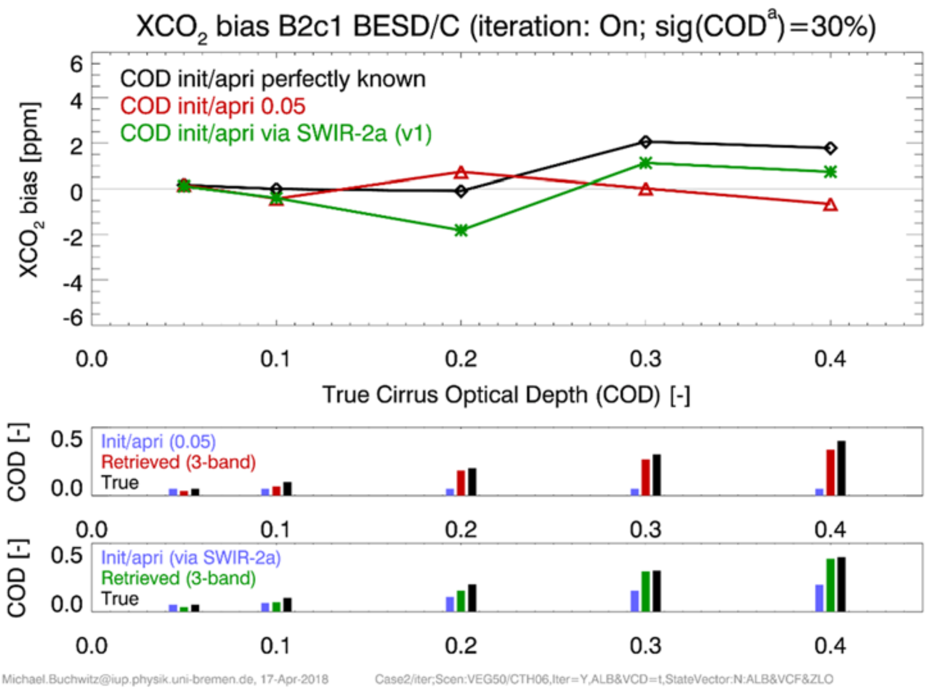

Figure 63: As
Figure 62 but with iteration.

10.1. Summary and conclusions SWIR-2a

It is clear – from published investigations using simulated and real satellite data – that strongly saturated water (SSW) bands (e.g., SWIR-2a) provide information on elevated (> 4-5 km) scattering layers (cirrus, elevated aerosols).

Currently SSW bands are used by some XCO_2 algorithms for identification and flagging (removal) of scenes contaminated by elevated scattering layers.

Note:

- Even „only“ detection and flagging is important as it ensures reliable detection of (potentially) very problematic scenes (footprints). Information on such scenes would be available prior to time consuming 3-band retrievals. This is relevant as processing time will be an issue (as each of the foreseen CO_2 satellites will have approximately 10 times the number of OCO-2 footprints).

The following has been investigated in this study (apart from the literature study results summarized above): Can SWIR-2a also help to improve the XCO_2 single footprint accuracy and/or to increase the yield via improved *a priori* information on cirrus optical depth (COD) from the SWIR-2a spectral region ?

The results shown in this section suggest that the answer is No.

Reason: The simulated retrievals have not shown any robust improvements. In fact, it has been shown that biases can even be worse for nearly ideal cases (where, for example, all is perfectly known except cirrus altitude). This is interpreted as a clear indication that improving the accuracy will hardly be possible.

The underlying reason for this is that COD information from other spectral regions (in particular from the NIR band) is already very good (at least for simulations) and that additional information from SWIR-2a does not to help to improve the accuracy.
Note that this conclusion is consistent with (unpublished) findings from SRON & UoL based on real GOSAT data

Based on these results the following is recommended for the MRD: Coverage of the SWIR-2a spectral region (e.g., the 1938-1940 nm region investigated here) should be included as a goal requirement but not necessarily as a threshold requirement („very good to have but not mandatory“).

11. Acronyms and abbrevations

Acronym	Meaning
ABL	Algorithm Baseline
AOD	Aerosol Optical Depth
ATBD	Algorithm Theoretical Basis Document
BESD	Bremen optimal EStimation DOAS
BESD/C	BESD algorithm used for CarbonSat assessments
BL	Boundary Layer
CA	Continental Average (aerosol scenario)
CarbonSat	Carbon Monitoring Satellite
CC	Continental Clean (aerosol scenario)
CCI	Climate Change Initiative (of ESA)
CL	Close Loop
CNES	Centre national d'études spatiales
COD	Cloud Optical Depth
CP	Continental Polluted (aerosol scenario)
CS	CarbonSat
CTH	Cloud Top Height
DE	Desert (aerosol scenario)
DES	Desert (surface albedo)
DOAS	Differential Optical Absorption Spectroscopy
DOF	Degrees of Freedom
EE8	Earth Explorer No. 8 (satellite)
ENVISAT	Environmental Satellite
ESA	European Space Agency
FR	Final Report
FWHM	Full Width at Half Maximum
GHG	Greenhouse Gas
GHG-CCI	Greenhouse Gas project of ESA's Climate Change Initiative (CCI)
GM	Gain Matrix
GMM	Gain Matrix Method
GOSAT	Greenhouse Gases Observing Satellite
ISRF	Instrument Spectral Response Function
IUP-UB	Institute of Environmental Physics (Institut für Umweltphysik), University of Bremen, Germany
MLS	Mid-latitude summer (profiles)
MODIS	Moderate resolution Imaging Spectrometer
MRD	Mission Requirements Document
NIR	Near Infra Red (band)
OCO	Orbiting Carbon Observatory
OE	Optimal Estimation

OPAC	Optical Properties of Aerosol and Clouds
RfMS	Report for Mission Selection
RMSE	Root Mean Square Error
RTM	Radiative Transfer Model
SCIAMACHY	Scanning Imaging Absorption Spectrometers for Atmospheric Chartography
SCIATRAN	Radiative Transfer Model under development at IUP
SIF	Sun-Induced Fluorescence
SNR	Signal to Noise Ratio
SSI	Spectral Sampling Interval
SSP	Spectral Sizing Point
SSR	Spectral Sampling Ratio
SW1 or SWIR-1	SWIR 1 band
SW2 or SWIR-2	SWIR 2 band
SWIR	Short Wave Infrared
SZA	Solar Zenith Angle
TOA	Top of atmosphere
VCF	Vegetation Chlorophyll Fluorescence
VEG	Vegetation (surface albedo)
VIIRS	Visible Infrared Imaging Radiometer Suite
VMR	Volume Mixing Ratio

12. References

/Bovenmann et al., 2010/ Bovensmann, H., Buchwitz, M., Burrows, J. P., Reuter, M., Krings, T., Gerilowski, K., Schneising, O., Heymann, J., Tretner, A., and Erzinger, J., A remote sensing technique for global monitoring of power plant CO_2 emissions from space and related applications, Atmos. Meas. Tech., 3, 781-811, 2010.

/Bovenmann et al., 2014/ Bovensmann, H., M. Buchwitz, M. Reuter, T. Krings, J. Heymann, H. Boesch, J. Landgraf, CarbonSat Earth Explorer 8 Candidate Mission "Level-2 and Level-1B Requirements Consolidation Study", Final Report ESA Study CarbonSat Earth Explorer 8 Candidate Mission "Level-2 and Level-1B Requirements Consolidation Study ", ESA Contract No 4000105676/12/NL/AF, Version 2.2, Date: 18. July 2014, Doc.ID: IUP-CS-L1L2-FR-01, 2014.

/Bovenmann et al., 2015/ Bovensmann, H., M. Buchwitz, M. Reuter, T. Krings, J. Heymann, H. Boesch, J. Landgraf, CarbonSat Earth Explorer 8 Candidate Mission "Level-1 Level-2 (L1L2) Performance Assessment Study ", Final Report ESA Study, ESA Contract No 4000109814/13/NL/FF/lf, Version 1.0, Date: 11. December 2015, Doc.ID: IUP-CS-L1L2-II-FR-01, 2015.

/Buchwitz et al., 2013a/ Buchwitz, M., M. Reuter, H. Bovensmann, D. Pillai, J. Heymann, O. Schneising, V. Rozanov, T. Krings, J. P. Burrows, H. Boesch, C. Gerbig, Y. Meijer, and A. Loescher, Carbon Monitoring Satellite (CarbonSat): assessment of atmospheric CO_2 and CH_4 retrieval errors by error parameterization, Atmos. Meas. Tech., 6, 3477-3500, 2013.

/Buchwitz et al., 2013b/ Buchwitz, M., H. Bovensmann, M. Reuter, J. Heymann, O. Schneising, et al., CARBONSAT: ERROR ANALYSIS FOR PRIMARY LEVEL 2 PRODUCTS XCO_2 AND XCH_4 AND SECONDARY PRODUCT VEGETATION CHLOROPHYLL FLUORESCENCE FOR NADIR OBSERVATIONS OVER LAND, ESA Living Planet Symposium, Sept 9-13, 2013, Edinburgh, UK, conference proceedings ESA Special Publication SP-722 (on CD-ROM), link: http://www.iup.uni-bremen.de/sciamachy/NIR_NADIR_WFM_DOAS/2846996buchwitz.pdf, 2013.

/Buchwitz et al., 2015/ Buchwitz, M., Bovensmann, T. Krings, M. Reuter, V. V. Rozanov, P. Liebing, J. Landgraf, F. Alkemade, Mission Requirements Analysis and Level 2 Error Characterization for CarbonSat Nadir Observations over Land - WP 1100, 2000 & 4100 Report, ESA Study CarbonSat Earth Explorer 8 Candidate Mission "Level-1 Level-2 (L1L2) Performance Assessment Study" ESA Contract No 4000109814/13/NL/FF/lf, Version 1.2, 3 Dec 2015, Doc ID: IUP-CS-L1L2-II-TNnadir, 2015.

/Buchwitz et al., 2017/ ESA Climate Change Initiative (CCI) Product Validation and Intercomparison Report (PVIR) for the Essential Climate Variable (ECV) Greenhouse Gases (GHG) for data set Climate Research Data Package No. 4 (CRDP#4), Version 5.0, 9. Feb. 2017, link: http://www.esa-ghg-cci.org/?q=webfm_send/352, 2017.

/Ciais et al., 2015/ Ciais, P., et al.: Towards a European Operational Observing System to Monitor Fossil CO_2 emissions - Final Report from the expert group, http://www.copernicus.eu/main/towards-european-operational-observing-system-monitor-fossil-co2-emissions, pp. 68, October 2015, 2015.

/CS MRD v1.0, 2011/ ESA, CarbonSat – Candidate Earth Explorer Opportunity Mission – Mission Requirements Document, Issue 1, Revision 0, 8 July 2011, ESA Mission Science Division, Reference EOP-SMA/2232/PI-pi, 2011.

/CS MRD v1.2, 2013/ ESA, CarbonSat – Candidate Earth Explorer Opportunity Mission – Mission Requirements Document, Issue 1, Revision 2, 23 May 2013, ESA Mission Science Division, Reference EOP-SMA/2232/PI-pi, 2011.

/CS RfMS, 2015/ ESA, Report for Mission Selection: CarbonSat, ESA SP-1330/1 (2 volume series), European Space Agency, Noordwijk, The Netherlands. link: http://esamultimedia.esa.int/docs/EarthObservation/SP1330-1_CarbonSat.pdf, 2015.

/Eldering et al., 2017/ Eldering, A., O'Dell, C. W., Wennberg, P. O., Crisp, D., Gunson, M. R., Viatte, C., Avis, C., Braverman, A., Castano, R., Chang, A., Chapsky, L., Cheng, C., Connor, B., Dang, L., Doran, G., Fisher, B., Frankenberg, C., Fu, D., Granat, R., Hobbs, J., Lee, R. A. M., Mandrake, L., McDuffie, J., Miller, C. E., Myers, V., Natraj, V., O'Brien, D., Osterman, G. B., Oyafuso, F., Payne, V. H., Pollock, H. R., Polonsky, I., Roehl, C. M., Rosenberg, R., Schwandner, F., Smyth, M., Tang, V., Taylor, T. E., To, C., Wunch, D., and Yoshimizu, J.: The Orbiting Carbon Observatory-2: first 18 months of science data products, Atmos. Meas. Tech., 10, 549-563, https://doi.org/10.5194/amt-10-549-2017, 2017.

/Galli et al., 2014/ Galli, A., Guerlet, S., Butz, A., Aben, I., Suto, H., Kuze, A., Deutscher, N. M., Notholt, J., Wunch, D., Wennberg, P. O., Griffith, D. W. T., Hasekamp, O., Landgraf, J., The impact of spectral resolution on satellite retrieval accuracy of CO_2 and CH_4, Atmos. Meas. Tech., Volume 7, Issue 4, pp.1105-1119, 2014.

/Guerlet et al., 2013/ Guerlet, S., Butz, A., Schepers, D., et al., Impact of aerosol and thin cirrus on retrieving and validating XCO_2 from GOSAT shortwave infrared measurements, J. Geophys. Res., VOL. 118, 4887–4905, doi:10.1002/jgrd.50332, 2013.

/Hess et al., 1998/ Hess, M., P. Koepke, and I. Schult, Optical Properties of Aerosols and Clouds: The software package OPAC, Bull. Am. Met. Soc., 79, 831-844, 1998.

/Heymann et al., 2012/ Heymann, J., H. Bovensmann, M. Buchwitz, J. P. Burrows, N. M. Deutscher, J. Notholt, M. Rettinger, M. Reuter, O. Schneising, R. Sussmann, and T. Warneke SCIAMACHY WFM-DOAS XCO_2: reduction of scattering related errors, Atmos. Meas. Tech., 5, 2375-2390, 2012.

/Heymann et al., 2015/ Heymann, J., M. Reuter, M. Hilker, M. Buchwitz, O. Schneising, H. Bovensmann, J. P. Burrows, A. Kuze, H. Suto, N. M. Deutscher, M. K. Dubey, D. W. T. Griffith, F. Hase, S. Kawakami, R. Kivi, I. Morino, C. Petri, C. Roehl, M. Schneider, V. Sherlock, R. Sussmann, V. A. Velazco, T. Warneke, and D. Wunch, Consistent satellite XCO_2 retrievals from SCIAMACHY and GOSAT using the BESD algorithm, Atmos. Meas. Tech., 8, 2961-2980, 2015.

/Landgraf et al., 2017/ Landgraf, J., J. aan de Brugh, A. Butz, K. Graf, Specification of Instrument Spectral Sizing Concepts, Spectral Errors and Geo-Physical Scenarios, Technical Note, SRON-CSS-TN-2016-002, 21-Feb-2017, version 3, pp. 20, 2017.

/Landgraf et al., 2017b/ Landgraf, J., J. aan de Brugh, A. Butz, K. Graf, Specification of Instrument Spectral Sizing Concepts, Spectral Errors and Geo-Physical Scenarios, Technical Note, SRON-CSS-TN-2016-002, 20-May-2017, version 4, pp. 21, 2017.

/Rascher et al., 2009/ Rascher, U., Agati, G., Alonso, L., Cecchi, G., Champagne, S., Colombo, R., Damm, A., Daumard, F., de Miguel, E., Fernandez, G., Franch, B., Franke, J., Gerbig, C., Gioli, B., Gomez, J. A., Goulas, Y., Guanter, L., Gutierrez-de-la-Camara, O´ ., Hamdi, K., Hostert, P., Jimenez, M., Kosvancova, M., Lognoli, D., Meroni, M., Miglietta, F., Moersch, A., Moreno, J., Moya, I., Neininger, B., Okujeni, A., Ounis, A., Palombi, L., Raimondi, V., Schickling, A., Sobrino, J. A., Stellmes, M., Toci, G., Toscano, P., Udelhoven, T., van der Linden, S., and Zaldei, A.: CEFLES2: the remote sensing component to quantify photosynthetic efficiency from the leaf to the region by measuring sun-induced fluorescence in the oxygen absorption bands, Biogeosciences, 6, 1181–1198, doi:10.5194/bg-6-1181-2009, 2009.

/Reuter et al., 2010/ Reuter, M., Buchwitz, M., Schneising, O., Heymann, J., Bovensmann, H., and Burrows, J. P., A method for improved SCIAMACHY CO_2 retrieval in the presence of optically thin clouds, Atmos. Meas. Tech., 3, 209-232, 2010.

/Reuter et al., 2011/ Reuter, M., Bovensmann, H., Buchwitz, M., et al. (2011), Retrieval of atmospheric CO_2 with enhanced accuracy and precision from SCIAMACHY: Validation with FTS measurements and comparison with model results, J. Geophys. Res., 116, D04301, doi:10.1029/2010JD015047.

/Reuter et al., 2017a/ Reuter, M., M. Buchwitz, O. Schneising, S. Noel, V. Rozanov, H. Bovensmann, J. P. Burrows, A Fast Atmospheric Trace Gas Retrieval for Hyperspectral Instruments Approximating Multiple Scattering - Part 1: Radiative Transfer and a Potential OCO-2 XCO_2 Retrieval Setup, Remote Sens., 9, 1159, doi:10.3390/rs9111159, 2017.

/Reuter et al., 2017b/ Reuter, M., M. Buchwitz, O. Schneising, S. Noel, H. Bovensmann, J. P. Burrows, A Fast Atmospheric Trace Gas Retrieval for Hyperspectral Instruments Approximating Multiple Scattering - Part 2: Application to XCO_2 Retrievals from OCO-2, Remote Sens., 9, 1102, doi:10.3390/rs9111102, 2017.

/Rodgers 2000/ Rodgers, C. D.: “Inverse Methods for Atmospheric Sounding: Theory and Practice”, World Scientific, Singapore, 2000.

/Rodgers and Connor, 2003/ Rodgers, C. D. and B. J. Connor, Intercomparison of remote sounding instruments, J. Geophys. Res., Vol. 108, No. D3, 4116, pp. 1-13, 2003.

/Rozanov et al. 2014/ Rozanov, V.V., A.V. Rozanov, A.A. Kokhanovsky, J.P. Burrows: Radiative transfer through terrestrial atmosphere and ocean: Software package SCIATRAN. Journal of Quantitative Spectroscopy and Radiative Transfer, http://dx.doi.org/10.1016/j.jqsrt.2013.07.004, Vol. 133, p. 13–71, 2014.

/VIIRS Cloud Mask ATBD, 2014/ GSFC JPSS CMO, Joint Polar Satellite System (JPSS) VIIRS Cloud Mask (VCM) Algorithm Theoretical Basis Document (ATBD), Aug. 5, 2014, Revision E, Goddard Space Flight Center, Greenbelt, Maryland, 2014.

***** End of Document *****